공학박사 학위논문

Various allotropes of diamond nanoparticles and their contribution to the growth of diamond in hot filament chemical vapor deposition

Hot-filament 화학 기상 증착에서의 다이아몬드 나노입자의 다양한 동소체와 다이아몬드의 성장 거동

2021 년 2 월

서울대학교 공과대학원
재료공학부
김 환 영

Various allotropes of diamond nanoparticles and their contribution to the growth of diamond in hot filament chemical vapor deposition

지도교수 황 농 문

이 논문을 공학박사학위논문으로 제출함

2021년 2월

서울대학교 대학원
재료공학부

김 환 영

김환영의 박사학위논문을 인준함
2021년 2월

위 원 장	김 영 운	(인)
부위원장	황 농 문	(인)
위 원	김 미 영	(인)
위 원	박 진 우	(인)
위 원	김 근 수	(인)

Abstract

Various allotropes of diamond nanoparticles and their contribution to the growth of diamond in hot filament chemical vapor deposition

Hwan-Young Kim

Department of Materials Science and Engineering

The Graduate School

Seoul National University

The nanoparticles were captured on the membrane of the transmission electron microscope (TEM) grid in the hot filament chemical vapor deposition (HFCVD) diamond process and the captured nanoparticles were observed by high resolution TEM. i-Carbon, hexagonal diamond, and n-diamond and cubic-diamond were identified. To confirm the relationship between the crystal structure of the nanoparticle and methane concentration, we

analyzed the d-spacing values of the captured nanoparticles. Observation of various carbon allotropes in the same sample suggested the coexistence of them in the gas phase during HFCVD. ~ 600 nanoparticles, which were captured for 10 s at 6 conditions of the capture temperatures of 900 ° C, 600 ° C and 300 ° C and the gas mixtures of 1% CH_4-99% H_2 and 3% CH_4-97% H_2, were analyzed for phase identification using high-resolution transmission electron microscopy(HR-TEM) and fast Fourier transformation(FFT). Hexagonal diamond, i-carbon, n-diamond, and cubic diamond were identified. The observation of two or more carbon allotropes captured on the same membrane suggested their coexistence in the gas phase during HFCVD. The crystal structure of carbon allotropes was related with the size of nanodiamond. Also, the effect of charging on the stability of nanodiamond structures has not been studied experimentally. We succeeded in capturing nanoparticles on the floating and grounded SiO, carbon, and graphene membranes of a copper transmission electron microscope grid during HFCVD. Nanoparticles captured on the grounded membrane consisted mainly of i-carbon, whereas those captured on the floating membrane consisted mainly of cubic diamond and n-diamond. We examined the effect of charge on the crystal structure

of nanodiamonds captured for 10 s under various conditions. ~ 200 nanoparticles were analyzed for phase identification using HR-TEM and FFT. Four carbon allotropes were identified. In order to control the stability of nanodiamonds, we controlled the number of electrons by increasing the filament temperature from 2100 °C to 2300 °C and filament bias from − 100 V to + 50 V at 1% methane concentration. ~ 700 nanoparticles were analyzed for phase identification using HR-TEM and FFT. The crystal structure of carbon allotropes was related with the size of nanodiamond. The crystal structure of nanoparticles affected the crystal structure of diamond deposited for 8 h. Confirmation of various carbon allotropes provides new insight into the nanodiamond synthesis in the gas phase and the growth mechanism of HFCVD diamond.

Table of Contents

List of Figures

1000 °C.

Fig. 6. Schematics of (a) the HFCVD system with the capturing apparatus for capturing nanoparticles on the TEM membrane and (b) the capturing apparatus.

Fig. 7. (a) TEM image of nanoparticles captured on the TEM membrane of the Cu grid with a capture time of 10 s, (b) HRTEM image of the white square in (a), (c) a higher magnification of the nanoparticle in the white circle of (b) and (d) the FFT image obtained from the Fig. 7. (c).

Fig. 8. HRTEM and FFT images of four carbon allotropes. (a) i-carbon at the gas mixture of 3 % CH_4 - 97 % H_2, (b) hexagonal diamond at the gas mixture of 1 % CH_4 - 99 % H_2, (c) n-diamond at the gas mixture of 3 % CH_4 - 97 % H_2, and (d) cubic diamond at the gas mixture of 1 % CH_4 - 99 % H_2.

Fig. 9. The number of nanoparticles with the d-spacing values obtained from 150 d-spacing values of ~ 100 nanoparticles captured at the gas mixture of (a) 1 % CH_4 - 99 % H_2 and at capture temperature of 900 °C, (b) at the gas mixture of 1 % CH_4 -

99 % H_2 and at capture temperature of 600 °C, (c) at the gas mixture of 1 % CH_4 – 99 % H_2 and 300 °C, (d) at the gas mixture of 3 % CH_4 – 97 % H_2 and 900 °C, (e) at the gas mixture of 3 % CH_4 – 97 % H_2 and at capture temperature of 600 °C, and (f) at the gas mixture of 3 % CH_4 – 97 % H_2 and at capture temperature of 300 °C.

Fig. 10. HRTEM images of nanoparticles captured at the gas mixture of 1 % CH_4 – 99 % H_2 at the capture temperature of (a) 900 °C, (b) 600 °C, (c) 300 °C and at the gas mixture of 3 % CH_4 – 97 % H_2 at the capture temperature of (d) 900 °C, (e) 600 °C, and (f) 300 °C.

Fig. 11. Distributions of the size of 100 captured nanoparticles captured at the gas mixture of 1 % CH_4 – 99 % H_2 at the capture temperature of (a) 900 °C, (b) 600 °C and (c) 300 °C and captured at the gas mixture of 3 % CH_4 – 97 % H_2 at the capture temperature of (d) 900 °C, (e) 600 °C and (f) 300 °C.

Fig 12. FESEM images of diamond particles deposited at the gas mixture of (a) 1 % CH_4 – 99 % H_2 and (d) 3 % CH_4 –97 % H_2 for deposition time of 8 h on the bare silicon substrate. (b) and (e) are the higher magnification of (a) and (d), respectively, and (c) and (f)

are the higher magnification of (b) and (e), respectively.

Fig. 13. FESEM images of diamond film deposited for 8 h on the pretreated silicon substrate. (a) and (b) are top view. (c) and (d) are cross section of (a) and (b).

Fig. 14. (a) and (b) are Raman spectra of diamond film of Fig. 13 (c) – (d).

Fig. 15. Schematics of the experimental apparatus for capturing carbon nanoparticles. The left figure is the HWCVD reactor with a capturing system. The right figure illustrates how the carbon and SiO membranes are made electrically grounded and floating condition. Nanoparticles were captured on grounded and floating carbon and SiO membranes under the same HFCVD condition.

Fig. 16. STEM images of nanoparticles captured for capturing time of 10 s (a) on the SiO membrane on the quartz holder (floating condition), (b) on the SiO membrane on the stainless-steel holder (grounded condition), (c) on the carbon membrane on the quartz holder (floating condition), and (d) on the carbon membrane on the stainless steel-holder (grounded condition) at the filament

temperature of 2000 °C and the capture temperature of 600 °C at the gas mixture of 3 % CH_4 – 97 % H_2.

Fig. 17. TEM images of nanoparticles captured on the graphene membrane of the TEM Cu grid (a) on the quartz holder (floating condition) and (b) on the stainless-steel holder (grounded condition) at the capture temperature of 600 °C and the gas mixture of 1 % CH_4-99 % H_2.

Fig. 18. HRTEM and FFT images of four carbon allotropes such as (a) cubic diamond (JCPDS6-0675), (b) n-diamond (JCPDS43-1104) captured on the floating membrane and (c) hexagonal diamond (JCPDS19-0268) and (d) i-carbon (52) captured on the grounded membrane.

Fig. 19. Frequency of d-spacing values of nanoparticles captured at 1 % CH_4 – 99 % H_2. The data were obtained by analyzing 300 d-spacing values out of ~ 200 nanodiamonds.

Fig. 20. Size distribution of nanoparticles captured (a) on the quartz holder (floating condition) and (b) on the stainless-steel holder (grounded condition), respectively.

Fig. 21. FESEM images of diamonds particles deposited for deposition time of 8 h on the bare silicon substrate (a) on the sapphire plate on the stainless-steel holder (floating condition) and (b) on the stainless-steel holder (grounded condition). (c) and (d) are magnified images of a diamond particle of (a) and (b), respectively.

Fig. 22. Raman spectra of deposited diamond particles deposited (a) on the floating substrate (Fig. 21 (a)) and (b) on the grounded substrate (Fig. 21 (b)).

Fig. 23. Schematic diagram of the experimental system with capturing apparatus.

Fig. 24. TEM image of nanoparticles captured for 10 s on the graphene membrane of the TEM Cu grid. Nanoparticles are black small spot in Fig. 24 (a). (b) HRTEM image of the white box in (a). (c) a higher magnification of a nanoparticle in the white circle of (b). (d) The selected are electron diffraction pattern of the crystalline nanoparticle in (c). (e) i-carbon with 2.43 Å d-spacing value. (f) FFT image of (e).

Fig. 25. The number of nanoparticles with d-spacing values of the captured nanoparticles, which obtained 450 d-spacing values of ~300 nanodiamonds. The nanoparticles were captured at filament temperature of 2100 °C, 2200 °C, and 2300 °C at the gas mixture of 1 % CH_4 - 99 % H_2, respectively.

Fig. 26. HRTEM image of nanoparticles captured at filament temperature of (a) 2100 °C, (b) 2200 °C, and (c) 2300 °C. And, (d-f) are the magnified HRTEM images of (a-c), respectively.

Fig. 27. The classification of ~ 100 nanoparticles at each conditions.

Fig. 28. Average size of the captured nanoparticles at each filament bias ranging of - 100 V to +50 V.

Fig. 29. Deposition behavior of diamond particles. (a) and (c) at filament temperature of 2100 °C, (b) and (d) at filament temperature of 2300 °C.

Fig. 30. Deposition behavior of diamond film at filament bias (a) 0 V, (b) -5 V, (c) -10 V, (d) -20 V, and (e) - 40 V.

Fig. 31. FESEM images of diamond particles deposited on the Si substrate at a filament temperature of 2100 °C. The diamond particles (a–d) were deposited at 1 % CH_4 – 99 % H_2. The low magnification image of diamond particles (a–d) deposited for 4 h and 8 h, respectively. (c–d) are the high magnification images, respectively, of (a–b). The diamond particles (e–h) were deposited at 3 % CH_4 – 97 % H_2. The low magnification image of diamond particles (e–h) deposited for 4 h and 8 h, respectively. (g–h) are the high magnification images, respectively, of (e–f). (e–f) are the low magnification image of diamond particles deposited for 4 h and 8 h, respectively.

Fig. 32. FESEM images of diamond particles deposited on the Si substrate at a filament temperature of 1900 °C. The diamond particles (a–d) were deposited at 1 % CH_4 – 99 % H_2. The low magnification image of diamond particles (a–d) deposited for 4 h and 8 h, respectively. (c–d) are the high magnification images, respectively, of (a–b). The diamond particles (e–h) were deposited at 3 % CH_4 – 97 % H_2. The low magnification image of diamond particles (e–h) deposited for 4 h and 8 h, respectively. (g–h) are the high magnification images, respectively, of (e–f).

(e–f) are the low magnification image of diamond particles deposited for 4 h and 8 h, respectively.

Fig 33. Raman spectra of deposited particles in Figs. 31 and 32. (a) the Raman spectra of the diamond particle in Fig. 31 (d). (b) the Raman spectra of the diamond particles in Fig. 31 (h). (c) the Raman spectra of the diamond particle in Fig. 32 (d). (d) the Raman spectra of the diamond particle in Fig. 32 (h).

Fig. 34. Optical microscope images of the filament surface (a) at a filament temperature of 2100 °C at the gas mixture of 1 % CH_4 – 99 % H_2 and (b) at a filament temperature of 2100 °C at the gas mixture of 3 % CH_4 – 97 % H_2, (c) at a filament temperature of 1900 °C at the gas mixture of 1 % CH_4 – 99 % H_2, and (d) at a filament temperature of 1900 °C at the gas mixture of 3 % CH_4 – 97 % H_2.

Fig. 35. Thermodynamic calculations of the equilibrium mole fraction of carbon precipitation at gas mixture of 1 % CH_4 – 99 % H_2 and 3 % CH_4 – 97 % H_2 by using a Thermo–Calc software based on a SGTE (Scientifica Group Thermodata Europe) database [56].

Fig. 36. Current measured at filament temperatures of 1900 °C,

2000 °C and 2100 °C. The light gray bars show the current measurement at 1 % CH_4 – 99 % H_2 and the dark gray bars show the current measurement at 3 % CH_4 – 97 % H_2.

Fig. 37. TEM images of carbon nanoparticles captured at the gas mixture of 3 % CH_4 – 97 % H_2 for 15 s on the SiO membrane of the TEM grid. (a–b) are the STEM images of the nanoparticles captured at 1900 °C and 2100 °C, respectively. (c–d) are the HRTEM images of (a–b), respectively.

Fig. 38. HRTEM images of carbon nanoparticles for 10 s on the carbon membrane of the TEM grid. (a) shows the nanoparticles captured at 1900 °C at 3 % CH_4 – 97 % H_2 (b) after 2 s (c) 4 s.

Table 1. The experimentally observed d–spacing values with those for four carbon allotropes such as cubic diamond, n–diamond, hexagonal diamond, and i–carbon.

Chapter 1. Introduction

Technical development for synthesizing the diamond has made great strides for understanding the various carbon allotropes such as i-carbon, hexagonal diamond, n-diamond and cubic diamond. Thin i-carbon films have been chiefly produced by the ion-beam deposition method [1] and by radio frequency plasma decomposition of hydrocarbon gases. [2] Gogotsi et al. [3] reported that nano and micro crystalline diamond-structured carbon, with cubic and hexagonal structure, were synthesized by extracting silicon from silicon carbide in chlorine-containing gases at ambient pressure and temperatures. Hirai and Kondo [4] developed a rapid cooling technique in the shock compression of graphite sheets and found a new allotrope of carbon referred to as 'n-diamond' (new-diamond), since its lattice parameter is close to that of diamond. Yamada et al. [5] reported that two kinds of diamond-like carbon crystals, n-diamond and i-carbon, together with diamond were found in a detonation product of high explosive (RDX)/graphite mixtures.

As the diamond size decreases, the phase stability of the diamond also changes and the diamond becomes a more stable structure than

the graphite phase. Verechshagin [6] predicted that the most stable phase of the detonation diamond was 3 nm, and observed nanodiamond below 4 nm at 3000 °C. Barnard et al. [7] investigated the relationship between the size of the nanodiamonds and the phase stability of carbon nanoparticles. They showed that the bucky diamond occupies a coexistence region, spanning the calculated upper limit of fullerene stability and the lower limit of nanodiamond stability. However, the relationship between the size of nanoparticle and the carbon allotropes such as i-carbon, hexagonal diamond, n-diamond and cubic diamond have not been studied yet.

The purpose of this paper is to research the relationship between crystal structure of the nanoparticles and the size of the nanoparticles. Park et al. [8] succeeded to confirm the generation of diamond nanoparticles in the gas phase under the synthesis condition of diamond films by HFCVD. To captured the nanodiamonds, we used a capturing apparatus, which is loaded with a transmission electron microscope (TEM) grid membrane was exposed for 10 s. We investigated the effect of the various process parameter to understand the crystal structure of nanoparticles and their contribution to the diamond growth. This thesis experimentally examined the possibility that the charge can be an essential factor

for synthesizing the diamond nanoparticles during hot-filament chemical vapor deposition (HFCVD). Chapter 1 describes the theory of charged nanoparticle, gas phase generation of diamond nanoparticles, charge induced stabilization on the surface structure of nanodiamond, and the effect of process parameter on the crystal structure of the various carbon allotropes. (TEM).

1.1 Theory of Charged Nanoparticle

Hwang suggested that diamond synthesized at low pressure by CVD grow by clusters formed in the gas phase in 1996. [9] He suggested that CVD diamonds grow by non-classical crystallization. However, it was difficult to provide a direct experimental evidence for the non-classical crystallization. The first paper (Hwang and Yoon 1996) suggested the 'charged cluster model', which was called as a 'theory of charged nanoparticle(TCN)'. In TCN, the role of electric charges in the nanoparticles is important factor because charges play a crucial role in non-classical crystallization.

When the silicon and the iron substrates were placed side by side under the same processing condition of HFCVD, the crystalline diamond is growing on the silicon substrate while a porous soot structure is evolved on the iron substrate as shown in Fig. 1. This results imply that the growth mechanisms of diamond and soot should be closely related to one another. If the growth mechanism of soot is understood, such understanding would provide great insight as to the growth mechanism of diamond. Those of soot commonly observed in the field of combustion and flame. Soot is regarded as aggregates of carbon particles and grown in the gas phase. The gas phase aggregation of soot has been explained by the

ionic mechanism, which suggest that soot is aggregates of charged carbon cluster. [10−12]

The growth rate of soot on the iron substrate in Fig. 1 is almost 10 times higher than that of diamond on the silicon substrate. The growth rate of soot is hard to understand by the atomic hydrogen hypothesis because the graphite should be etched by the atomic hydrogen. In addition, the iron substrate is known to be harmful to the quality of diamond film. Based on the catalytic effect of iron on the diamond growth, the growth rate of soot should not be higher than that of diamond. Hwang suggested that the charge transfer rates would be related to the growth rate of diamond and soot.

The previous reports of the CVD diamond process such as formation of diamond along the convex edge can be explained by the charged cluster model. This phenomenon can be approached by assuming the charge−induced nucleation of the diamond clusters in the gas phase. When diamond nanoparticles were generated in the gas phase, the initiation of the diamond particles on the substrate is not by nucleation, but by landing of the charged nanoparticles. Due to the highest electric field gradient, the charged nanoparticles are expected to land on the convex sites.

Based on these theories, various materials and systems have been

set up to demonstrate the charged cluster model in many studies. Differential mobility analyzer (DMA) can be used to directly measure the charged nanoparticles which were generated in the gas phase during HFCVD. Besides, faraday cups can be used to measure the size distribution of the charged nanoparticles in the mass. (Fig. 3) A DMA separates charged nanoparticles according to their electrical mobility and can be used to produce aerosols of known size and number concentration. Using this system, Hwang's group confirmed the existence of charged nanoparticles in the growth of nanostructures of Carbon [13], Silicon [14], Silicon Nitride [15], ZnO [16], and GaN [17], and furthermore, by controlling these particles, the relationship between the electrical sign and the deposition behavior was investigated. (Figs. 4 and 5)

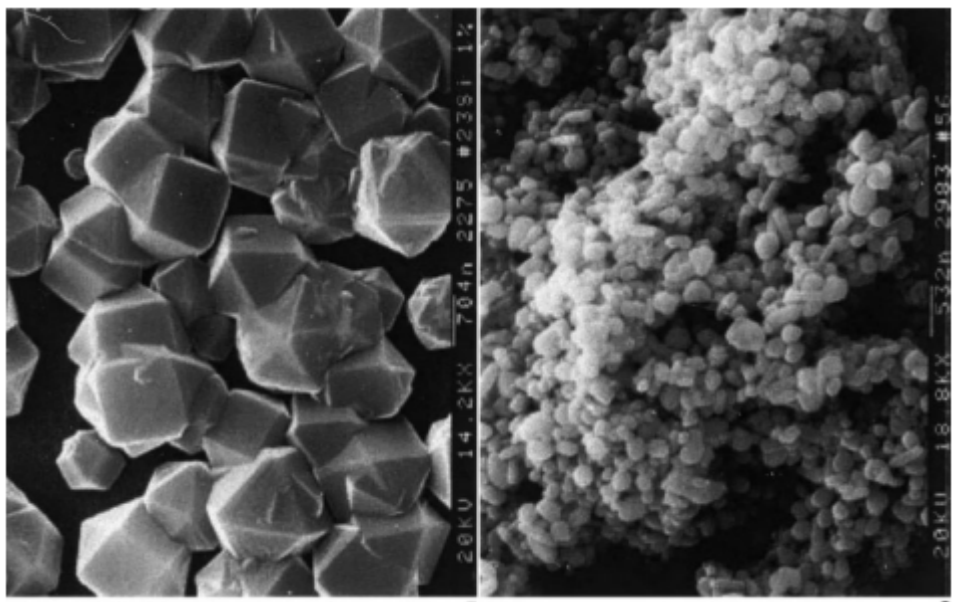

Fig. 1. SEM images of (a) diamond particles deposited on a silicon substrate, (b) soot particles deposited on an iron substrate at a flow rate, 100 sccm, of 1 % CH_4 – 99 % H_2 gas mixture for 2 h under 20 torr at a filament temperature of 2200 °C and a substrate temperature of 990 °C. The substrates were placed side by side during hot wire diamond CVD [13, 18].

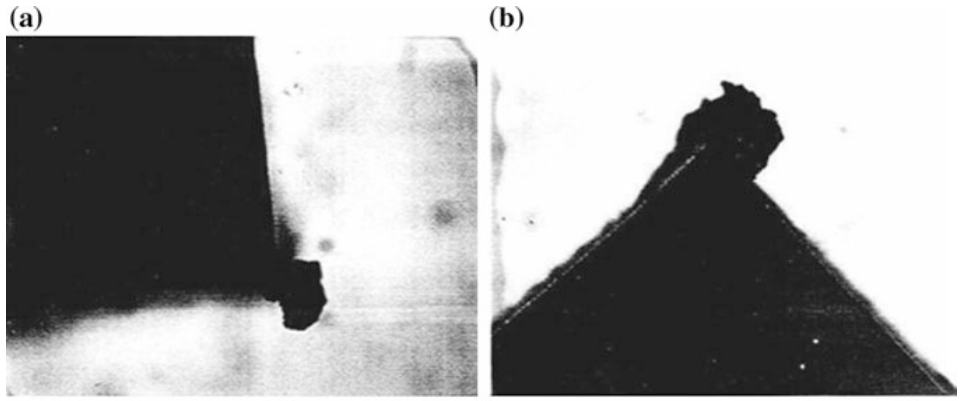

Fig. 2. the preferential growth of soot particles at the corner of the iron substrate.

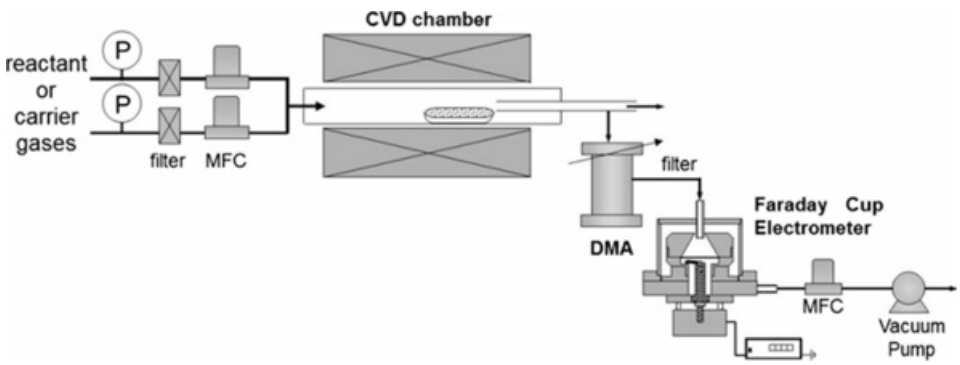

Fig. 3. Schematic of experimental set-up for the CVD reactor with the DMA-FCE system for measurements of charged nanoparticles (CNPs) generated at the gas phase during atmospheric CVD.

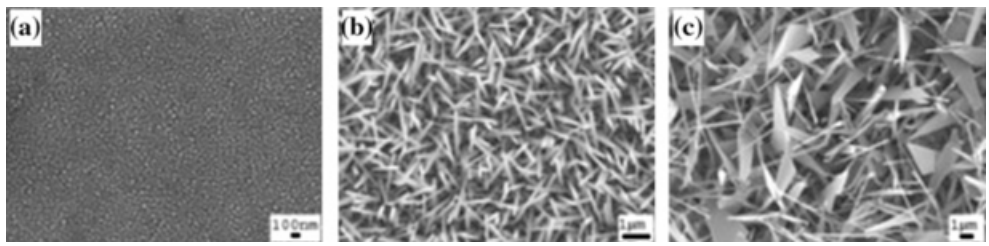

Fig. 4. FESEM images of ZnO nanowires at furnace temperatures of (a) 800 °C, (b) 900 °C, and (c) 1000 °C and at an oxygen flow rate of 10 sccm.

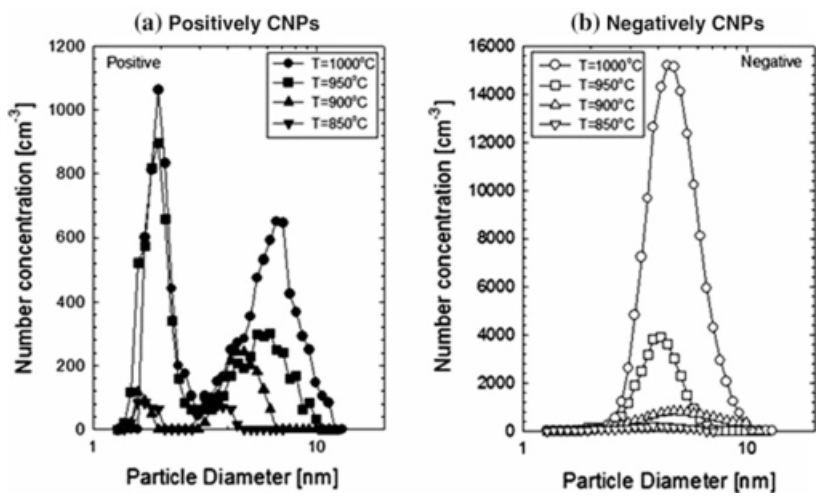

Fig. 5. The size distribution of (a) positively and (b) negatively charged ZnO nanoparticles at furnace temperatures from 850 °C to 1000 °C.

1.2 Gas-phase generation of diamond nanoparticles

The charges or ions are known to be strong heterogeneous sites for nucleation, which is known as ion-induced nucleation well established in the Wilson cloud chamber experiment [18-20].

In the Wilson cloud chamber experiment, the amount of supersaturated medium is large whereas the amount of ions is rather small. As a result, charged nuclei instantly grow into the visible size, which reveals the track of high energy particles. In the diamond CVD process, however, the amount of supersaturated carbon is relatively small whereas the amount of charges is huge. As a result, supersaturated carbon is divided into each charge, becoming invisible nanometer-sized charged diamond particles.

Generation of the diamond nanoparticles in the gas phase is supported by the well-known phenomenon of simultaneous diamond deposition and graphite etching. When graphite is used as a substrate for synthesizing diamond via gas activation (e.g., via plasma or a hot filament), diamond deposits on the graphite and simultaneously graphite etches away into the gas phase [21]. However, comparison of the chemical potential of carbon in diamond (μ_C^{dia}), graphite (μ_C^{gra}) and the gas phase (μ_C^{gas}) reveals that this phenomenon would violate the second law of thermodynamics if

diamond is deposited by an individual atom. Specifically, graphite is more stable than diamond, which indicates that $\mu_C^{gra} < \mu_C^{dia}$. Therefore, if stable graphite is etched away, which indicates $\mu_C^{gas} < \mu_C^{gra}$, one would expect the less-stable diamond to be also etched away because $\mu_C^{gas} < \mu_C^{dia}$ [22-23]. However, simultaneous etching of graphite and deposition of diamond indicates that $\mu_C^{gas} < \mu_C^{gra}$ and $\mu_C^{gas} > \mu_C^{dia}$, which obviously violates the second law of thermodynamics.

To avoid the violation of the second law of thermodynamics, Hwang and Yoon [24] suggested that diamond should be nucleated in the gas phase and the gas-phase nuclei should be the building block of diamond films. Furthermore, Hwang et al. [9] suggested that gas phase generated-diamond nuclei should be negatively charged. Jeon et al. [25-26] confirmed the generation of negatively-charged nanoparticles using a hot filament chemical vapor deposition (HFCVD) process via an energy analyzer and a Wien filter. Park et al. [8] demonstrated the existence of diamond nanoparticles in the gas phase using an HFCVD system. Gas phase nucleation of diamond was also reported by other groups [27-29].

1.3 Relationship between the size and the phase stability of diamond

As the nanodiamond size decreases, the phase stability of the diamond also changes and the nanodiamond becomes a more stable structure than the graphite phase. A number of theoretical models have been proposed regarding the stability of carbon nanoparticles [30-31]. These models predict that for particles under 5 – 6 nm in diameter nanocrystalline diamond is more stable than graphite. However, when the size of a nanoparticle becomes smaller, exfoliation (surface delamination of a diamond) occurs on the surface of the nanodiamond. Verechshagin [6] predicted that the most stable phase of the detonation diamond was 3 nm, and observed nanodiamond below 4 nm at 3000 °C. Barnard et al. [7] investigated the relationship between the size of the nanodiamonds and the phase stability of carbon nanoparticles. At ~ 2.0 nm < D < ~ 2.2 nm, it was confirmed to be bucky-diamond and nanodiamond structure. When ~ 1.7 nm < D < ~ 2.0 nm, it has bucky-diamond and carbon-onions, and when ~ 1.4 nm < D < ~ 1.7 nm, it becomes bucky-diamond and fullerenes structure. Eventually, the fullerene structure becomes the most stable phase after the bucky-nanodiamond phase. However, if (111) is 76 % or more, a core-

shell type structure and if (111) is 76 % or less, a single or double-layer shell is formed. The reason is that the multiple layers play an important role in preventing the sp^3 bonding on the surface of the nanoparticle from relaxing into a shell structure with sp^2 bonding. As such, the surface of nanoparticle is closely related to the size of the nanoparticles.

1.4 Charge induced stabilization on the surface structure of nanodiamond

The presence of atomic hydrogen has been considered to be a crucial factor in the low pressure synthesis of diamond [32-34]. One point of view has claimed that atomic hydrogen etches selectively the nondiamond carbon phase or cleans the growing diamond surface providing reactive sited for further growth. In another point of view, it was suggested that adsorbed hydrogen atoms stabilize the diamond surface over the reconstruction into sp^2-bonded graphitic layers. However, recent reports on the successful synthesis of diamond without atomic hydrogen suggested the existence of an unknown microscopic mechanism [35-36]. The surface of the nanodiamond can be stabilized through charging. Park et al. [37] confirmed that the diamond was more stable than the graphite by increasing the excess charge. Park calculate the charged unit cell without a spurious long-ranged interaction. His model showed the geometry of optimized structure was transformed to a partially graphitized structure. As increasing the numbere of excess electrons in the cluster, the graphite terminated structure becomes less and less favored. Lai et al. [38] studied the surface and structure of bucky-diamonds with increasing charge state.

They suggested that charging of hydrogeneated nanodiamonds could achieve the spontaneous release of atomic hydrogen. Besides, their model showed the charge-induced dehydrogenation. In addition to this, they confirmed that the phase transition from a bucky-diamond to an onion-like structure was dependent on extra charge. Anionic charging saturates dangling bonds of carbon atoms at the surface resulting in the disappearance of reconstructed and graphitized layers at the surface, while cationic charging partly breaks the connection between the core and shell forming a new layer of graphene-like carbons. However, when induced charge in bucky-diamonds approaches the threshold, the coordination and hybridization of the carbon atoms at the interface between shell and core will be greatly altered. Too much charge leads to destruction of individual bucky-diamond upon reaching the mechanical failure limit, which is dependent on both the morphology of the structure and the sign of charge. At this stage, cationic charging breaks the graphene-like surface of bucky-diamonds and results in several fullerenic fragments of graphene nano-flakes. By contrast, anionic charging only removes individual carbon atoms from the surface and leaves an entirely sp^3-hybridised diamond nanoparticle. Charging saturates dangling bonds of carbon atoms at the surface, the disappearance of reconstructed and graphitized layers at the

surface was confirmed.

Chapter. 2 Various allotropes of diamond nanoparticles generated in the gas phase during hot filament chemical vapor deposition (HFCVD)

The nanoparticles were captured on the transmission electron microscope (TEM) grid membrane by a hot filament chemical vapor deposition (HFCVD) and the grid membrane was observed by TEM. I-carbon, hexagonal diamond, and n-diamond and cubic-diamond were identified. To confirm the relationship between the crystallinity of the nanoparticle and process conditions, we analyzed the d-spacing values of the captured nanoparticles. Relative proportion of d-spacing values of captured nanoparticles suggest the coexistence of carbon allotropes at the gas phase in HWCVD. Not only they showed the coexistence of carbon allotropes, but also the crystal structure of carbon allotropes showed size dependence. This is because they have different surface stability depending on the size and shape of the particles. Because the size is very important to stabilize the surface energy, which was related to the graphitization of diamond nanoparticles. Chapter 2 shows observation of various carbon allotropes at 6 process conditions and their size dependence.

2.1 Generation of diamond nanoparticles during HFCVD

Nanodiamonds have been synthesized by using various methods such as laser ablation [40], ion irradiation of graphite [41], detonation [42], plasma-assisted CVD [43], electron irradiation of carbon onions [44], ultrasound cavitation [45] and ball milling of high-pressure/high-temperature diamond [46]. Laser ablation, detonation, and ball milling methods are used commercially, with detonation being the most common approach. Nanodiamonds are applied to medical diagnostics, biological studies and quantum technologies because the optical color-centres in diamond offer well-defined optical transitions and long-lived spin quantum states with stable entanglement [47-49]. However, the nanodiamonds synthesized by detonation method tend to be agglomerated and to include impurity defects, making the difficult for them to be applied to optical applications [50-51].

For applications of nanodiamonds, synthesizing the non-agglomerated high quality nanodiamonds is requied. The generation of non-agglomerated diamond nanoparticles in the gas phase was confirmed under the synthesis condition of diamond films by HFCVD [8]. This result opened the way that non-agglomerated

high quality nanodiamonds can be synthesized using a HFCVD reactor. Here we investigated the crystal structure of nanodiamonds and the relationship between the crystal structure and the processing conditions. For this, by using a capturing apparatus under various processing conditions, nanodiamonds were captured on a graphene membrane of a transmission electron microscope (TEM) grid during HFCVD. The analysis of the nanoparticles by high resolution TEM (HR-TEM) and fast Fourier transformation (FFT) revealed four carbon allotropes: i-carbon, n-diamond, hexagonal diamond, and cubic diamond. The nanoparticles were captured at capture temperatures of 900 °C, 600 °C and 300 °C at the gas mixtures of 1 % CH_4 - 99 % H_2 and at 3 % CH_4 - 97 % H_2. We investigated the size distribution for understanding the relation between the size of nanodiamonds and the crystal structure. Besides, we confirmed that the crystal structure of the nanoparticles was related to the crystal structure of deposited diamond.

2.2 Experimental procedure

Preparation of nanoparticles

The HFCVD reactor with the capturing apparatus is shown schematically in Fig 6. The three 0.5 mmϕ tungsten wires were twisted into a nine-turn coil of 8 mmϕ. The filament temperature was 2100 °C and the process pressure was 20 Torr. By using a mass flow controller, CH_4 and H_2 were supplied as a gas mixture at 1 standard cubic centimeter per minute (sccm) and 99 sccm or at 3 sccm and 97 sccm, respectively.

Capturing the nanoparticles at high temperature such as 900 °C was difficult because of the thermal damage or etching of carbon by atomic hydrogen. Several membranes were tested. For example, the SiO membrane (SiO Type-A, Ted Pella, Inc., Redding, CA, USA) proved very weak to thermal damage above ~ 600 °C. The carbon membrane (ultrathin carbon type-A; Ted Pella, Inc.) was easily etched away at a capture temperature of 900 °C. After many trials, we succeeded in capturing the nanoparticles by using a graphene membrane (6-8 layers of graphene film; Ted Pella, Inc.), as it can withstand thermal damage during the capture time of 10 s.

The capturing apparatus could be pushed to the capture zone as needed and pulled toward the chamber wall. The distance between

the capture zone and the capture temperature was apart from 6 mm, 30 mm and 50 mm, where the temperature of the capture zone was, respectively, 900 ± 50 °C, 600 ± 50 °C and 300 ± 50 °C. Before capturing process, the filament was carburized at 2100 °C for 24 hrs at 1 % CH_4 – 99 % and at 3 % CH_4 – 97 % H_2, respectively. After supplying the gas mixture of CH_4 and H_2 for 30 min, capturing was done at the filament temperature of 2100 °C. The quartz holder loaded with the TEM grid was pushed to the capture zone, and the grid was exposed for 10 s. After that, the quartz holder was pulled toward the chamber wall. Captured nanoparticles were analyzed by HR-TEM (JEM-2100F; JEOL Ltd., Tokyo, Japan).

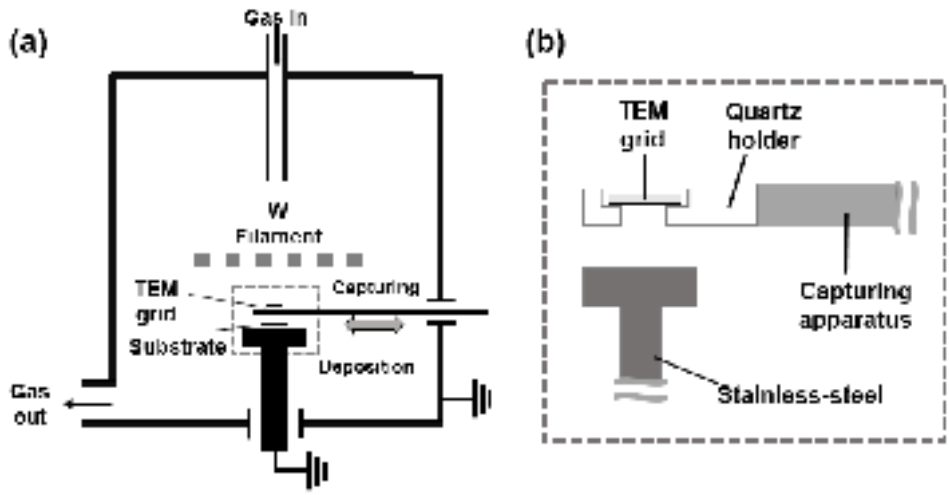

Fig. 6. Schematics of (a) the HFCVD system with the capturing apparatus for capturing nanoparticles on the TEM membrane and (b) the capturing apparatus.

Indexing of nanoparticles

Even though some nanoparticles were polycrystalline or aggregated, most of them were single crystals. From the FFT image of each nanoparticle, d-spacings and the angles were determined. Joint Committee on Powder Diffraction Standards (JCPDS) data of the reported carbon allotropes were used to create unit cells of various carbon allotropes for the indexing of nanoparticles. We encountered two difficulties in identifying the phase of single-crystalline carbon nanoparticles. The first was the coexistence of various carbon allotropes, and the second was that those carbon allotropes showed the similar d-spacing values. As a result, several d-spacings and lattice angles of the carbon allotropes needed to be classified. In total of ~ 600 nanoparticles were chosen to determine the size and d-spacing by DigitalMicrograph (Gatan, Inc., Pleasanton, CA, USA) at 6 conditions of the capture temperature of 900 ^{o}C, 600 ^{o}C and 300 ^{o}C and the gas mixtures of 1 % CH_4 - 99 % H_2 and 3 % CH_4 - 97 % H_2. 900 d-spacings were obtained from ~ 600 nanoparticles. The d-spacings were classified from JCPDS of the reported various carbon allotropes. We used lattice angles of the reported carbon structures, from i-carbon to cubic diamond, to identify the crystal structure of individual nanoparticles.

Current measurement

We measured the current between the substrate and the ground, which would represent the density of electrons emitted from the hot filament. The feedthrough, which was connected to the picoammeter (model 6487; Keithley Instruments, Cleveland, OH, USA), was apart from the 30 mm below the filament. The number density of captured nanoparticles was measured by ImageJ software (ImageJ, National Institutes of Health, Bethesda, MD, USA).

Deposition of diamond particles

n-Diamond and cubic diamond were dominant in the gas mixture of 1 % CH_4 - 99 % H_2, whereas nanoparticles of i-carbon allotropes were dominant in the gas mixture of 3 % CH_4 - 97 % H_2. The morphology of diamond particles would be affected by the crystal structure of the nanoparticles. To study this, diamond particles were deposited for 8 h on Si substrates under substrate temperature and filament of 900 ^{o}C and 2100 ^{o}C, respectively. To observe diamond particles, the Si substrate was not pretreated because the pretreatment tends to produce diamond films. The Si substrate was apart from 6 mm below the hot filament. The microstructure of the diamond particles was observed by field-emission scanning electron microscopy (FE-SEM; SU70; Hitachi Ltd., Tokyo, Japan).

2.3 Result & Discussion

Identification of nanoparticles

We analyzed ~ 600 captured nanoparticles and could identify 4 kinds of carbon allotropes: i-carbon, n-diamond, hexagonal diamond and cubic diamond. For example, Fig. 7 (a) shows a TEM image of nanoparticles on the graphene membrane of the Cu grid for a capture time of 10 s and at a gas mixture of 1 % CH_4 - 99 % H_2 at capture temperature of 900 ^oC, using a filament temperature of 2100 ^oC. Fig. 7 (a) shows that 2 ~ 7 nm nanoparticles are randomly distributed on the membrane. In Fig. 7 (b), the HRTEM image shows the magnified image of the white square in Fig. 7 (a). Fig 7(c) is the magnified image of the nanoparticle in the white circle of Fig 7 (b), showing the lattice image of the nanoparticle with a diameter of ~ 5 nm. The FFT image obtained from the nanoparticle in Fig. 7 (c) is shown in Fig. 7 (d). The FFT image in Fig 7 (d) indicated that the nanoparticle has an n-diamond structure with the (200) forbidden plane. This is the way how to identify and classify the observed nanoparticles.

To index the phase of the observed nanoparticles, the reported values of carbon allotropes were compared with both d-spacings

and lattice angles determined from the FFT image. The observed nanoparticles were classified into four carbon allotropes: i-carbon, n-diamond, hexagonal diamond, and cubic diamond, as shown in Fig. 8, respectively. The nanoparticle in Fig. 8 (a) was captured for 10 s at the capture temperature of 900 °C with the filament temperature of 2100 °C and gas mixture of 3 % CH_4 - 97 % H_2. The FFT image in Fig. 8 (a) shows the cubic phase diamond along the <110> zone axis. Vora et al. [52] investigated an i-carbon film containing an unknown cubic phase having a lattice parameter of 4.25 Å. They confirmed that d-spacings of 2.43 and 2.12 Å of the phase were assigned to the (111) and (200) planes, respectively. This crystal structure is called i-carbon [53-55]. D-spacings of 2.42 and 2.10 Å in Fig. 8 (a) were assigned, respectively, to the (111) and (200) planes of the cubic phase with a lattice parameter 4.2 Å, which are nearly similar with the lattice parameter reported by Vora et al. [52]. We observed i-carbon nanoparticles had a d-spacing range of 2.36 - 2.54 Å. From the observed d-spacings, we measured the variation in the lattice parameter over the range of 4.1-4.4 Å. In addition to these, the lattice angles of 54° and 70° shown in Fig. 8 (a), which are between the (111) and (200) planes and between the two (111) planes, respectively, matched with those of i-carbon.

The nanoparticle in Fig. 8 (b) was captured at capture temperature of 300 °C with the filament temperature of 2100 °C and the gas mixture of 1 % CH_4 – 99 % H_2. The FFT image in Fig 8. (b) shows the hexagonal diamond phase along the <100> zone axis. HR–TEM and FFT images show the (100), (002), and (102) lattice planes of hexagonal diamond. The lattice angles of 43° and 90° in Fig 8 (b), which are between the (002) and (102) planes and between the (100) and (002) planes, respectively, matched those of a hexagonal diamond structure (JCPDS No.19–0268).

The conditions of the nanoparticle shown in Fig. 8 (c) were the same as those in Fig. 8 (a). The FFT image in Fig 8 (c) includes n–diamond phase along the <110> zone axis. HR–TEM and FFT images display the (111) and (200) lattice planes of n–diamond. The (200) plane is forbidden plane which was not observed in the cubic diamond. The lattice angles of 54° and 70° in Fig 8c, which are between the (111) and (200) planes and between two (111) planes, respectively, matched those of n–diamond (JCPDS No.43–1104).

The nanoparticle in Fig. 8 (d) was captured at 900 °C with the filament temperature of 2100 °C and the gas mixture of 1 % CH_4 – 99 % H_2. The FFT image in Fig 8 (d) shows a cubic diamond phase

along the <110> zone axis and the two (111) planes and the (220) plane of cubic diamond (Fd3m). HR-TEM and FFT images show d-spacings of 2.06 and 1.25 Å, which correspond to the (111) and (220) planes of cubic diamond, respectively. The lattice angles of 35° and 70° in Fig. 8 (a), which are between the (111) and (220) planes and between the two (111) planes, respectively, match with those of cubic diamond (JCPDS No.6-0675).

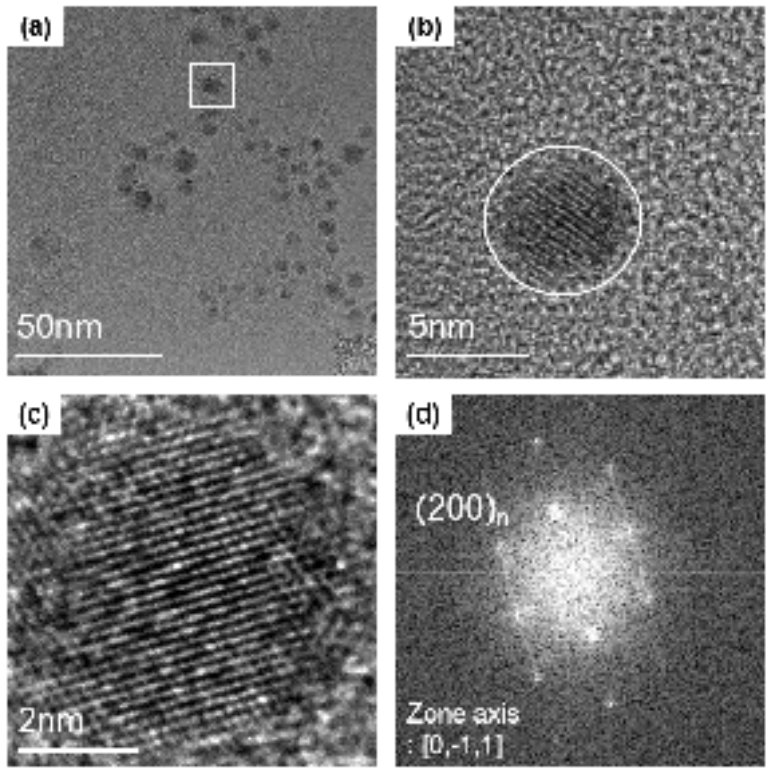

Fig. 7. (a) TEM image of nanoparticles captured on the TEM membrane of the Cu grid with a capture time of 10 s, (b) HRTEM image of the white square in (a), (c) a higher magnification of the nanoparticle in the white circle of (b) and (d) the FFT image obtained from the Fig. 7. (c).

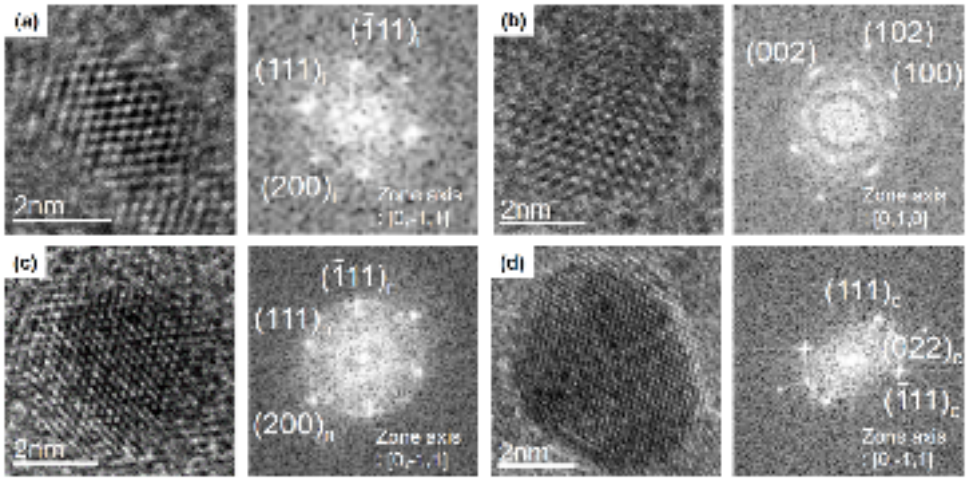

Fig. 8. HRTEM and FFT images of four carbon allotropes. (a) i-carbon at the gas mixture of 3 % CH_4 - 97 % H_2, (b) hexagonal diamond at the gas mixture of 1 % CH_4 - 99 % H_2, (c) n-diamond at the gas mixture of 3 % CH_4 - 97 % H_2, and (d) cubic diamond at the gas mixture of 1 % CH_4 - 99 % H_2.

Captured nanoparticles under various processing conditions

The dependence of the crystal structure of captured nanoparticles on the capture temperature and the methane concentration was investigated by analyzing the crystal structure of the captured nanoparticles at 900 °C, 600 °C and 300 °C on the gas mixture of 1 % CH_4 – 99 % H_2 and 3 % CH_4 – 97 % H_2. Fig. 9 (a–c) and (d–f) show the number of nanoparticles with observed d–spacing values of the captured nanoparticles, respectively, which were captured at 1 % CH_4 – 99 % H_2 and 3 % CH_4 – 97 % H_2 at the filament temperature of 2100 °C. Fig. 9 shows 150 d–spacing values out of ~ 100 nanoparticles for each membrane. The number of the d–spacing values in Fig. 9 would be related to the XRD relative intensity of the polycrystal of various carbon allotropes. The number of the d–spacing values could be used to estimate the fraction of the phase of the nanoparticles. By using the reported values for the carbon allotrope in JCPDS, we classified the observed d–spacing values. We made an ~ 3 % approximation to correspond to carbon allotropes of JCPDS.

In Fig. 9 (a), nanoparticles, captured at 900 °C and the gas mixture was 1 % CH_4 – 99 % H_2, show the number of 1 for 2.42 Å

and the number of 97 for 2.06 Å. In addition, in Fig 9 (c), nanoparticles captured at 300 °C show the number of 39 for 2.42 Å and the number of 60 for 2.06 Å. However, in Fig. 9 (d), nanoparticles, captured at 900 °C and the gas mixture was 3 % CH_4 – 97 % H_2, show the number frequency of 78 for 2.42 Å and the number frequency of 35 for 2.06 Å. On the other hand, in Fig 9 (f), nanoparticles captured at 300 °C show the number of 55 for 2.42 Å and the number frequency of 54 for 2.06 Å. The number of nanoparticles for 2.06 Å at 1 % CH_4 – 99 % H_2 in Fig. 9 (a–c) is larger than that at 3 % CH_4 – 97 % H_2 in Fig 9 (d–f) at all capture temperatures.

Based on the tendency of the d–spacing values, we confirmed that the fraction of the carbon allotropes was depended on the temperature of capture zone. At the gas mixture of 1 % CH_4 – 99 % H_2, the number of nanoparticles with 2.06 Å increases as the capture temperature increases. However, at the gas mixture of 3% CH_4 – 97 % H_2, the number of nanoparticles with 2.06 Å decreases as the capture temperature increases. Fig. 9 (a–c) shows that the number of cubic diamond and n–diamond increase as the capture temperature increases from 300 °C to 900 °C at the gas mixture of 1 % CH_4 – 99 % H_2. However, Fig 9 (d–f) shows that the number of

captured i-carbon nanoparticles increases as the capture temperature increases from 300 °C to 900 °C at the gas mixture of 3 % CH_4 - 97 % H_2.

Table 1 shows the comparison the observed d-spacing values and those reported values for cubic diamond, n-diamond, hexagonal diamond, and i-carbon. The XRD relative intensity (I/I_{111}) of various carbon allotropes is shown in Table 1. For n-diamond by H. Vora model, the XRD relative intensities of (111) and (200) are 100 and 100, respectively, whereas for cubic diamond, the corresponding intensities are 100 and 0, respectively. As mentioned above, the experimentally observed d-spacing of forbidden plane (200) indicates the existence of n-diamond. If nanoparticles show a high fraction of the number of (111) plane but none of (200) plane in FFT images, then it implies that most of the observed nanoparticles would mainly consist of cubic diamond. Although the ratio of the relative XRD intensity of (111) to (200) was 1 for the reported n-diamond in Table 1, the observed number of d-spacing ratio of (111) to (200) shown in Fig 9 (a) was 5. The d-spacing ratio of the observed nanoparticles, which were captured at 900 °C with the filament temperature of 2100 °C and the gas mixture of 1 % CH_4 - 99 % H_2, was five-fold larger than the ratio of the XRD

relative intensities. This result shows that the nanoparticles captured at capture temperature of 900 °C in Fig 9 (a) would mainly consist of cubic diamond rather than that of n-diamond.

The d-spacing of 2.42 Å belongs to i-carbon whereas the d-spacing of 2.06 Å belongs to cubic diamond, n-diamond, hexagonal diamond, and some of i-carbon. Therefore, the larger number of 2.06 Å than that of 2.42 Å indicates that cubic diamond, n-diamond, and hexagonal diamond is a major phase with i-carbon being a minor phase. To understand the relationship between the observed 2.06 Å and the number of i-carbon, we should compare the data in Fig. 9 (a) and (b). Because If i-carbon had a high relative intensity of 2.42 Å, then we should count a 2.42 Å in Fig. 9 (a). But the number of 2.42 Å was not rarely observed in that capture condition, which implies that the 2.42 Å would be obtained from not i-carbon but the cubic diamond, hexagonal diamond, and n-diamond. Similarly, the lower fraction of 2.06 Å than that of 2.42 Å indicates that i-carbon is a major phase with cubic diamond or n-diamond being a minor phase. Fig. 9 shows that the observed number of a 2.06 Å d-spacing for 1 % CH_4 - 99 % H_2 was much larger than that for 3 % CH_4 - 97 % H_2. Additionally, the number of observed nanoparticles for the 2.42 Å d-spacing, which was very high

fraction for 3 % CH_4 – 97 % H_2, is highly related to i–carbon. Thus, the nanoparticles for 3 % CH_4 – 97 % H_2 consisted mainly of i–carbon, whereas those for 1 % CH_4 – 99 % H_2 consisted mainly of cubic diamond, n–diamond, and hexagonal diamond.

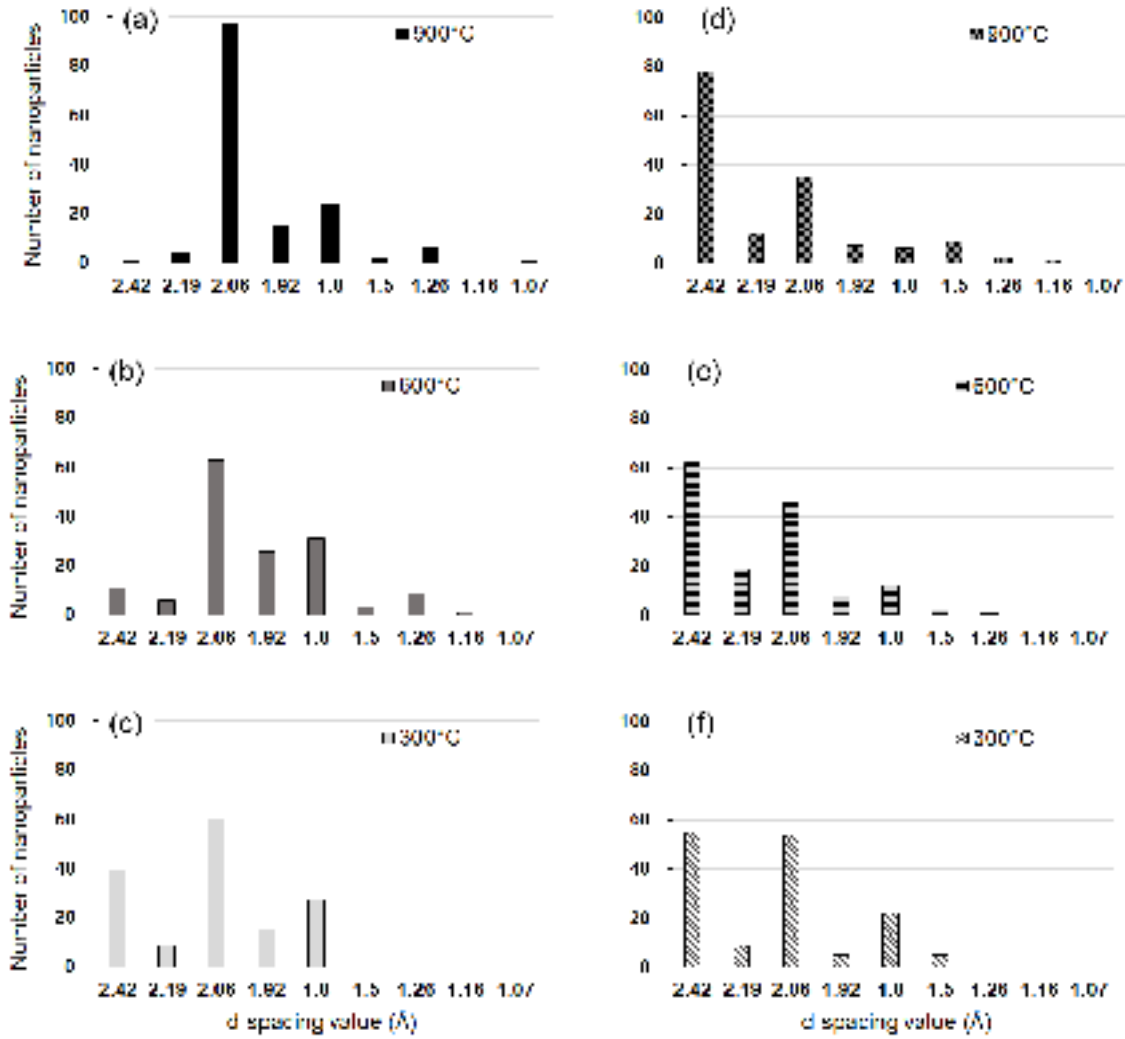

Fig. 9. The number of nanoparticles with the d−spacing values obtained from 150 d−spacing values of ~ 100 nanoparticles captured at the gas mixture of (a) 1 % CH_4 – 99 % H_2 and at capture temperature of 900 °C, (b) at the gas mixture of 1 % CH_4 – 99 % H_2 and at capture temperature of 600 °C, (c) at the gas mixture of 1 % CH_4 – 99 % H_2 and 300 °C, (d) at the gas mixture of

3 % CH_4 – 97 % H_2 and 900 °C, (e) at the gas mixture of 3 % CH_4 – 97 % H_2 and at capture temperature of 600 °C, and (f) at the gas mixture of 3 % CH_4 – 97 % H_2 and at capture temperature of 300 °C.

Table 1. The experimentally observed d-spacing values with those for four carbon allotropes such as cubic diamond, n-diamond, hexagonal diamond, and i-carbon.

Cubic-diamond (observed)		Cubic diamond (JCPDS#6-0675)			n-Diamond (observed)		n-Diamond (JCPDS#43-1104)			Hexagonal diamond (observed)		Hexagonal diamond (JCPDS#19-0268)			i-Carbon (observed)		i-Carbon [ref. 52]	
d (Å)	hkl	d (Å)	hkl	I/I_{max}	d (Å)	hkl	d (Å)	hkl	I/I_{max}	d (Å)	hkl	d (Å)	hkl	I/I_{max}	d (Å)	hkl	d (Å)	hkl
										2.18	100	2.18	100	100	2.48	111	2.48	111
2.06	111	2.06	111	100	2.06	110	2.06	111	100	2.06	002	2.06	002	100	2.10	200	2.12	200
										1.93	101	1.93	101	50				
					1.78	200*	1.78	200*	100						1.78	211	1.74	211
										1.50	102	1.50	102	25	1.47	220	1.50	220
1.26	220	1.26	220	25	1.26	220	1.26	220	100			1.26	110	75			1.26	311
												1.16	103	50				
												1.09	020	50				
		1.07	311	10			1.07	311	100			1.07	112					

* Forbidden reflections in Fd3m

Size dependence on the crystal structure of nanoparticles

In Fig. 10, the TEM images of nanoparticles captured under 6 different conditions shows the nanoparticles were randomly distributed on the membranes. 6 different conditions were at capture temperature of 900 °C, 600 °C and 300 °C at the gas mixture of 1 % CH_4 – 99 % H_2 and 3 % CH_4 – 97 % H_2, respectively. At the gas mixture of 1 % CH_4 – 99 % H_2, there was a tendency that the average size of nanoparticles in Fig 10 (a–c) decreases with decreasing capturing temperature. On the other hand, at the gas mixture of 3 % CH_4 – 97 % H_2, there was a tendency that the average size of nanoparticles in Fig 10 (d–f) increases with decreasing capturing temperature from 900 °C to 300 °C. To make a more quantitative analysis of the size, the size distribution of the nanoparticles was measured from the observed TEM image.

In Fig. 11, the size distributions were measured from 100 nanoparticles for each condition. At a gas mixture of 1 % CH_4 – 99 % H_2, when the temperature of capture zone decreased from 900 °C to 300 °C, the average size of the nanoparticles decreased from ~ 4.5 nm to ~ 3.2 nm. At 3 % CH_4 – 97 % H_2, however, when the temperature of capture zone was decreased from 900 °C to 300 °C,

the average size of the nanoparticles increased from ~ 3.1 nm to ~ 3.8 nm. The average size of the nanoparticles which show 2.42 Å was ~ 3 nm regardless of the methane concentration and the capture temperature.

By comparing Fig. 9 with Fig. 11, it can be said that the average size of nanoparticles has a higher correlation with the number of 2.06 Å than with the capture temperature. In other words, there is a high correlation that the larger the size the larger the number of cubic diamond, n-diamond, and hexagonal diamond and the smaller the size the larger the number of i-carbon. This result implies the possibility that the stability of the crystal structure of nanodiamonds should depend on the size.

Considering this possibility, we made a literature survey on the dependence of the stability of nanodiamonds on the size. As the size of nanodiamond decreases, the phase stability of the nanodiamond also changes, and the nanodiamond becomes a more stable structure than the graphite phase. [7, 39] From the results, the crystal structure of the nanoparticles would be related to the size of nanoparticles. According to a previous study on the size of nanoparticles produced in the gas phase of a HFCVD diamond process via a Wien filter using differential pumping, the

nanoparticles contained only ~ 250 carbon atoms at 1.5 % CH_4 – 98.5 % H_2 [26]. These nanoparticles would be primary nanoparticles. The nanoparticles in Fig 10 are expected to form by coalescence of primary nanoparticles. Because the size of the nanoparticle was depended on the capturing time. [8]

The question is then cubic diamond, n-diamond, and hexagonal nanoparticles more prevalent with 1 % CH_4 – 99 % H_2? Moreover, why are i-carbon nanoparticles mainly formed with 3 % CH_4 – 97 % H_2? Previously, Hwang et al. [9] suggested that the diamond nanoparticles is stabilized by the negative charge. To compare the amount of electrons at the gas phase between the gas mixtures of 1 % CH_4 – 99 % H_2 and 3 % CH_4 – 97 % H_2, we measured the current at the location 30 mm away from the hot filament at filament temperature of 2100 °C using the gas mixtures of 1 % CH_4 – 99 % H_2 and 3 % CH_4 – 97 % H_2. At the gas mixture of 1 % CH_4 – 99 % H_2, The current was −24.9 μA/cm^2, which was almost three-fold larger than that of −8.3 μA/cm^2 measured with 3 % CH_4 – 97 % H_2. The thermionic emission depends on the work function of the surface of the hot filament. If the filament is coated with graphite, which is shown by the phase diagram calculated by Thermo-Calc [56] to occur at 3% CH4-97% H2, the filament surface changes

from tungsten carbide to graphite. Under these conditions, the work function of the filament surface would increase from 3.6 eV for tungsten carbide [57] to 4.8 eV for graphite [58], which could explain the three-fold discrepancy in the current readings. A relative deficiency in electrons at 3 % CH_4 - 97 % H_2 would likely induce the sp^2 bond of i-carbon. On the other hand, relatively abundant electrons at 1 % CH_4 - 99 % H_2 would tend to stabilize the sp^3 bond of nanodiamond, which would result in cubic diamond or n-diamond. [37-38].

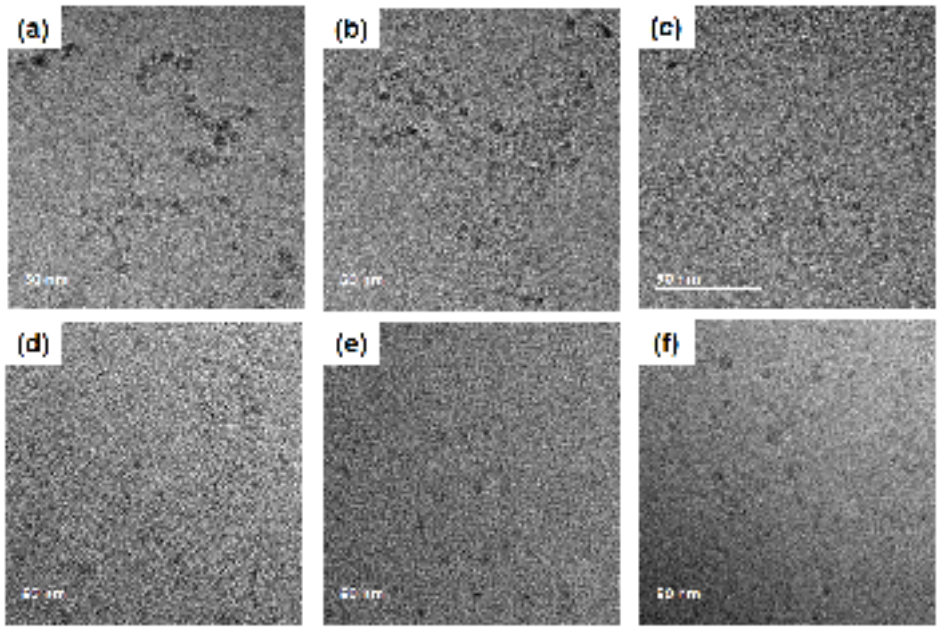

Fig. 10. HRTEM images of nanoparticles captured at the gas mixture of 1 % CH_4 – 99 % H_2 at the capture temperature of (a) 900 °C, (b) 600 °C, (c) 300 °C and at the gas mixture of 3 % CH_4 – 97 % H_2 at the capture temperature of (d) 900 °C, (e) 600 °C, and (f) 300 °C.

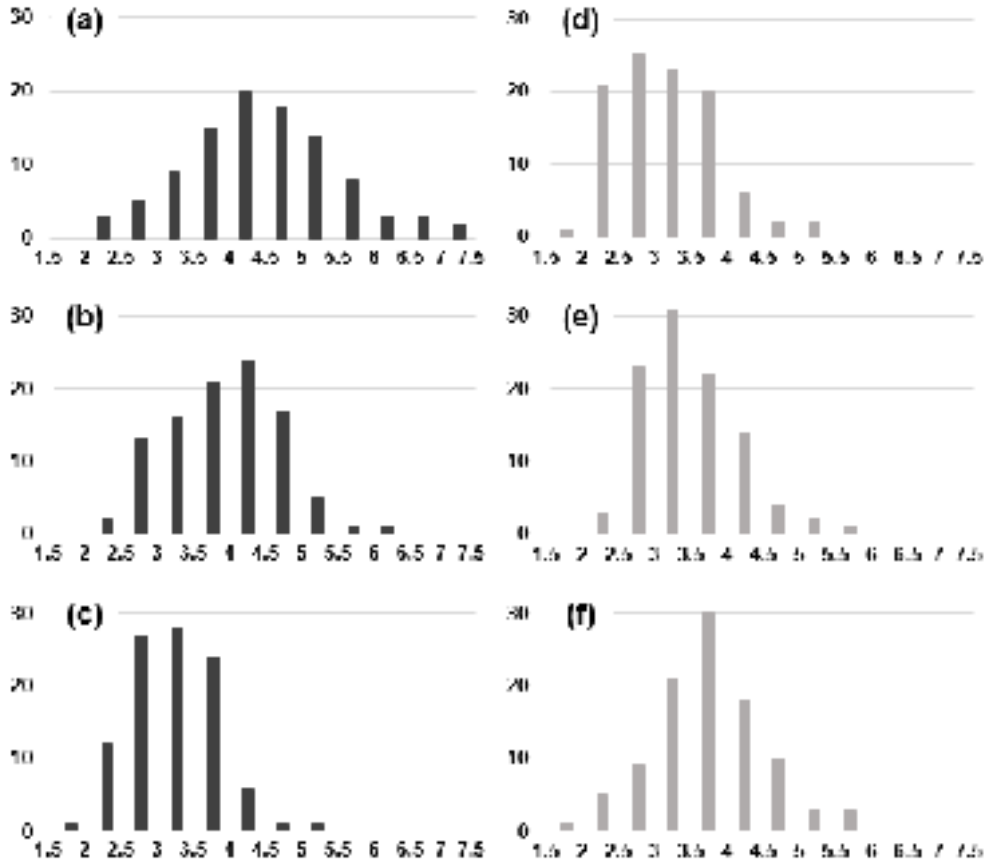

Fig. 11. Distributions of the size of 100 captured nanoparticles captured at the gas mixture of 1 % CH_4 – 99 % H_2 at the capture temperature of (a) 900 °C, (b) 600 °C and (c) 300 °C and captured at the gas mixture of 3 % CH_4 – 97 % H_2 at the capture temperature of (d) 900 °C, (e) 600 °C and (f) 300 °C.

Diamond nanoparticles at the capture temperature of 300 °C

The other parameter, which is related to the size, is the temperature. The size of a nanodiamonds that become stabilization depends on the temperature. At 25 °C, the particle size that becomes the crossing point between the diamond structure and the graphite structure is 10.2 nm, but at 800 °C, it exists at 4.8 nm. And the phase transition from diamond to graphite depends not only on the difference in free energies of the phase but also on the activation energy of the phase transition. As the size decreased, the activation energy would decrease, and the phase transition temperature from diamond to graphite would decrease. Size effects may cause graphitization to become more desirable with smaller nanodiamonds. However, Gamarnik [39] did not reveal the energetic preferences for graphitization to occur better with smaller diamonds. Because when he annealed the nanodiamonds, a coalescence of nanoparticles accompanied.

However, in the capture experiment, it was an appropriate experiment to confirm this because the nanoparticles were captured for a sufficiently short time before annealing occurred. The average

size of the nanodiamonds at a methane concentration of 1 % and a capture temperature of 900 °C is ~ 4.8 nm. A direct comparison between experimental results and computational analysis [39] is difficult. However, one possibility that differs from the calculation results is that the surface of the membrane does not reach 900 °C during the capture process, so larger diamond nanoparticles may be present.

From a thermodynamic perspective, deposition and etching are opposite irreversible processes and cannot occur simultaneously. The driving force may be deposition only or etching only. If the driving force is for irreversible etching of stable graphite, it must be for irreversible etching of less stable diamond. At 1 % CH_4 – 99 % H_2, carbon rapidly stabilizes the gas phase at around 500 °C, and at 3 % CH_4 – 97 % H_2, the gas phase becomes stable at slightly lower temperatures. And at 300 °C, the gas phase of both 1 % CH_4 – 99 % H_2 and 3 % CH_4 – 97 % H_2 becomes stable. [59–60] And diamonds synthesized by CVD are formed relatively easily on a graphite surface [61]. The viewpoint of the atomic growth unit, graphite is the most disadvantageous substrate for the diamond growth because graphite is no additional barrier for nucleation. Besides, the growth barrier of graphite would be much smaller than the

nucleation barrier of diamonds on graphite. Thermodynamically, capturing the nanodiamond on a carbon membrane at capture temperature of 300 °C is contrary to the thermodynamic result and Yarbroug's claim, which the atom was the deposition unit. [22] For these reasons, pre-existing diamond clusters in the gas phase land on the graphite substrate should be assumed to explain this phenomenon.

Although hydrogen etching effect can be beneficial in decreasing cluster size, an electric charge instead of hydrogen is necessary for the low-pressure synthesis of diamond. Palnichenko et al. [62] succeeded in diamond synthesis by applying electric pulse discharge using high purity graphitic electrodes in a helium gas environment, and Yoshimoto et al. [63] synthesized diamond in laser ablation in a hydrogen-free environment. Gruen et al. [64] synthesized diamond nanostructure by a discharge of C_{60} in Ar plasma without hydrogen or oxygen. The above results experimentally support that the charge is related to the stabilization of diamonds in the absence of hydrogen. A charge is related to the stability of carbon and has two major effects in gas phase nucleation. The first is that charge interferes with brownie coagulation between clusters. Charged clusters can maintain nanometer-size because

coagulation is disturbed. [24, 65] The second effect is to form an electrical double layer on the cluster surface. So the diamond clusters retain dielectric diamond clusters rather than conducting graphite clusters. [66] Glasner and Sunagawa [67–71] confirmed that high capillary pressure increases diamond stability. Furthermore, it was considered that a strong ion–induced dipole interaction for the dielectric diamond cluster was created. Therefore, the phenomenon that stable graphite etching and metastable diamond deposition simultaneously occur is explained as the formation of charged nanoparticles in the gas phase due to the charge effect.

It can be seen that the nanoparticles generated in the gas phase are falling from a high temperature to low temperature as they move away from the filament. The average size decreases as the temperature decreases from 900 °C to 300 °C at 1 % CH_4 – 99 % H_2, whereas the average nanoparticle size increases at 3 % CH_4 – 97 % H_2. This cannot be explained from a conventional thermodynamic point of view. We would suppose that charged particles are produced in the gas phase. The reason that the size of the nanoparticles increases as the capture temperature decreases under the condition of 3 % CH_4 – 97 % H_2 maybe that coalescence

occurs between the particles while the nanoparticles go from high temperature (6mm distance from the filament) to low temperature (30mm distance from the filament). The reason for this possibility is that the Coulomb repulsion between nanoparticles is weak because there are not enough electrons in the gas phase of 3 % CH_4 – 97 % H_2. On the other hand, at 1 % methane concentration, the size of the nanoparticles decreases as the capture temperature goes down from 900 °C to 300 °C. Because the amount of free electrons in the gas phase is large, the nanoparticles are charged. As a result, the Coulomb repulsion prevents coalescence between the nanoparticles. In the meantime, atomic etching occurs because the driving force of atomic etching is increasing thermodynamically. So, as the capture position is lowered, the particle size is getting smaller at around 300 °C.

In Fig. 10, at the gas mixture of 1 % CH_4 – 99 % H_2, the number of nanoparticles increases from 163 to 508 per 1000nm^2 as the capture temperature decreases from 900 °C to 300 °C, while at the gas mixture 3 % CH_4 – 97 % H_2, as the capture temperature decreases from 900 °C to 300 °C, the number of nanoparticles decreases from 147 to 77 per 1000nm^2. The decrease in the number of nanoparticles as the capture temperature decreases is

explained by thermodynamically atomic etching. However, as the capture temperature decreases, the increase in the number of captured nanoparticles is not explained by this.

There are two possibilities. The first is that as the capture position moves away from the filament, the amount of electrons decreases, so the amount of charge on the membrane decreases, and more charged nanoparticles are captured. Table 6 shows that the amount of electrons is less at the gas mixture of 3 % CH_4 – 97 % H_2 than at the gas mixture of 1 % CH_4 – 99 % H_2. However, the amount of precursor is higher at 3 % CH_4 – 97 % H_2 than at 1 % CH_4 – 99 % H_2. So, a charge state per nanoparticle at the gas mixture 1 % CH_4 – 99 % H_2 might be higher than at the gas mixture 3 % CH_4 – 97 % H_2. If nanoparticles had a high charge state, they would close to the cubic structure diamond. Diamond is not atomically etched compared to graphite. So the nanoparticles at the gas mixture 1 % CH_4 – 99 % H_2 might not be easily etched. In this case, if there are few electrons in the membrane, many nanoparticles may be captured at the gas mixture 1 % CH_4 – 99 % H_2. On the other hand, due to atomic etching, few nanoparticles may be captured at the gas mixture 3 % CH_4 – 97 % H_2.

The second possibility is that multiply charged nanoparticles might have a charge distribution in HWCVD. Blažek et al. [72] investigated the time fluctuation of charge on an individual cluster by using the MC simulation. In the case of the HWCVD, due to thermionic emission from the hot-filament, free electrons are emitted and existed at the gas phase. The charge state of nanoparticles and carbon radicals depends on time and electron density in the gas phase. If carbon radicals can maintain a sufficiently high charge state even away from the filament, ion induced nucleation may occur and the nanoparticle with high charging state might not be etched by atomic hydrogen. However, nanoparticles with a stochastically low charge state might be atomically etching. In this case, atomic etching and ion-induced nucleation may occur simultaneously. If this is true, the charged particle theory with the quantum mechanical approach would explain the unsolved classical perspective in crystal growth.

Comparing the captured nanoparticles and deposited diamond

To compare deposition behavior between the gas mixtures of 1 % CH_4 – 99 % H_2 and 3 % CH_4 – 97 % H_2, a bare Si substrate without the pretreatment was used for deposition at 900 °C for 8 h under the same processing conditions as those under which the nanoparticles were captured. Fig. 12 shows SEM images of diamond particles deposited on the Si substrate. Since the Si substrate was not pretreated, diamond particles instead of films were grown even after deposition for 8 h. The diamond particles deposited using the gas mixture of 1 % CH_4 – 99 % H_2 are shown in Fig. 12 (a) with successively higher magnification images shown in Fig. 12 (b–c). The diamond particles deposited using the gas mixture of 3 % CH_4 – 97 % H_2 are shown in Fig. 12 (d), with a higher magnification image shown in Fig. 12 (e) and an even higher one shown in Fig. 12 (f).

The diamond particles in Fig. 12 (a–c) show well–developed (100) facets, whereas those in Fig. 12 (d–f) show ball–like or cauliflower–like structures with numerous nanosized nodules on the surfaces. The particle size in Fig. 12 (b) is smaller than that shown in Fig. 12 (e). When comparing the crystal structures of captured nanoparticles and diamond particles deposited for 8 h, the

nanoparticles captured at 1 % CH_4 – 99 % H_2 were grown as well-faceted diamond particles, whereas the nanoparticles at 3 % CH_4 – 97 % H_2 were grown as cauliflower diamond particles. These results suggest that the crystal structure of the nanoparticle affects the crystal structure of the deposited diamond.

In Fig. 13 (c-d), thin-film at the gas mixture of 3 % CH_4 – 97 % H_2 hardly grew compared to the gas mixture of 1 % CH_4 – 99 % H_2 thin film. Compared to the amount of precipitation, this is the very opposite result. This phenomenon can be interpreted that graphite is more easily etched by atomic hydrogen than diamond. [73] When comparing the Raman results (Fig. 14 (a-b)), the value of I_D/I_G is greater at 1 % CH_4 – 99 % H_2. This tells us that a thin film deposited at 3 % CH_4 – 97 % H_2 has a more graphitic structure and explains that etching occurs more easily at 3 % CH_4 – 97 % H_2. In the case of a thin-film deposited at a concentration of 1 % CH_4 – 99 % H_2, it can be seen that the thin-film was thickly grown, which shows that etching is not easily performed. When comparing the relationship between the crystallinity of the captured nanoparticles and the thin-film, Fig. 9 (a) shows that the nanoparticles captured at 1 % CH_4 – 99 % H_2 and a capture temperature of 900 °C mainly have 2.06 Å. Due to a property of diamond-like structure, it seems

that these nanoparticles are involved in thin-film growth where etching does not occur easily. On the other hand, at 3 % CH_4 - 97 % H_2, the nanoparticles, which were related with 2.52~2.40 Å, would be involved in thin-films growth where etching occur easily.

Fujita [74-75] proposed that large nanoparticles grow non-epitaxial particles, whereas small nanoparticles grow epitaxial particles because they have like-liquid property. Particles with liquid-like properties are called magic size small clusters and have a magic-size of 1 to 2 nm. The smaller it grows epitaxially, this makes well-defined facets. And large clusters make secondary nuclei on a growing surface and grow in cauliflower form. According to Iijima [76], as the size increases, the liquid-like property is lost. Jeon [25] confirmed the nanodiamond particle size using an ion mobility analyzer in HWCVD. In the 3 % CH_4 - 97 % H_2condition, the nanoparticle size is large, so it loses the liquid-like property and has a cauliflower form. In the 1 % methane concentration condition, the size is small and has a liquid-like property. However, this result presents a different possibility from the previous results. In this result, it was confirmed that the average size of nanoparticles at 3 % CH_4 -97 % H_2 and the capture temperature of 900 °C is smaller than the average size of nanoparticles at 1 % CH_4

– 99 % H_2 and the capture temperature of 900 °C. In Fig. 13 (c–b), respectively, the facet diamond film was grown at 1 % CH_4 – 99 % H_2 and the cauliflower structure was grown at 3 % CH_4 – 97 % H_2. So, these results would suggest that even if the nanoparticle size is small, there is a possibility that the crystallinity of the nanoparticle affects the crystallinity of the diamond.

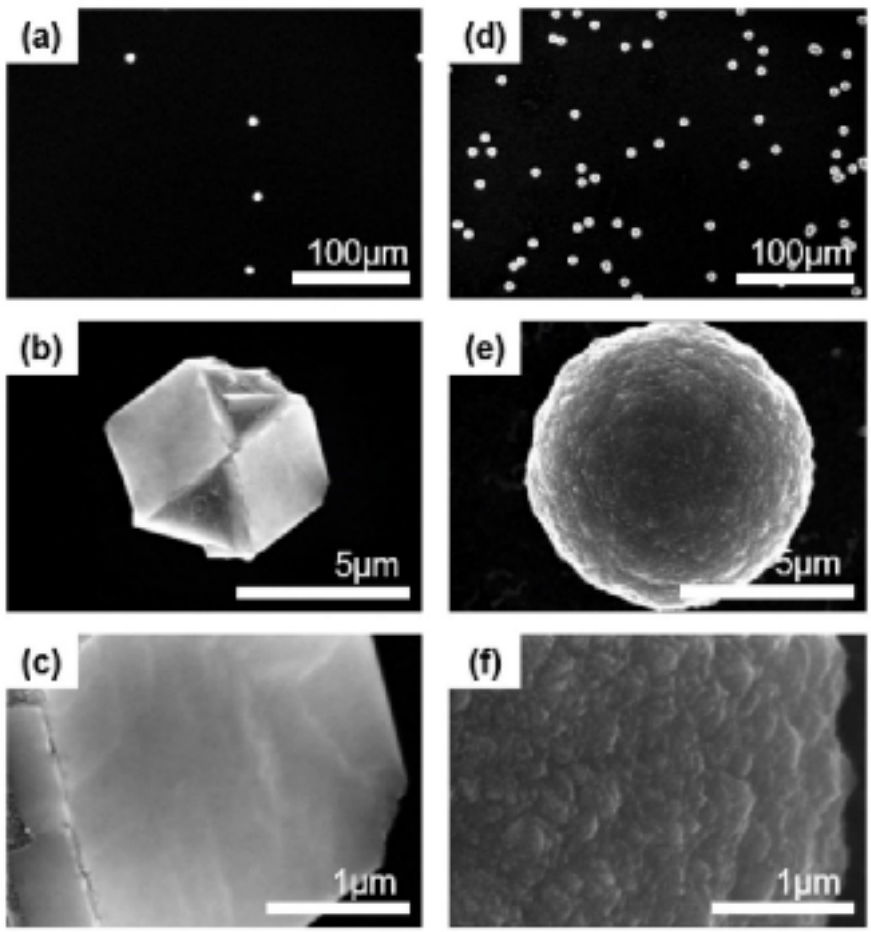

Fig 12. FESEM images of diamond particles deposited at the gas mixture of (a) 1 % CH_4 – 99 % H_2 and (d) 3 % CH_4 –97 % H_2 for deposition time of 8 h on the bare silicon substrate. (b) and (e) are the higher magnification of (a) and (d), respectively, and (c) and (f) are the higher magnification of (b) and (e), respectively.

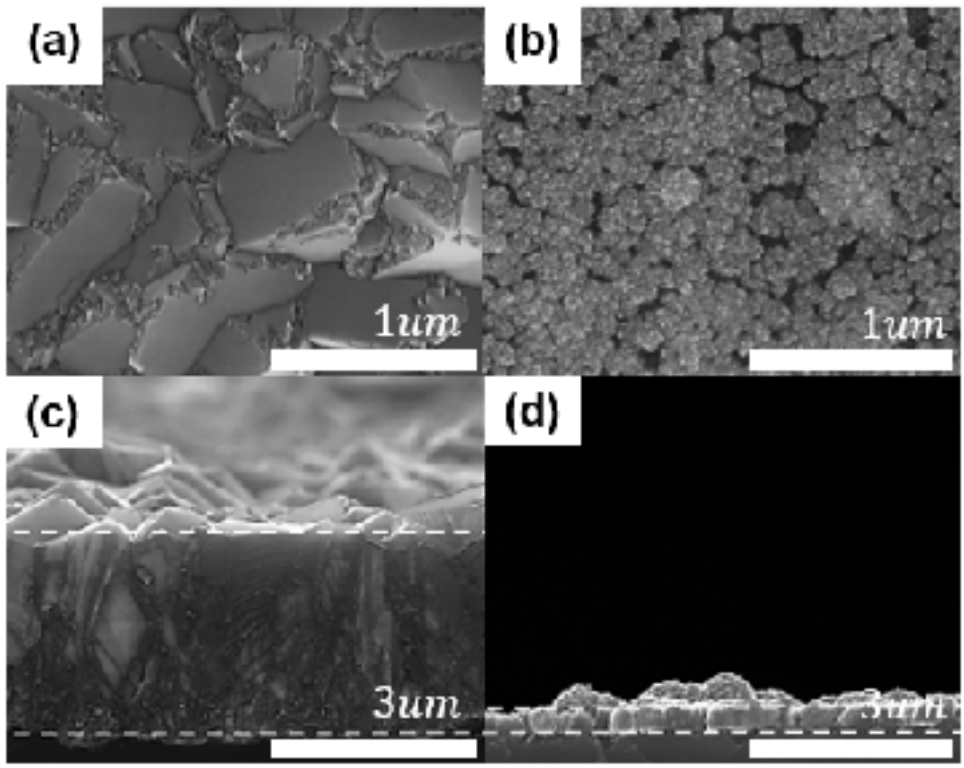

Fig. 13. FESEM images of diamond film deposited for 8 h on the pretreated silicon substrate. (a) and (b) are top view. (c) and (d) are cross section of (a) and (b).

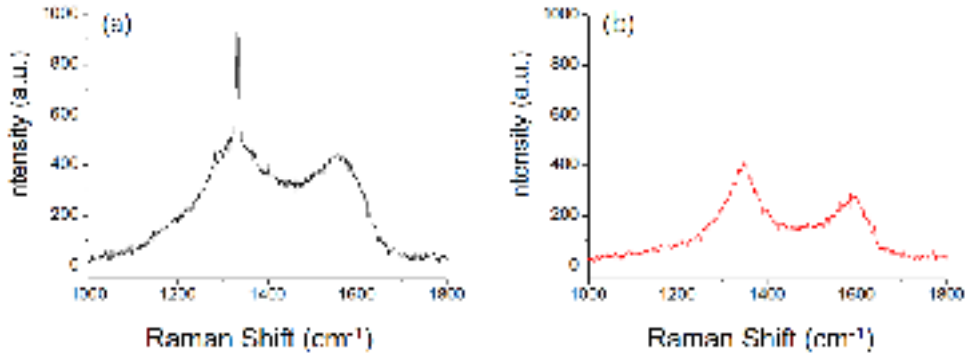

Fig. 14. (a) and (b) are Raman spectra of diamond film of Fig. 13 (c) – (d).

2.4 Conclusion

About 600 nanoparticles captured in the HFCVD diamond process at various experimental conditions were analyzed by HRTEM and FFT images and identified as cubic diamond, n-diamond, hexagonal diamond and i-carbon. Quantitative analysis was used to analyze the captured nanoparticles. Also, the allotropes of diamond coexist under certain conditions was confirmed. The cubic diamond, n-diamond, and hexagonal diamond become more stable as the size increases and i-carbon becomes more stable as the size decreases in the size range of 2 ~ 7 nm of nanoparticles generated in the gas phase of HFCVD. Moreover, the relationship between the crystal structure of nanodiamond and the deposited diamond particles was confirmed. Diamond crystals deposited for 8 h under the condition of the capture temperature of 3 % CH_4 - 97 % H_2, where mainly i-carbon nanoparticles were captured, have ball-like or cauliflower-like structures, whereas diamond crystals deposited for 8 h under the condition of the capture temperature of 900 °C and 1 % CH_4 - 99 % H_2, where mainly cubic diamond and n-diamond nanoparticles were captured, have well-developed (100) facets.

Chapter. 3 Comparison of diamond nanoparticles captured on the floating and grounded membranes in the HFCV D

Negatively charged diamond nanoparticles are known to be generated in the gas phase of the hot filament chemical vapor deposition (HFCVD) process. However, the structures of these nanoparticles remain unknown. Also, the effects of charging on the stability of nanodiamond structures has not been studied experimentally. Here, we examine the charge effect on the crystal structure of captured nanodiamonds by using the floating and grounded carbon membrane. Using a capturing apparatus system, we succeeded in capturing various allotropes of diamonds such as i-carbon, hexagonal diamond, and n-diamond. To compare the crystallinity of the nanoparticles captured on the floating membrane and the grounded membrane, we analyzed the number of d-spacing values of the nanodiamonds. Nanoparticles captured on the floating membrane consisted mainly of cubic diamond and n-diamond, whereas those captured on the grounded membrane consisted mainly of i-carbon. Besides, the effect of nanoparticle charge on the crystallinity of grown diamond particles was studied by comparing the deposition behavior between electrically floating and

grounded silicon substrates.

3.1 Negatively charged diamond nanoparticles in HFCVD

It took nearly 40 years to characterize and isolate dispersed nanoparticles 4–5 nm in diameter [77–78]. Hydrocarbon, C_nH_m, with hydrogen atoms terminating all dangling bonds of surface carbon atoms, is also considered a surface structure of nanodiamonds [79]. The presence of atomic hydrogen is a crucial factor in the low–pressure synthesis of diamond [7, 30, 80–81]. However, Recent studies show the synthesis of diamond without atomic hydrogen. [63–64] The high–purity diamond micro–particles were synthesized by using electric pulse discharge in a low–pressure process. [62] Yoshimoto et al. [63] reported that the nucleation and growth of diamond by vapor deposition in a hydrogen–free, pure oxygen environment to form crystals on a single–crystal sapphire substrate. The above results experimentally support that the charge is related to the stabilization of diamonds. Barnard et al. [82] used computer simulation to investigate the effect of the charge on the stability of the surface of nanodiamond. She reported that a specific amount of charge stabilized the surface of sp^2–bonded carbon atoms and induced the dehydrogenation from the surface of the nanodiamonds. Besides,

anionic charging can prevent the phase transition between bucky-diamonds and onion-like structures related to graphitized layers at the surface. [37]

The structure of nanodiamonds can be changed in response to variations in the conditions of external stimuli. For example, a transformation from bucky-diamonds to onion-like carbons can be occurred by the annealing at a specific temperature. [33-38] The transformation of bucky-diamonds into carbon onions and onion-like-carbon (OLC) under electron irradiation has been observed in situ by high-resolution transmission electron microscopy (HRTEM) and electron energy loss spectroscopy (EELS). [83-84] However, it is difficult to confirm the effect of charge on the phase transition of nanodiamonds at the atomistic level experimentally. So, there has not been much research on the effect of charge on the crystallinity of nanodiamond.

Hwang et al. [9] suggested that the charges such as electrons and ions are heterogeneous nucleation sites for the supersaturated carbon vapor in hot-filament chemical vapor deposition (HFCVD). Besides, they assumed that the charges might lead to negatively charged nuclei clusters. The generation of carbon nanoparticles in the HFCVD process was experimentally confirmed using the energy

analyzer and Wien filter. [25-26] Recent study shows that the negatively charged diamond nanoparticles of 4-6 nm can be synthesized in HFCVD by capturing them on a membrane of the TEM grid. [44]

The purpose of this study is to investigate the charge-dependent crystallinity of diamond nanoparticles. To generate the negatively charged nanoparticles at the gas phase, we performed the experiments in the HFCVD. We compare the captured nanoparticles between floating and grounded membrane on a TEM grid. We pushed a capturing apparatus to the capture zone, and the grid was exposed for 10 s and pulled to the chamber wall. The captured nanoparticles were observed by the TEM. To confirm the effect of charge induced reconstruction of the nanoparticles on particle growth, we deposited the diamond for 8 h on floating and grounded Si substrates.

3.2 Experimental procedure

Preparation of nanoparticles

Using the capturing system in an HFCVD, which is schematically shown in Fig. 1, we captured the diamond nanoparticles. The filament consisted of three 0.5−mmϕ tungsten wires, which were twisted into a nine−turn coil of 8 mmϕ. The reaction pressure and filament temperature were 20 Torr and 2,000 ^{o}C 20 Torr, respectively. A ratio of CH_4 to H_2 of 1:99 or 3:97, using a mass flow controller. Before nanoparticle capture was initiated, the tungsten filament was carburized for 24 h at 1 % CH_4 – 99 % H_2 or 3 % CH_4 – 97 % H_2.

In order to investigate the negatively charged diamond nanoparticles, which were generated in the gas phase, we used the carbon membrane (lacey carbon film; Ted Pella, Inc, Redding, CA, USA), SiO membrane (Ted Pella, Inc.), and graphene membrane (6–8 layers of graphene film; Ted Pella, Inc.) of a copper (Cu) TEM grid. The carbon and SiO membranes were for scanning TEM (STEM) imaging. STEM images were taken by a Tecnai F20 TEM instrument (FEI, Hillsboro, OR, USA). The graphene membrane was for HR−TEM images from a JEM−2100F system (JEOL Ltd., Tokyo, Japan). The TEM grids were placed in a stainless steel

holder or quartz holder connected to the capturing apparatus. The capturing apparatus pushed to the capture zone as needed and pulled back towards the chamber wall. The grid was exposed at the capture zone for a capturing time of 10 s. The capture zone was located 30 mm below the hot filament because of thermal damage to the membranes at temperatures above ~ 650 °C. The temperature in the capture zone was 600 °C. Before pushing the capturing apparatus into the capture zone, the tungsten filament was additionally carburized for 30 min under the same conditions as those for diamond deposition.

Most of the observed nanoparticles were single crystals, which were chosen to identify the phase. To index the crystal structure of observed nanoparticles, we compared lattice parameters, lattice angles and reference to the information, which were provided by the JCPDS on the reported carbon allotropes. We analyzed 150 d-spacing values of ~ 100 nanoparticles on each membrane to identify the crystal structure of the captured nanoparticles. Four carbon allotropes of i-carbon, n-diamond, hexagonal diamond, and cubic diamond were identified from the HFCVD process.

We compared the deposition behavior of diamond particles between the electrically floating and grounded p-type <100> Si substrates on a p-type <100> Si substrate of 10 × 10 × 3 mm^3.

For the grounded substrate, the Si substrate was placed on the stainless-steel substrate holder was connected to the external ground. For the floating substrate, the Si substrate was placed on the sapphire plate of 10 × 10 × 1 mm^3, which was again was placed on the stainless-steel substrate holder. The diamond was deposited for 8 h on the Si substrate at the substrate temperature of 950 °C, with the substrate was apart from the 5 mm below the filament. The microstructure of the diamond particles was observed by FESEM (SU70, Hitachi). The deposited diamond was analyzed using a Raman spectrometer (LabRam HR Evolution, HORIBA) with a DPSS laser beam at an exciting radiation wavelength of 532.3 nm and a spot size of 1 μm.

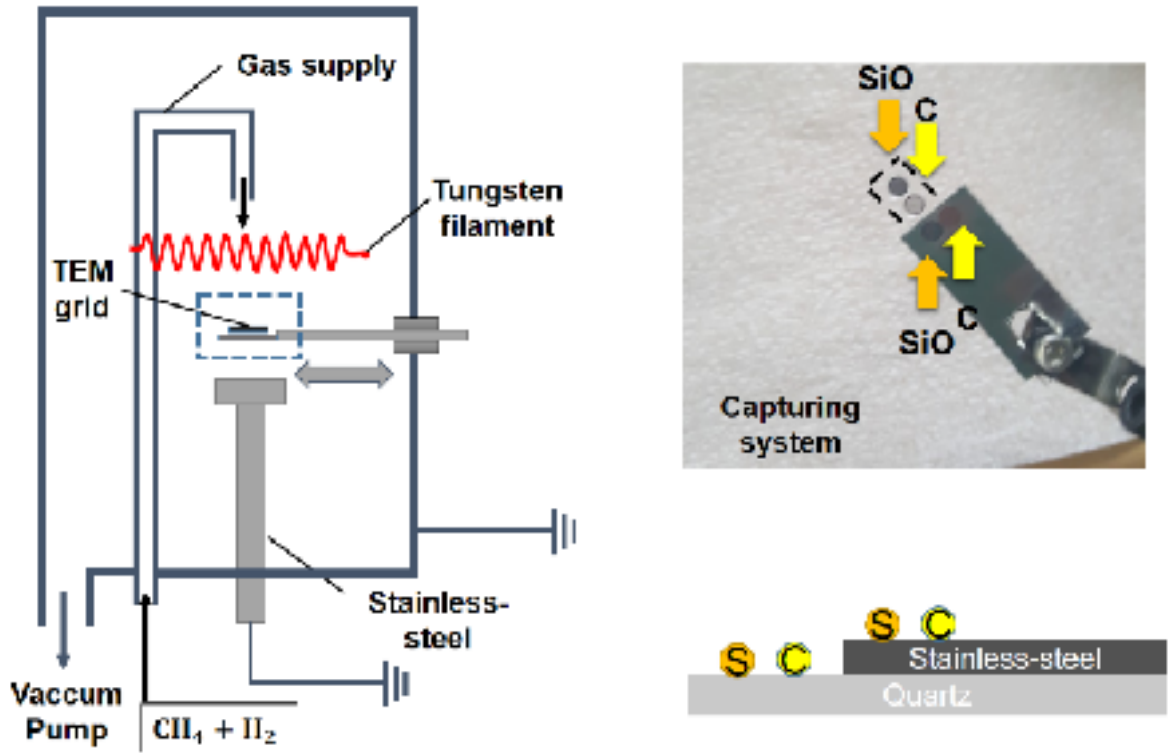

Fig. 15. Schematics of the experimental apparatus for capturing carbon nanoparticles. The left figure is the HWCVD reactor with a capturing system. The right figure illustrates how the carbon and SiO membranes are made electrically grounded and floating condition. Nanoparticles were captured on grounded and floating carbon and SiO membranes under the same HFCVD condition.

3.3 Result & Discussion

Charged nanoparticles in the gas phase

The nanoparticles in the gas phase are negatively charged. One possible route to negative charging [85] is the negative surface ionization of carbon molecules of high electron affinity such as C_2, which has an electron affinity of 3.54 eV [86]. When the carbon molecules attached on the surface of the hot-filament, then the ionization potential could be decreased because of the high electron affinity of C_2. After the attachment of C_2, those would easily take a charged state from the hot filament. The other possibility to negative charging is the ion-induced heterogeneous nucleation at the gas phase. When negatively charged carbon molecules act as a site for ion-induced nucleation, then they grow as charged nuclei. Another possible route to negative charging is neutral nucleation, followed by the attachment of electrons emitted from the hot filament.

We used several different types of membranes to investigate the electrical properties of nanoparticles. The negatively charged nanoparticles would be repelled when they landed on the surface of the substrate. Because the free electrons which were thermally emitted from the hot-filament would be trapped on the surface of

the substrate, which lead to the negatively charged state on the surface of the substrate. Due to the electrical potential energy, the charged nanoparticles had a Coulomb-repulsion interaction with the negatively charged surface of the substrate [85]. Fig. 16 (a-b) show STEM images of nanoparticles on SiO membranes. Fig. 16 (c-d) show STEM images of nanoparticles on the carbon membranes. In the setup shown in Fig. 16 (a) and (c), the membranes were placed on a quartz holder to create electrically floating conditions. In the setup shown in Fig. 16 (b) and (d), however, the membranes were placed on an electrically grounded stainless steel holder.

The average number densities of nanoparticles per μm^2 were 65, 283, 390, and 2,713 under the capture conditions shown in Fig. 16 (a-d), respectively, and the average nanoparticle size was 3.1, 3.3, 3.2, and 3.2 nm. The results would support the expectation which the negatively charged nanoparticles would be repelled from the negatively charged surface. The SiO membrane is an electrical insulator and the sheet resistivity of the SiO membrane almost 10^7 ohm per square. The average number density of nanoparticles on the SiO membrane using the grounded stainless holder (Fig. 16 (b)) was four-fold larger than that on the floating quartz holder (Fig. 16 (a)). The average number density of nanoparticles on the carbon

membrane of the grounded holder (Fig. 16 (d)) was seven-fold larger than that on the floating holder (Fig. 16 (c)).

In contrast, the average number densities of nanoparticles on the carbon membrane were 6-fold and 9.6-fold larger than those on the SiO membrane using the quartz and stainless steel holders, respectively. Because the carbon membrane is an electrical conductor and the sheet resistivity of the carbon membrane almost $10^{3\sim4}$ ohm per square. These results indicate that the charged nanoparticles would be repelled on the insulating surface, which is attributed to Coulomb repulsion between the negatively charged surface and the negatively charged nanoparticles.

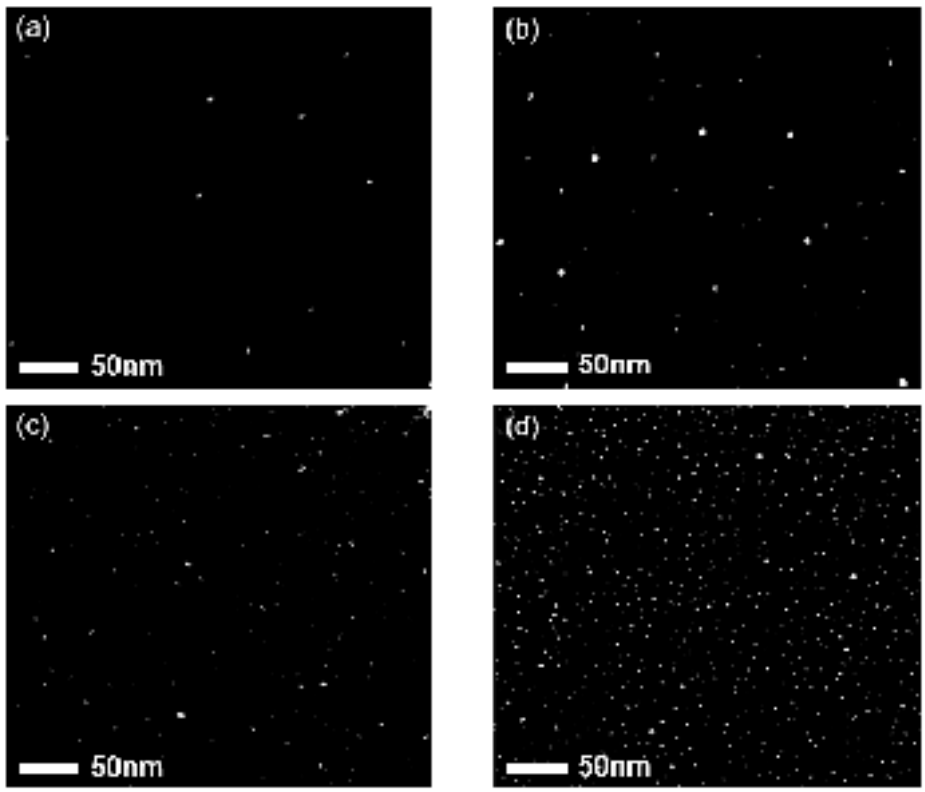

Fig. 16. STEM images of nanoparticles captured for capturing time of 10 s (a) on the SiO membrane on the quartz holder (floating condition), (b) on the SiO membrane on the stainless-steel holder (grounded condition), (c) on the carbon membrane on the quartz holder (floating condition), and (d) on the carbon membrane on the stainless steel-holder (grounded condition) at the filament temperature of 2000 °C and the capture temperature of 600 °C at the gas mixture of 3 % CH_4 - 97 % H_2.

Nanoparticles captured on the floating and the grounded membrane

Similar experiments were carried out with the gas mixture of 1 % CH_4 – 99 % H_2; however, the SiO membrane was much more damaged at the capture temperature of 600 °C with 1 % CH_4 – 99 % H_2 than with 3 % CH_4 – 97 % H_2. Moreover, the carbon membrane was completely etched away with the 1 % CH_4 – 99 % H_2 gas mixture. Thus, nanoparticle capture at 1 % CH_4 – 99 % H_2 failed at 600 °C. As such, the capture temperature was reduced to 300 °C for nanoparticle capture using the carbon membrane. The average size of the nanoparticles was ~10 nm, which indicated coalescence of the primary nanoparticles. HR-TEM observations revealed that those nanoparticles had an onion-like structure, implying that nanoparticles undergo a structural change in the amorphous carbon membrane.

Therefore, we used a graphene membrane at 300 °C to capture nanoparticles generated with 1 % CH_4 – 99 % H_2. Fig. 17 (a-b) show TEM images of nanoparticles captured on the graphene membrane of the Cu TEM grid. The capture time was 10 s at the capture temperature of 300 °C, and the filament temperature was 2,000 °C using 1 % CH_4 – 99 % H_2. In Fig. 17 (a), the graphene

membrane on the Cu grid was placed on the quartz holder in the floating condition. In Fig. 17 (b), the graphene membrane was placed on the stainless steel holder in the grounded condition. The average sizes of nanoparticles captured in the floating and grounded conditions were, respectively, 4.0 and 3.8 nm. The average number density of the nanoparticles captured in the grounded condition was 7.9 × 103 per μm^2, almost five times larger than that in the floating condition (1.6 × 103 per μm^2). These results confirmed that the build-up of negative charges on the floating membrane creates a repulsive Coulomb interaction with the negatively charged nanoparticles.

We observed that average size of the captured nanoparticles in the floating conditions was much larger than those in the grounded conditions. Its tendency was repeatedly observed in several re-experiments. Due to 10s capture time, heating rate on the surface of the membrane would be similar both the floating and grounded membrane. The reason why the observation of the smaller size of the nanoparticles on the grounded membrane would be related to the etching of the nanoparticles by the atomic hydrogen. To clarify the phenomena, we identified the crystal structure of the captured nanoparticles on the floating and grounded condition.

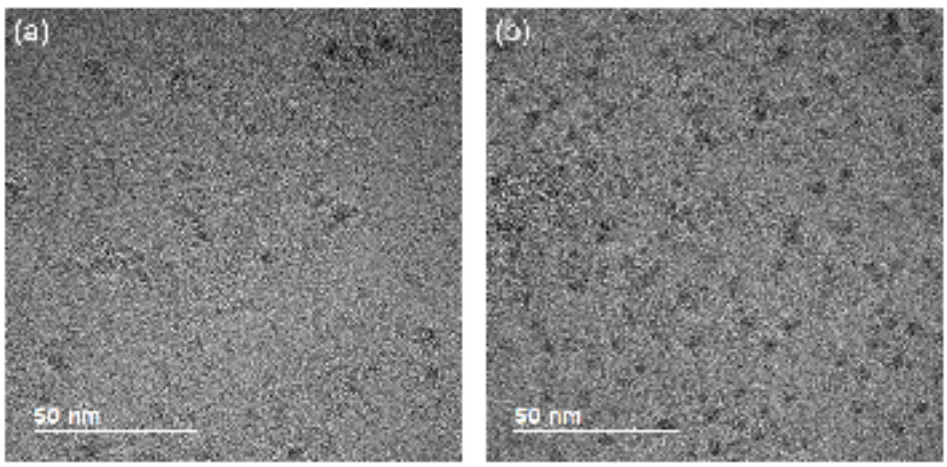

Fig. 17. TEM images of nanoparticles captured on the graphene membrane of the TEM Cu grid (a) on the quartz holder (floating condition) and (b) on the stainless-steel holder (grounded condition) at the capture temperature of 600 °C and the gas mixture of 1 % CH_4-99 % H_2.

Comparing the nanoparticles on the floating and on the grounded membrane

We examined the structures using HR-TEM to compare the crystal structure of the nanoparticles captured in floating and grounded conditions. Four carbon allotropes were identified: i-carbon, n-diamond, hexagonal diamond, and cubic diamond. The nanoparticles in Fig. 18 (a) were captured on the graphene membrane, which was placed on the quartz holder for 10 s at capture temperature of 300 °C and the filament temperature of 2,000 °C under the gas mixture of 1 % CH_4 - 99 % H_2. Fig. 18 (a) shows that the single-crystalline cubic diamond phase along the <110> zone axis. FFT and HR-TEM images show the two (111) planes of cubic diamond (Fd3m) and the d-spacing of 2.06 Å. In addition, the lattice angle of 70° in Fig. 18 (a), between the two (111) planes, matches that of cubic diamond (JCPDS No.6-0675).

The conditions used to capture the nanoparticles shown in Fig. 18 (b) were the same as those used to capture the nanoparticles in Fig. 18 (a). The FFT image in Fig. 18 (b) shows n-diamond phase along the <110> zone axis. FFT and HR-TEM images show the (111) and (200) lattice planes of n-diamond; the d-spacing value of 1.8 Å corresponds to the forbidden reflection (200) plane. The

lattice angles of 70° and 54° in Fig. 18 (b) are the angles, respectively, between the two (111) planes and between the (111) and (200) planes, representing n-diamond. A lattice angle of 54° between the (111) and (200) planes was observed for the n-diamond phase. It should be noted that cubic and hexagonal diamonds do not have a lattice angle of 54° between the (111) and (200) planes (JCPDS No.43-1104).

The nanoparticles shown in Fig. 18 (c) were the same as those used to obtain the results shown in Fig. 18 (a). The FFT image in Fig. 18 (c) shows single-crystalline hexagonal diamond along the <100> zone axis with d-spacings of 2.18, 2.06, and 1.50 Å, which were assigned to the (100), (002), and (102) lattice planes of hexagonal diamond, respectively. The d-spacing values of 2.18 Å and 1.50 Å are specific to hexagonal diamond. The lattice angles of 90° and 46° in Fig. 18 (b) were attributed to the angles between the (100) and (002) planes and between the (100) and (102) planes, respectively, of hexagonal diamond (JCPDS No.19-0268).

The conditions used to capture the nanoparticle shown in Fig. 18 (d) were the same as those shown in Fig. 18 (c). The FFT image in Fig. 18 (d) shows single-crystalline cubic-phase diamond along the <100> zone axis. The nanoparticle contained three lattice planes

with d-spacings of 2.46, 2.10, and 1.50 Å, corresponding to (111), (200), and (220), respectively, of the cubic phase with a lattice parameter of 4.2 Å. The lattice angles of 70°, 54°, and 35° in Fig. 18 (d) were also assigned, respectively, to the angles between the two (111) planes, between the (111) and (200) planes, and between the (111) and (220) planes of i-carbon. The i-carbon nanoparticles showed variation in the d-spacing value in the range of 2.36-2.54 Å; the lattice parameter of i-carbon had a range of 4.1-4.4 Å [30-31].

It was hard to distinguish the cubic diamond and the n-diamond structure. Because both phase structure had a same d-spacing values such as (111) and (220) lattice planes. Even though n-diamond could show the forbidden plane (200), some of them would not reflect the lattice plane or show only specific lattice plane in case of <100> zone axis. Not only n-diamond could show the 2.06 d-spacing values, but also hexagonal diamond and i-carbon structure show the 2.06 d-spacing values within 3% approximation. So only few cubic diamond nanoparticles can be identified by using the specific zone axis such as <110> axis including the (111) and (220) phase. In this case, the FFT image can be distinguished to the other carbon allotropes, which can't show such d-spacing values with specific lattice angles. To identify the fraction of the

captured nanoparticles, we counted the observed d-spacing values.

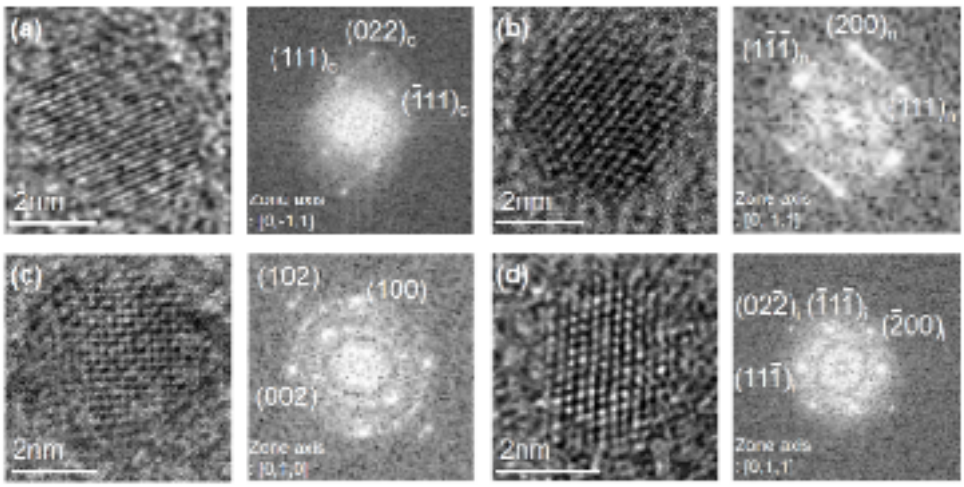

Fig. 18. HRTEM and FFT images of four carbon allotropes such as (a) cubic diamond (JCPDS6-0675), (b) n-diamond (JCPDS43-1104) captured on the floating membrane and (c) hexagonal diamond (JCPDS19-0268) and (d) i-carbon (52) captured on the grounded membrane.

Analysis of captured nanoparticles

For this, we analyzed the phase of the captured nanoparticles between graphene membranes in floating and grounded conditions. Fig 19 shows the number of the d-spacing values of the observed nanoparticles captured at 600 °C using the gas mixture of 1 % CH_4 - 99 % H_2 at a filament temperature of 2,000 °C. The number of nanoparticles shown in Fig. 19 were determined from 150 d-spacing values from ~ 100 nanoparticles for each membrane. For this, 300 d-spacing values were classified based on the reported d-spacing values which the crystal structure of carbon allotropes could have. The frequency of the d-spacing value in Fig. 19 should be closely related to the XRD intensity of the polycrystal. Because, as mentioned early page, the observed d-spacing values were not the relative intensity itself. However, if the number of observed d-spacing values was significantly enough, then the number of d-spacing values would represent the information of the crystal structure, which was correlated to the relative intensity of the observed nanoparticles. So 150 d-spacing values from ~ 100 nanoparticles were used to estimate the reliability and reproducibility.

By using the values reported by the JCPDS for the carbon

allotrope, we analyzed the d-spacing values. The observed d-spacings were assumed that those correspond to reported values from the JCPDS, if the d-spacing values were within ~ 3%. The nanoparticles captured on the grounded holder show that the number of nanoparticles were 66 and 38, assigned to the d-spacing values of 2.42 and 2.06 Å, respectively. The nanoparticles captured on the floating holder show that the number of nanoparticles were 41 and 64, assigned to the d-spacing values of 2.42 and 2.06 Å, respectively. The d-spacing of 2.42 Å belongs to i-carbon, whereas the d-spacing of 2.06 Å belongs to cubic diamond, n-diamond, and hexagonal diamond (diamond allotropes). Therefore, the large number of 2.06 Å than 2.42 Å in the floating condition in Fig. 19 indicates that diamond allotropes are a major phase, whereas i-carbon is a minor phase. Similarly, the small number of 2.06 Å than 2.42 Å in the grounded condition indicates that i-carbon is a major phase, whereas diamond allotropes are a minor phase.

Negative charge build up on the surface of the membrane would be expected to be much greater in the floating condition than in the grounded condition. According to the results shown in Fig. 19, such the crystal structure of diamond allotropes would be stabilized by the build-up of negative charge. The build-up of negative charges

or electrons on the grounded membrane would be much less than that on the floating membrane. Such a low charging state on the grounded membrane may be sufficient to change the nanoparticles from diamond allotropes to i-carbon, which might be related to the sp^2 or sp^{2+x} bond of carbon structure. However, there is no report on the relationship between the charging state and the carbon allotropes.

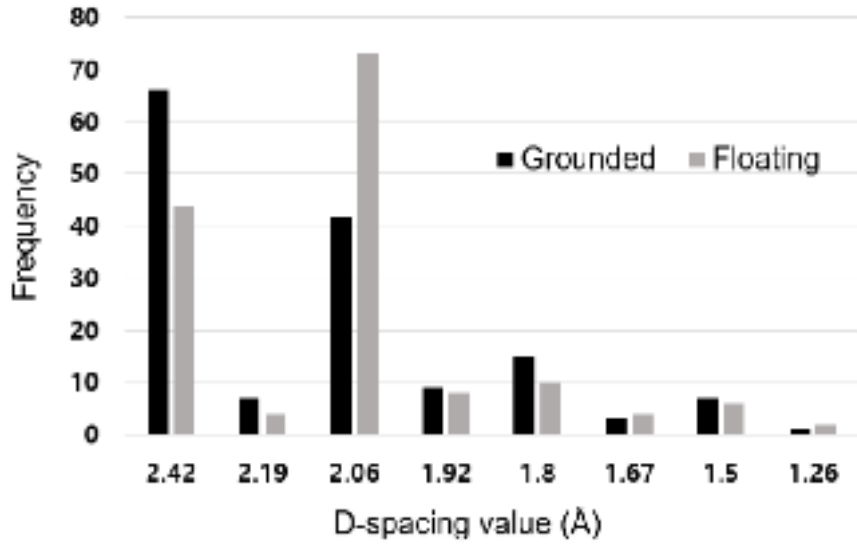

Fig. 19. Frequency of d−spacing values of nanoparticles captured at 1 % CH_4 – 99 % H_2. The data were obtained by analyzing 300 d−spacing values out of ~200 nanodiamonds.

Charge induced recrystallization of charged nanoparticles

In a previous study, Hwang et al. [9] suggested that negatively charged diamond are generated in the gas phase, and that these particles maintained the stability of diamond upon landing on the Si substrate. He assumed that when diamond nanoparticles landed on the Fe substrate, they would lose charge state. If diamond nanoparticles lost their stability, they would be transformed to graphitic carbon structure. Based on ab-initio simulations, Lai and Barnard [38] investigated that the negative charging of nanoparticles stabilizes sp^3 bonding of carbon, favoring the diamond structure, whereas positive charging stabilizes sp^2 bonding of carbon, favoring the graphite structure. Park et al. [37] also studied that negative charging of a cluster containing 165 carbon atoms stabilizes the diamond structure over the graphite structure.

However, the size of the nanoparticles should be considered to understand the stability of the carbon nanostructure. Because, it is well known that the crystal structure of nanoparticles is strongly related to the size of the nanoparticle. Due to surface stress of the nanostructure, the surface stress energy affects the stability of diamond nanoparticles ranging from ~ 1 to ~ 3.6 nm in diameter,

including through graphitization of the (111) surface to form fullerenic and onion-like structures [87-89]. Considering the reported studies about the correlation between the stability of the nanoparticles and the size dependence, we found that the different structure of nanoparticles between floating and grounded conditions may relate to the size difference. To clarify the size dependence of crystal structure, we measured the size distribution of nanoparticles.

Fig 20 (a-b) show the size distribution of nanoparticles captured on floating and grounded membranes. We analyzed 100 nanoparticles on each membrane. The average size of 100 nanoparticles on the floating membrane was 3.99 ± 0.16 nm with 95% confidence. On the grounded membrane, the average size of 100 nanoparticles on the grounded membrane was 3.87 ± 0.15 nm. The size distribution of the nanoparticles may affect the stability of the carbon allotrope. However, Fig. 20 shows that both nanoparticles on the floating and grounded conditions have similar size distributions. Fig. 20 also shows that the crystal structure depends strongly on the condition (floating or grounded). These results imply that the crystal structure of nanoparticles would be affected by the charging, as opposed to nanoparticle size.

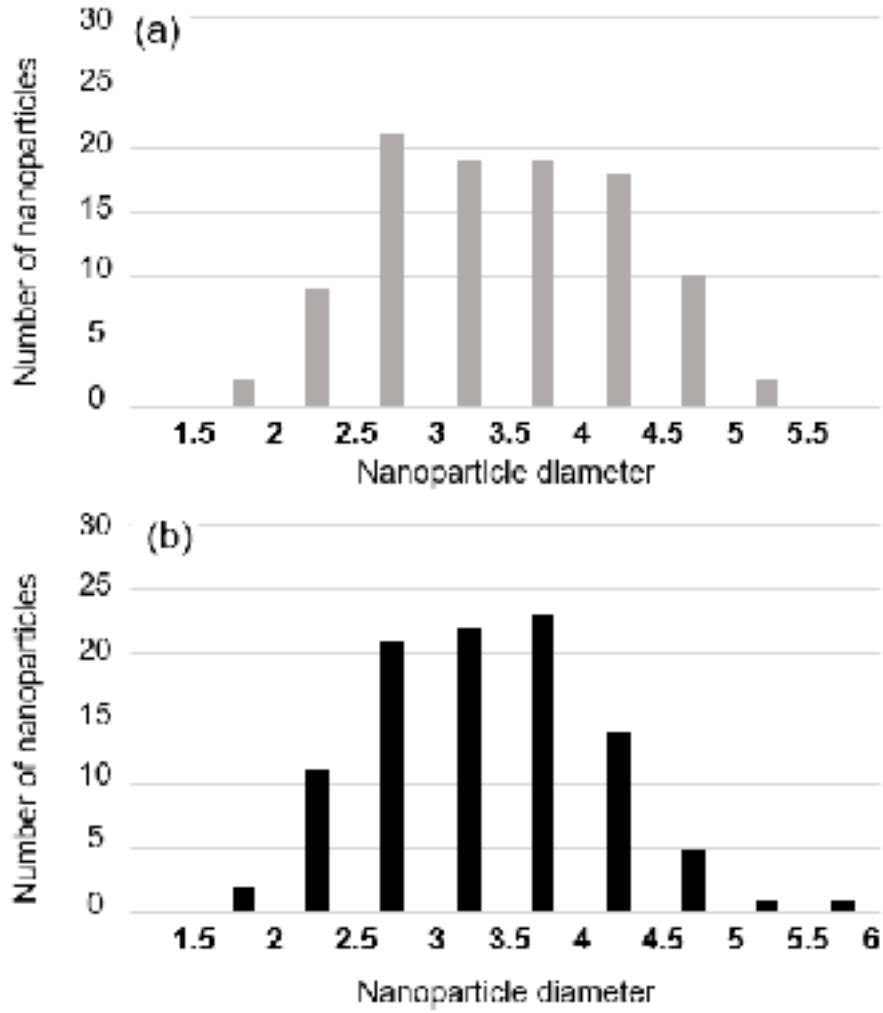

Fig. 20. Size distribution of nanoparticles captured (a) on the quartz holder (floating condition) and (b) on the stainless-steel holder (grounded condition), respectively.

Charged nanoparticles and their contribution to the growth of diamond

A bare Si substrates were used for diamond deposition at substrate temperature of 950 °C for 8 h under the same processing conditions as the nanoparticles that were captured to compare the deposition behavior between floating and grounded conditions. To make isolated diamond particles instead of diamond film, we used a bare Si substrate was used without pretreatment. For floating condition of the Si substrate, we inserted a 1 mm thick sapphire plate between the stainless steel holder and the Si substrate. For grounded condition of the Si substrate, the substrate was placed onto the stainless steel holder. We also considered the thermal conductivity and heat capacity of the sapphire plate. Even though the substrate temperature measured by thermo-couple was almost same in case of floating and grounded condition, we assumed that the temperature of the Si substrate on the plate was slightly higher than that of the stainless-steel holder. The distance between the filament and substrate was adjusted to equalize the temperatures of the Si substrates.

Fig 21 (a-b) show FE-SEM images of the deposited diamond particles on the bare Si substrate under floating and grounded

conditions, respectively. The average number density of diamonds deposited in the grounded condition was 445 per cm^2, whereas in the floating condition it was 142 per cm^2. The number density in the grounded condition was almost three-fold larger than that in the floating condition, similar to the result whereby the number density of nanoparticles captured under grounded conditions is larger than that under floating conditions. This results reflect that the possibility of the nucleation and growth of diamond particles on the Si substrate was related to the charged nanoparticles which depend on the Coulomb interaction between the substrate and the charged nanoparticles.

Fig. 21 (c-d) are higher magnification FE-SEM images of Fig. 21 (a-b), respectively. The diamond particle in Fig. 21 (c) deposited on the floating conditions has well-defined facets diamond particles, whereas that the diamond particle in Fig. 21 (d) deposited on the grounded conditions has an overall spherical shape with partially crystalline facets. The size of the diamond particles deposited under the grounded conditions was smaller than that obtained under the floating conditions.

The diamond particles in Fig. 21 (c-d) were analyzed by a Raman spectrometer with a spot size of 1 μm. Fig 22 (a-b) show the Raman spectra of the diamond particles deposited under the floating

and grounded conditions, respectively. The Raman spectra in Fig. 22 (a) show a sharp peak at 1,332 cm^{-1}, which indicates sp^3-bonded diamond. However, the Raman spectrum in Fig. 22 (b) shows broadening of the G-band [90-91]. The relative intensity (I_D /I_G) of the particle deposited in the grounded condition was lower than that in the floating condition. The Raman spectra results imply that the crystal structure of the diamond particles deposited on the floating conditions mainly consisted of sp^3-bonded high quality diamond, whereas the diamond particles deposited on the grounded conditions is relatively low fraction of sp^3-bonded low quality diamond.

Comparing the crystal structure of the captured particles and the crystal structure of deposited nanoparticles, the large number of nanoparticles associated with the 2.06 Å d-spacing in Fig. 19 is related to the intensity of the 1,332 cm^{-1} diamond Raman peak, and that corresponding to the 2.43 Å d-spacing corresponds to Raman broadening of the graphite Raman peak consisting of sp^2 bonded carbon [92-93]. Fig 21 (c-d) show that the size of the diamond particles deposited in the floating condition are larger than the size of the diamond particles deposited in the grounded condition. In this case, the particles deposited under grounded conditions would be easily etched by atomic hydrogen due to their graphite-like

structure [94−95], resulting in a smaller size. Both the size of the nanoparticles and the deposited diamond on the grounded condition shows a relatively small size of the nanoparticles and the deposited diamond on the grounded condition, respectively. From the above results, the growth rate of the diamond particles would be related to the stability of the sp^3 bond of the nanoparticles which were generated in the gas phase during HFCVD process.

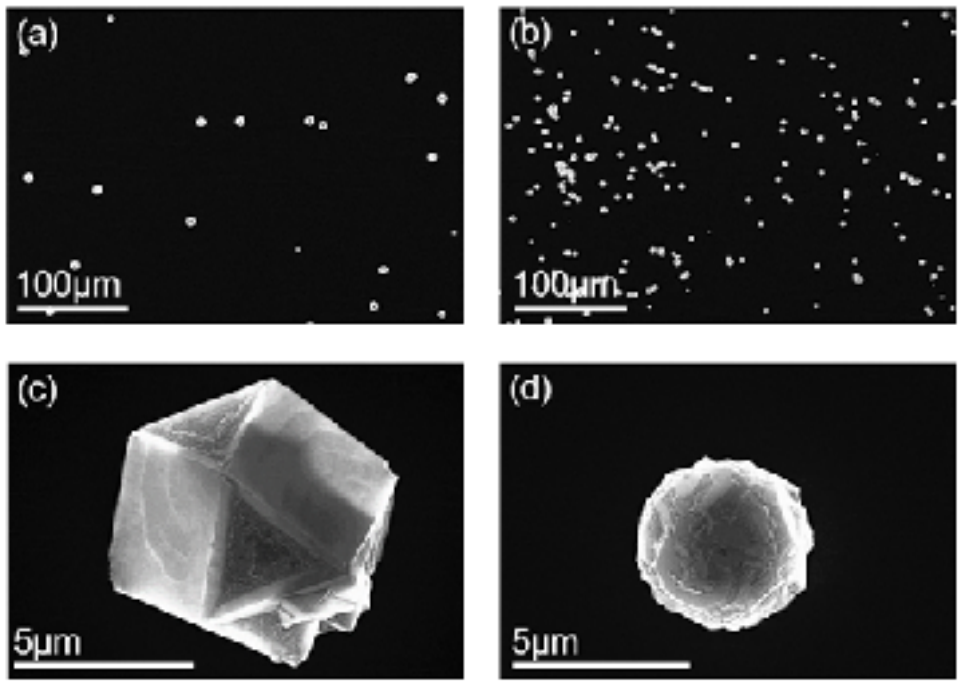

Fig. 21. FESEM images of diamonds particles deposited for deposition time of 8 h on the bare silicon substrate (a) on the sapphire plate on the stainless-steel holder (floating condition) and (b) on the stainless-steel holder (grounded condition). (c) and (d) are magnified images of a diamond particle of (a) and (b), respectively.

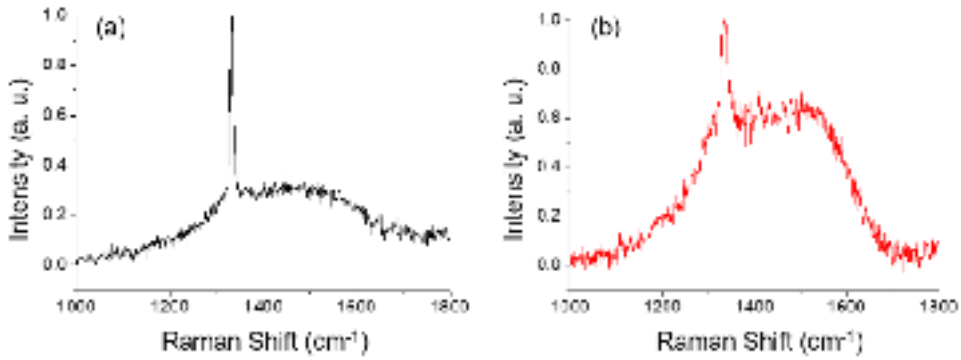

Fig. 22. Raman spectra of deposited diamond particles deposited (a) on the floating substrate (Fig. 21 (a)) and (b) on the grounded substrate (Fig. 21 (b)).

3.4 Conclusion

We confirmed that the number density of nanoparticles captured in the grounded condition was related to the electrically floating and grounded condition on the surface of the membrane. The number of nanoparticles in the grounded condition was larger than that in the floating condition. ~ 100 nanoparticles captured in the floating condition consisted mainly of diamond allotropes, whereas those captured in the grounded condition consisted mainly of i-carbon. Diamond particles deposited in the floating condition displayed an well-developed facets diamond particles, and had a high-intensity 1,332 cm^{-1} diamond Raman peak, whereas those deposited in the grounded condition showed an overall spherical shape with partially covered with crystalline facets with a broad G-band Raman peak. The results show that negative charging on the surface stabilize the sp^3 bonded crystal structure of nanoparticles, which contributes to the deposition of crystalline diamond with well-developed facets.

Ch. 4 Relationship between the electrons and the crystal structure of the captured nanoparticles in the HFCVD

From the above results, negatively charged diamond nanoparticles are stabilized on the floating condition. It means that charging state of the nanoparticles would relate to the stability of the nanoparticles. To make a high charging state of the captured nanoparticles, we increased the thermionic emission from the hot filament. First, we increased the filament temperature. A number of electrons from hot-filament was increased by increasing the filament temperature, following the law of thermionic emission by Richardson. Second, additional bias was applied to the hot-filament for increasing a number of electrons. The bias was increased from - 100 V to + 50 V at 3% methane concentration. ~500 nanoparticles were analyzed for phase identification using HR-TEM and FFT. Chapter 4 will discuss the relationship between the electrons and the crystal structure of captured nanoparticles.

4.1 Stabilization of diamond nanoparticles by using negative charging

Park et al. [8] confirmed that the nanoparticles generated at HWCVD were negatively charged. Because of thermionic emission from the hot-filament, the free electrons would occupy to the nanoparticles. An electric charge instead of hydrogen is necessary for the low-pressure synthesis of diamond. [62-64] The surface energy of the diamond nanoparticle would decrease due to the charges on the surface. [9] The phase transition from an onion-like structure to a bucky-diamond was related to the extra charge. Dangling bonds of carbon atoms were stabilized by charging and the graphitized layers disappeared. [34] Barnard et al. investigated the charge-induced restructuring and decomposition of bucky-diamonds. They confirmed that anionic charging saturates dangling bonds of carbon atoms at the surface. On the other hand, cationic charging breaks the surface structure between the core and shell forming a layer of graphene-like carbons. [82] They also investigated the charge-induced dehydrogenation. The breaking of the strong covalent C-H bonds is achieved through charging of hydrogenated nanodiamonds. [96] Not only charge stabilize the surface of the nanodiamond but also stabilize the diamond phase.

Park et al. confirmed that the diamond was more stable than the graphite by increasing the excess charge. [37] From the above results, we assumed that the free electrons emitted from the hot-filament might stabilize the nanoparticles generated at the gas phase. As a result, the shell structure might not be formed on the surface of the nanodiamonds.

Hwang et al. [15] suggested that diamond nanoparticles were generated at the gas phase. Besides, he investigated that diamond nuclei are negatively charged. Using the energy analyzer and Wien filter, Jeon et al. [25-26] investigated the generation of nanoparticles in the HWCVD. Park et al. [8] succeeded in synthesizing the diamond nanoparticles, which were generated at the gas phase under the processing condition of diamond films by capturing nanoparticles on a membrane of the TEM grid. Moreover, he confirmed that the nanoparticles were negatively charged. Barnard et al. [7] investigated that carbon nanoparticles would contain both sp^2 and sp^3 bonding simultaneously. The nanodiamond's surface can be stabilized by charging. Besides, they confirmed that the extra charge influenced the phase transition from the bucky-diamond to the onion-like structure. [80] Park et al. [37] confirmed that the diamond was more stable than the graphite by increasing the excess charge.

Considering these results, we controlled the crystal structure of captured nanodiamonds by increasing the electron density at the gas phase. To confirm the effect of electron density at the gas phase, we increased the filament temperature and applied the bias to the filament. For capturing the nanodiamonds, a capturing apparatus is pushed to the capture zone, exposed for 10 s and pulled to the chamber wall. The captured nanoparticles were analyzed by the transmission electron microscopy (TEM).

4.2 Experimental procedure

Fig. 1 show the schematic for the capturing apparatus. The filament consisted of three tungsten wires of 0.5 mmϕ, and those twisted to a 9−turn coil of 8 mmϕ. The reaction pressure was 20 torr. The gas mixture of CH_4 and H_2 was supplied at 100 standard cubic centimeters per minute (sccm), with a ratio of CH_4 to H_2 of 1:99 or 3:97, using a mass flow controller. To investigate the effect of the electrons on the crystallinity of diamond nanoparticles, we raised the filament temperature from 2100 °C to 2300 °C at 1 % methane concentration and the additional bias ranged of − 100 V ~ + 50 V at 3 % methane concentration. To maintain a constant capture temperature, the distance between the capture zone and filament was 50 mm, 53 mm, and 55 mm at filament temperature of 2100 °C, 2200 °C, and 2300 °C, where the temperature of capture zone was 300 °C. When the bias applied to the filament, the distance between the capture zone and filament was 30 mm, where the temperature of capture zone was 600 °C. To increase the reproducibility of experiments, capturing was done after 30 min of supplying the gas mixture of CH_4 and H_2. We pushed the capturing apparatus to the capture zone and pulled toward the chamber wall. Carburization for 30 min, which was the same as that of the

diamond deposition, was maintained before pushing the capturing apparatus into the capture zone. The quartz holder, which was loaded with the TEM grid, was pushed to the capture zone. The grid was exposed for a capturing time of 10 s. After that, the quartz holder was pulled out to the chamber wall. The TEM grid was placed in the quartz holder. graphene membrane (6-8 layers of Graphene Support film, TED PELLA, INC) were used to capture the diamond nanoparticles in the gas phase.

The diamond nanoparticles were analyzed by TEM (JEM-2100F, JEOL Ltd.). In total, ~ 700 nanoparticles, which were captured at the gas mixture of 1 % CH_4 - 99 % H_2 at each filament temperature of 2100 °C, 2200 °C, and 2300 °C and at the gas mixture of 3 % CH_4 - 97 % H_2 at each additional bias of - 100 V, - 50 V, 0V, and + 50 V, were analyzed for phase identification using HR-TEM and FFT. Some captured carbon nanoparticles were polycrystalline or aggregated. Most of them were single crystals, which were chosen to identify the phase. From the FFT image of each nanoparticle, lattice parameters and the angle between them could be determined. Besides, we measured an average size of 100 nanoparticles at each filament temperature of 2100 °C, 2200 °C, and 2300 °C. The current at the gas phase was measured by Picoammeter (Model 6487, Keitheley). Feedthrough, which was connected with Picoammeter,

was located below 30mm from the filament.

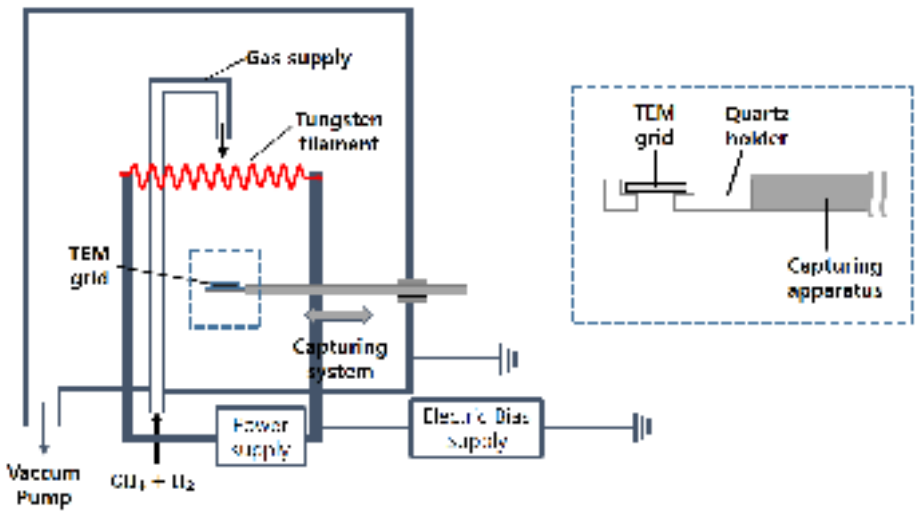

Fig. 23. Schematic diagram of the experimental system with capturing apparatus.

4.3 Result & discussion

Thermionic emission from the hot-filament

Fig. 24 (a) is the TEM image showing the nanoparticles on the graphene membrane with the Cu grid for a capture time of 10 s at the capture temperature of 300 °C under the condition of the hot filament temperature of 2100 °C at the gas mixture of 1 % CH_4 - 99 % H_2. The dark spots are the nanoparticles. The white square in Fig. 24 (a) is Fig. 24 (b). Fig. 24 (b) is the HRTEM image showing the captured nanoparticles, which are distributed randomly on the membrane. The nanoparticle pointed by the white arrow in Fig. 24 (b) is in Fig. 24 (c). The HRTEM image in Fig. 24 (c) shows that the nanoparticle has a diameter of ~ 3.8 nm and 2.06 Å of crystalline lattice spacing, which indicates the (111) lattice planes of diamond. The SAED pattern recorded from the nanoparticle in Fig. 24 (c) is shown in Fig. 24 (d). The SAED pattern in Fig. 24 (d) shows a single crystalline diamond structure. The FFT image in Fig. 24 (e) shows the i-carbon phase structure along the <110> zone axis. The HRTEM image in Fig. 24 (f) shows that the nanoparticle has d-spacings of 2.43 and 2.12 Å of the phase to the (111) and (200) forbidden planes of cubic phase structure with a lattice parameter 4.2 Å, respectively. This phase is i-carbon [52] The

SAED pattern in Fig. 24 (f) have a lattice angle of 70° between the two lattice planes with the same d-spacing of 2.42 Å, and of 54° between the d-spacings of 2.42 and 2.10 Å. which are between the two (111) planes and between the (111) and (200) planes, respectively, matched with those of i-carbon.

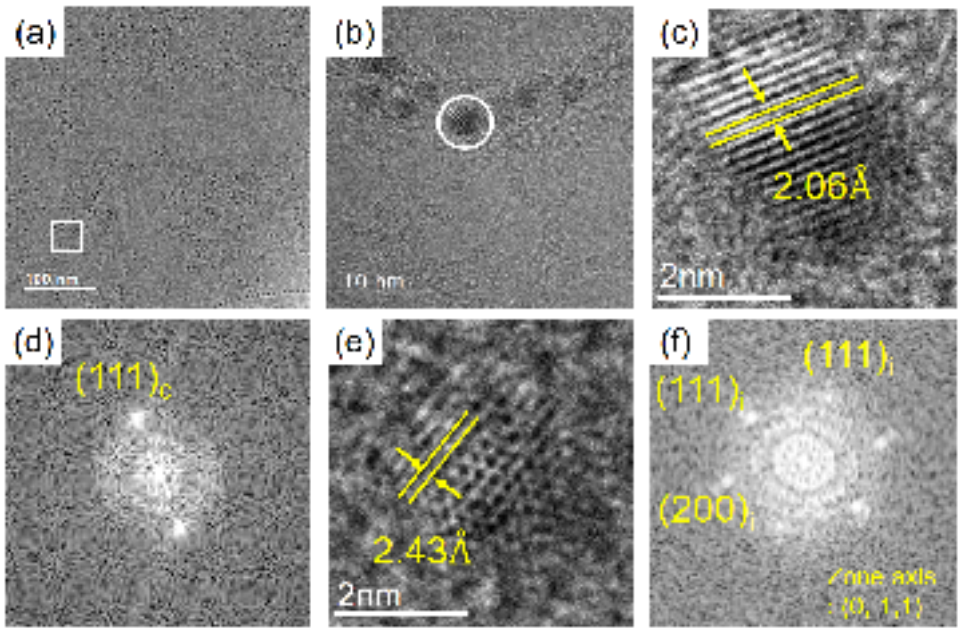

Fig. 24. TEM image of nanoparticles captured for 10 s on the graphene membrane of the TEM Cu grid. Nanoparticles are black small spot in Fig. 24 (a). (b) HRTEM image of the white box in (a). (c) a higher magnification of a nanoparticle in the white circle of (b). (d) The selected are electron diffraction pattern of the crystalline nanoparticle in (c). (e) i-carbon with 2.43 Å d-spacing value. (f) FFT image of (e).

Analysis of the captured nanoparticles

We analyzed 150 d-spacings of ~100 nanoparticles at each filament temperature. The fraction of observed d-spacing values was related to the filament temperature. The number of d-spacing values is a summation of observed d-spacing values of the captured nanoparticles from FFT images. The number of the d-spacing is closely related to the relative intensity of the d-spacing, which can be obtained from X-ray diffraction (XRD) of a polycrystal.

Fig. 25 shows the number of observed d-spacing values of captured nanoparticles at the filament temperature of 2100 °C, 2200 °C, and 2300 °C. The observed d-spacing values were approximately counted to the d-spacing values that the carbon allotropes could have. At the filament temperature of 2100 °C, the nanoparticles show that the number of 2.06 Å is 58, and the number of 2.42 Å is 43. However, the nanoparticles, which were captured at the filament temperature of 2200 °C, show that the number of the 2.42 Å is zero, and the frequency of the 2.06 Å is 98. At the filament temperature of 2300 °C, the nanoparticles show that the number of 2.06 Å is 110, and the number of 2.42 Å is zero. The number of 2.06 Å d-spacing increases as increasing the filament temperature from 2100 °C to 2300 °C. Fig. 25 indicates that the number of captured cubic diamonds increases as increasing the filament temperature from 2100 °C to 2300 °C.

As shown in Fig. 26, the nanoparticles, which were captured at filament temperature of 2100 °C, 2200 °C, and 2300 °C, were

randomly distributed on the TEM membranes. We observed one hundred nanoparticles to measure the average size of the nanoparticles at filament temperature of 2100 °C, 2200 °C, and 2300 °C. By increasing filament temperature from 2100 °C to 2300 °C, the average size of the nanoparticles increases from 3.5 nm to 4.4 nm. We observed that the average size of the nanoparticles is proportional to the number of 2.06 Å d-spacing.

For investigating the relationship between the electrons and the nanoparticles, we considered the surface energy of nanoparticles. As mentioned early, a high-charge state of the nanoparticle stabilized the sp^3 bond of the surface of a nanoparticle. When charging saturates dangling bonds of carbon atoms at the surface, the disappearance of reconstructed and graphitized layers at the surface was confirmed. We assumed that a charge state of nanoparticle might depend on an electron density in the gas phase. We expected that increasing electrons in the gas phase might maintain a higher level of the charge state of the surface. [82]

To increase the electron density at the gas phase, we tried to increase the filament temperature. By increasing filament temperature, the thermionic emission from the filament increased from 2100 °C to 2300 °C. Quantitatively, current were −24.9, −38.6 and −56.8 uA/cm^2 for filament temperature of 2100 °C, 2200 °C and 2300 °C, respectively. As filament temperature increases, the number of 2.06 Å d-spacing increases. From the results, we

confirmed that relatively abundant electrons at filament temperature of 2300 °C would tend to stabilize the sp^3 bond of nanodiamond.

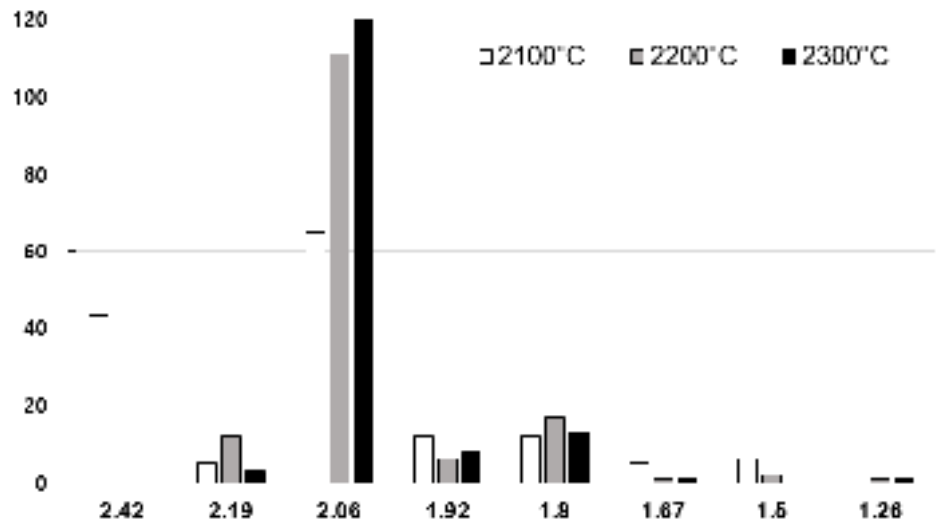

Fig. 25. The number of nanoparticles with d-spacing values of the captured nanoparticles, which obtained 450 d-spacing values of ~300 nanodiamonds. The nanoparticles were captured at filament temperature of 2100 °C, 2200 °C, and 2300 °C at the gas mixture of 1 % CH_4 - 99 % H_2, respectively.

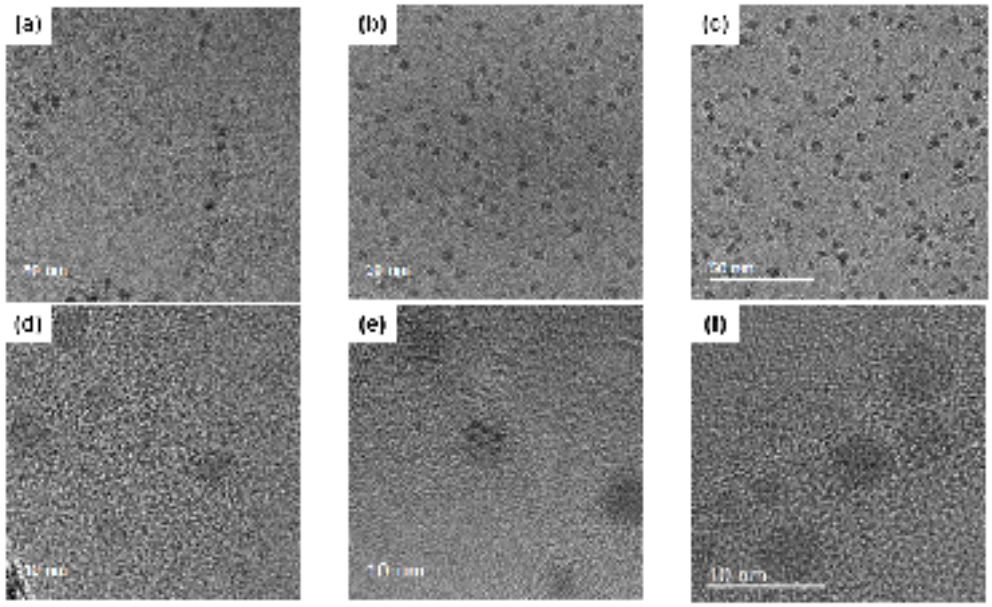

Fig. 26. HRTEM image of nanoparticles captured at filament temperature of (a) 2100 °C, (b) 2200 °C, and (c) 2300 °C. And, (d–f) are the magnified HRTEM images of (a–c), respectively.

Bias effect on the crystal structure of captured nanoparticles

A filament bias was one of the methods to increase the electron density at the gas phase. By increasing the additional bias from − 100 V to + 50 V at the gas mixture of 3 % CH_4 – 97 % H_2, the thermionic emission from the filament decreased from − 100 V to + 50 V. Quantitatively, current were −16.2, −13.6, 6.2 and −4.3 uA/cm^2 for the additional bias of − 100 V, − 50 V, 0 V, and + 50 V, respectively. To investigated the relationship between the electrons and the nanoparticles, we captured the nanoparticles on the graphene membrane at the filament temperature of 2100 °C and the capture temperature of 600 °C with the filament bias ranged – 100 V to +50 V.

Fig. 27 shows that the classification of ~ 100 nanoparticles at each filament condition ranging of – 100 V ~ + 50 V. The total 400 nanoparticles were classified as four carbon allotropes; i−carbon, n−diamond, hexagonal diamond, and cubic diamond. As increasing the filament bias from – 100 V to + 50 V, the number of i−carbon increased and the number of n−diamond decreased. The cubic diamond was observed in the filament bias – 100 V and – 50 V, but not observed in the filament bias 0 V and + 50 V. In case of the

hexagonal diamond, it was hard to find the relationship between the filament bias and the number of the hexagonal diamond.

Considering the measurement of the number of electrons at the gas phase, the tendency of the number of the classified carbon allotropes coincides to the tendency of the number of electrons. One thing that should be considered to understand the nanoparticles is the size effect on the nanoparticles. In chapter 1, the effect of size is important to the stability of the crystal structure of the nanoparticles. To clarify the effect of charge on the stability, we measured the average size of the observed nanoparticles by comparing the nanoparticles with 2.42 Å (only observed in i-carbon) and the nanoparticles with 2.06 Å. (mainly observed in diamond allotropes)

Fig. 28 shows the average size of the captured nanoparticles at each filament bias. And the average size of the observed nanoparticles at each filament bias had a ~ 3 nm. This results would imply that the nanoparticles which were charged by the electrons at the gas phase would be stabilized by the electrons. In addition to this, the different crystal structure means that they had a different potential energy originated by the geometry of the crystal structure. Not only potential energy, but also chemical bonding was also

related to the crystal structure of the nanodiamond. Considering above all physical and chemical properties of the crystal structure, the almost same size of the nanoparticles at each experiment condition means the stability of the nanoparticles was changed by the electrons, which determined the charge state of the nanoparticle. As a result, it seems that the nanoparticles which were generated at the gas phase would be multiply charged by the electrons.

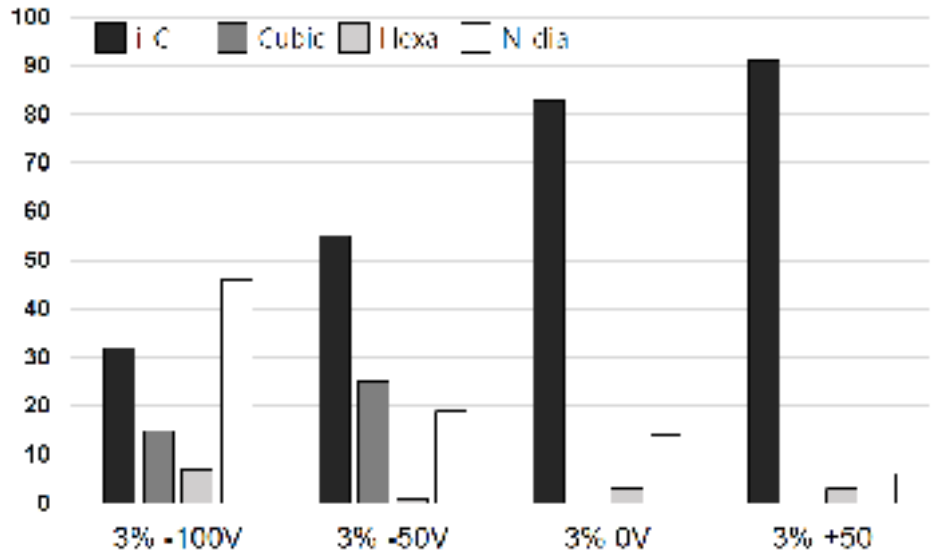

Fig. 27. The classification of ~ 100 nanoparticles at each conditions.

nm	-100V	-50V	0V	+50V
2.42 Å	3.14	3.24	3.00	2.98
2.06 Ä	2.92	3.26	3.32	2.89

Fig. 28. Average size of the captured nanoparticles at each filament bias ranging of – 100 V to +50 V.

Effect of electrons on the Deposition rate of diamond particles

To understand the relationship between the crystal structure of the deposition behavior of diamond, we deposited the diamond by controlling the filament temperature and the filament bias. In chapter 3, we already considered the relationship between the captured nanoparticles and the deposited diamond particles. The results showed that the deposition rate of the diamond particle increased as increasing the fraction of the diamond allotropes, whereas the deposition rate decreased as increasing the fraction of the i-carbon.

Electrons thermally emitted from the hot-filament increased as increasing the filament temperature. In Fig. 25, the number of diamond allotropes increased as increasing the filament. To confirm the growth rate of the diamond particles, we deposited the diamond particles at filament temperature Fig. 29 shows the diamond particles deposited at filament temperature of 2100 °C and 2300 °C. To set the same substrate temperature for deposition time, we located the substrate below the 6 mm and 10 mm from the hot-filament at filament temperature of 2100 °C and 2300 °C, respectively.

Fig. 25 (a-b) show the deposition behavior of the diamond particles deposited at filament temperature of 2100 °C and 2300 °C, respectively. The results show that the number density of the diamond particles at filament temperature of 2300 °C are larger than those at that of 2100 °C. Fig. 25 (c-d) are the magnified FESEM images of (a-b), respectively. It shows that the quality of the diamond particles almost same at both filament temperatures.

Even though the size of the diamond particles at the filament temperature of 2100 °C is slightly larger than those at that of 2300 °C, the nucleation rate on the surface of the substrate at filament temperature of 2300 °C is much faster than those at that of 2100 °C. This results are inconsistent with the results of the deposition behavior on the grounded conditions as mentioned at chapter 3. Fig. 26 (a) and (c) show that the number density of the nanoparticles increased as increasing the filament temperature. Considering the results, one possibility is related to the ion-induced nucleation of diamond nanoparticles generated at the gas phase. If the number of electrons at the gas phase increased, ion-induced nucleation also increased. Then the number of charged clusters in the gas phase would be stabilized by the electrons and might be existed as a cluster at the gas phase. After the nucleation of the diamond particle was induced by the supersaturation of the diamond

nanoparticles at the gas phase, then the diamond nanoparticles at the gas phase would be easily landed on the surface of the diamond particles on the substrate.

The preferential attachment of the diamond nanoparticles on the deposited diamond was interpreted by three major factors. First is the catalyst effect of charge on the surface of the diamond structure. Second is the electrostatic potential by the negatively charged nanoparticles for decreasing the surface energy of the nanoparticles. Third is the negative electron affinity of the diamond. Considering the all the chemical properties of diamond, if diamond nanoparticles were sufficiently generated at the gas phase, the deposition behavior could be changed from the diamond particles at filament temperature of 2100 °C to 2300 °C. To confirm the effect of electron on the growth of diamond film, we deposited the diamond film at filament bias 0 V ~ − 40V.

Fig. 30 shows the diamond films deposited at filament temperature of 2100 °C and a gas mixture of 3 % CH_4 – 97 % H_2. As decreasing the filament bias, the growth rate of diamond film increased. Because the electrons stabilized the crystal structure of the diamond nanoparticles and restrain the atomic hydrogen etching. As a result, the growth rate of diamond film is increased as increasing

the number of electrons at the gas phase.

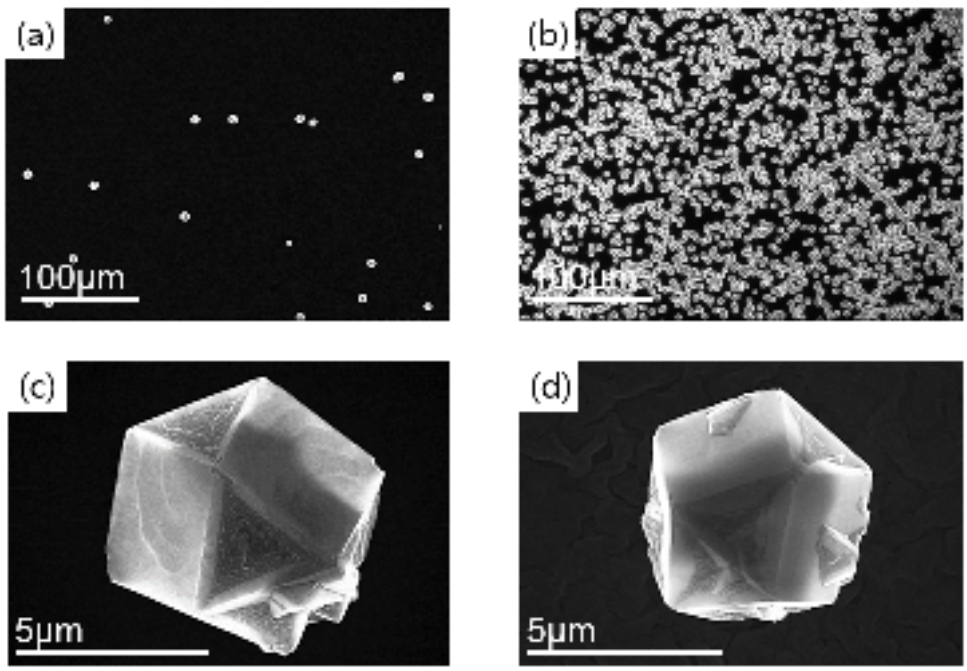

Fig. 29. Deposition behavior of diamond particles. (a) and (c) at filament temperature of 2100 °C, (b) and (d) at filament temperature of 2300 °C.

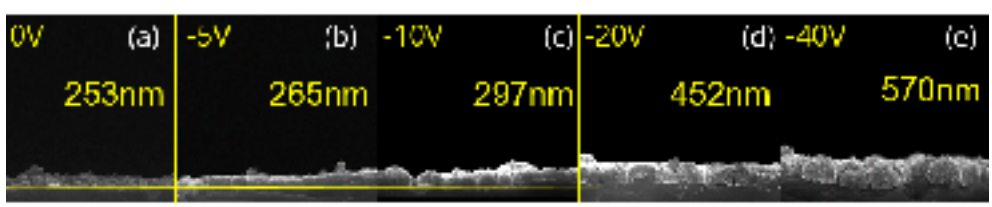

Fig. 30. Deposition behavior of diamond film at filament bias (a) 0 V, (b) −5 V, (c) −10 V, (d) −20 V, and (e) − 40 V.

4.4 conclusion

It is shown that the diamond allotropes can be synthesized by increasing the filament temperature and decreasing the filament bias. In this chapter, we confirmed that the electrons at the gas phase related to the crystal structure of the nanoparticles. By increasing the filament temperature from 2100 °C to 2300 °C, we confirmed that the number of captured nanoparticles and deposited particles increased. To clarify the effect of electrons on the growth rate of the diamond particles, we applied the additional bias on the filament ranging of 0 V ~ −40 V. The growth rate of the diamond film increased as decreasing the filament bias. The results show that the growth rate of diamond film could be enhanced by increasing the number of electrons at the gas phase.

Chapter.5 Unusual diamond growth rate at the low filament temperature in the HFCVD

The growth rate of diamond increased with increasing methane concentration at the filament temperature of 2100 °C. However, it decreased with increasing methane concentration from 1 % CH_4 – 99 % H_2 to 3 % CH_4 – 97 % H_2 at filament temperature of 1900 °C. This unusual diamond the growth rate at low filament temperature would be related to the non-diamond phase, which is then etched faster by atomic hydrogen, resulting in a decrease in the growth rate of diamond at low filament temperature. At 1 % CH_4 – 99 % H_2, graphite was only partly covered on the filament at 1900 °C but was not coated on the filament at 2100 °C. At 3 % CH_4 – 97 % H_2, however, graphite was fully covered on the hot filament both at 1900 °C and 2100 °C. The number of electrons thermally emitted from the hot filament was decreased when the surface of the filament was fully covered by Graphite coating. The number of electrons at 1 % CH_4 – 99 % H_2 was 13 times more than that at 3 % CH_4 – 97 % H_2 at the filament temperature of 1900 °C. The formation of the non-diamond phase, which is etched faster than diamond, resulting in a lower growth rate, was affected by the lower number of electrons at 3 % CH_4 – 97 % H_2.

5.1 Stabilization of diamond nanoparticles by using negative charging

In this chapter 5, we introduce the unusual deposition behavior of diamond, which is difficult to explain by the conventional concept of crystal growth. In the CVD process, the growth rate of films generally increases with increasing concentration of precursor. However, we observed that the deposition rate of diamond decreased with increasing the methane concentration from 1 % CH_4 – 99 % H_2 to 3 % CH_4 – 97 % H_2 at low filament temperature of 1900 °C. The purpose of this chapter is to understand the unusual dependence of the deposition behavior of the diamond growth at low filament temperature.

To investigate the unusual deposition behavior, we deposited the diamond particles at filament temperatures of 1900 °C and 2100 °C and at methane concentrations of 1 % CH_4 – 99 % H_2 and 3 % CH_4 – 97 % H_2. The unusual deposition behavior is related to the graphite coating on the filament surface. In addition to this, we revealed that the unusual deposition behavior could not be explained by filament coating alone. We confirmed that the number of electrons emitted from the hot filament would be more directly related to the unusual deposition behavior at the filament temperature of 1900 °C.

5.2 Experimental procedure

We used the filament consisted of three tungsten wires of ϕ 0.5 mm. The filament was carburized for 24 hr at a gas mixture 1 % CH_4 – 99 % H_2 and 3 % CH_4 – 99 % H_2, respectively. The reactor pressure was 20 Torr, and the filament temperature varied from 2100 °C to 1900 °C. CH_4 and H_2 were supplied as a gas mixture 1 % CH_4 – 99 % H_2 and 3 % CH_4 – 99 % H_2. We used a 1 cm x 1 cm silicon wafer substrate. The substrate temperature is targeted at 900 °C. The temperature was measured by a K-type thermocouple. The silicon substrate was not pretreated to deposit isolated diamond particles. The microstructure of the diamond particles was analyzed by FE-SEM (SU70. Hitachi Ltd., Tokyo, Japan), with an acceleration voltage of 15 kV.

We used a capturing system in the reactor to capture the diamond nanoparticles generated in the gas phase. The SiO membrane on the Cu grid for transmission electron microscope (TEM) (SiO Type-A, Ted Pella, Inc., Redding, CA, USA), on which nanoparticles were captured for 15 s, was placed on the quartz holder. The probe could be pushed from the chamber wall to the capture zone at capture temperature of ~ 600 °C and then pulled back toward the chamber wall. We observed that the SiO membrane was tended to be easily

thermally damaged during HFCVD. As a result, the capturing temperature of ~ 600 ^{o}C was the maximum to capture the nanoparticles for capturing time of 15 s.

We measured the number of electrons thermally emitted from the hot filament with the stainless steel probe installed in the feedthrough, connected to a picoammeter (model 6487; Keithley Instruments, Cleveland, OH, USA) outside the chamber.

5.3 Result & discussion

Unusual dependence of diamond growth rate

Fig. 31 shows the diamond particles deposited on the bare silicon substrate at the filament temperature of 2100 °C under the methane concentration of 1 % and 3 %. Fig. 31 (a–b) are the low magnification FESEM images of diamond particles deposited for 4 h and 8 h, respectively, at the gas mixture of 1 % CH_4 – 99 % H_2. Fig. 31 (c–d) are the high magnification FESEM images, respectively, of Fig. 31 (a–b). Fig. 31 (e–f) are the low magnification FESEM images of diamond particles deposited for 4 h and 8 h, respectively, at 3 % CH_4 – 97 % H_2. Fig. 31 (g–h) are the high magnification FESEM images, respectively, of Fig. 31 (e–f). We observed that the number density and the size of diamond particles increased with increasing methane concentration from 1% to 3% at the filament temperature of 2100 °C.

However, at the filament temperature of 1900 °C, the tendency of the number density and the size of diamond particles on methane concentration is reversed as shown in Fig. 32, where the diamond particles were deposited at the methane concentration of 1 % and 3 %. Fig. 32 (a–b) are the low magnification FESEM images of

diamond particles deposited for 4 h and 8 h, respectively, at 1 % CH_4 – 99 % H_2, with Fig. 32 (c–d) being the respective high magnification FESEM images. Fig. 32 (e–f) are the low magnification FESEM images of diamond particles deposited for 4 h and 8 h, respectively, at 3 % CH_4 – 97 % H_2, with Fig. 32 (g–h) being the respective high magnification FESEM images. With increasing methane concentration from 1% to 3%, the number density and the size of diamond particles decreased, which is unexpected.

Therefore, the tendency of the growth rate between the filament temperatures of 2100 °C and 1900 °C is reversed. It was well known that the flux for the deposition was closely related to the methane concentration. If the methane concentration increased, the flux for the deposition would increase. However, why does the deposition rate decrease when the methane concentration increased at the filament temperature of 1900 °C? Based on the thermodynamic approach, those reversible tendency of the growth rate of diamond particles cannot be explained. One possibility for Fig. 32 would be that the etching rate in the condition using 1 % CH_4 – 99 % H_2 is lower than that using 3 % CH_4 – 97 % H_2. Then, the question arises as to why the etching rate in the condition using 1 % CH_4 – 99 % H_2 is lower than that using 3 % CH_4 – 97 % H_2.

Considering the above all results including the chapter 1, 2, 3, and 4, we can assume that the diamond deposited in the condition using 3 % CH_4 – 97 % H_2 has a higher content of a non–diamond phase such as amorphous carbon nanoparticles and i–carbon. As a result, the diamond deposited in the condition using 3 % CH_4 – 97 % H_2 would be etched faster than that using 1 % CH_4 – 99 % H_2. To examine the crystallinity of diamond particles shown in Figs. 31 and 32, we analyzed the particles by using a micro Raman spectrometer with a spot size of 1 □m. Fig. 33 shows the Raman spectra of the diamond particles shown in Figs. 31 and 32, which were deposited under the filament temperature of 2100 °C and 1900 °C at the methane concentration of 1 % and 3 %.

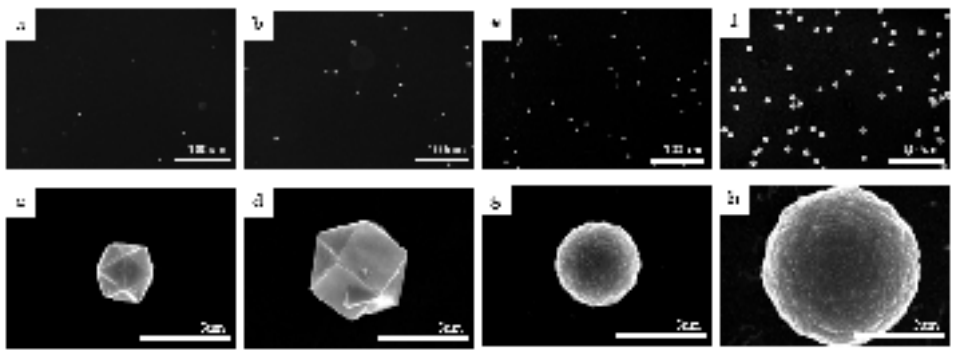

Fig. 31. FESEM images of diamond particles deposited on the Si substrate at a filament temperature of 2100 °C. The diamond particles (a–d) were deposited at 1 % CH_4 – 99 % H_2. The low magnification image of diamond particles (a–d) deposited for 4 h and 8 h, respectively. (c–d) are the high magnification images, respectively, of (a–b). The diamond particles (e–h) were deposited at 3 % CH_4 – 97 % H_2. The low magnification image of diamond particles (e–h) deposited for 4 h and 8 h, respectively. (g–h) are the high magnification images, respectively, of (e–f). (e–f) are the low magnification image of diamond particles deposited for 4 h and 8 h, respectively.

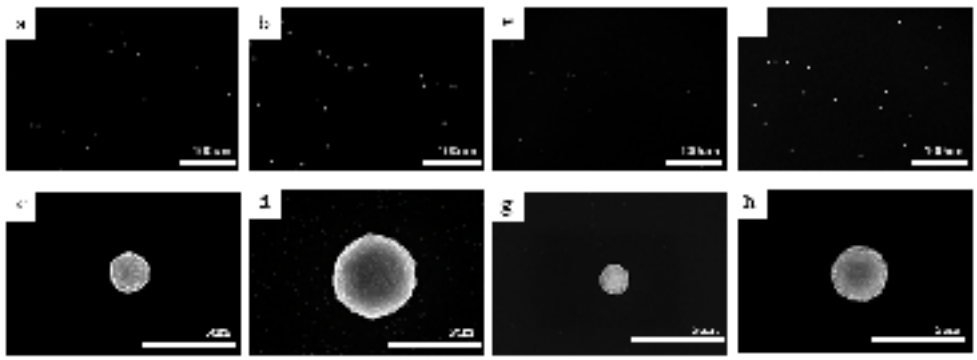

Fig. 32. FESEM images of diamond particles deposited on the Si substrate at a filament temperature of 1900 °C. The diamond particles (a–d) were deposited at 1 % CH_4 – 99 % H_2. The low magnification image of diamond particles (a–d) deposited for 4 h and 8 h, respectively. (c–d) are the high magnification images, respectively, of (a–b). The diamond particles (e–h) were deposited at 3 % CH_4 – 97 % H_2. The low magnification image of diamond particles (e–h) deposited for 4 h and 8 h, respectively. (g–h) are the high magnification images, respectively, of (e–f). (e–f) are the low magnification image of diamond particles deposited for 4 h and 8 h, respectively.

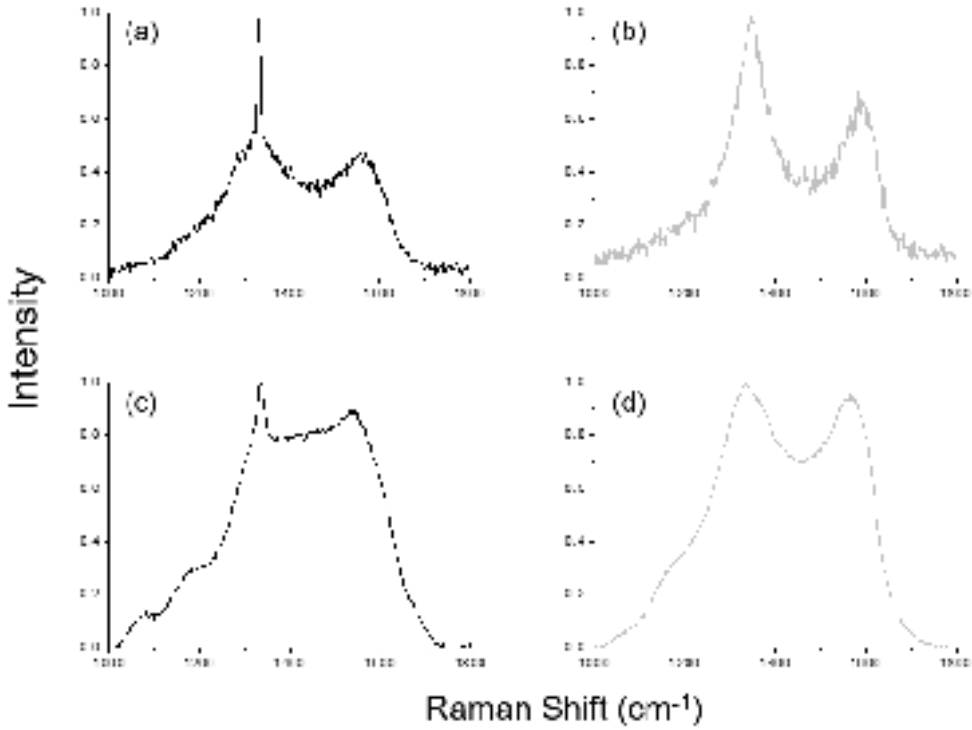

Fig 33. Raman spectra of deposited particles in Figs. 31 and 32. (a) the Raman spectra of the diamond particle in Fig. 31 (d). (b) the Raman spectra of the diamond particles in Fig. 31 (h). (c) the Raman spectra of the diamond particle in Fig. 32 (d). (d) the Raman spectra of the diamond particle in Fig. 32 (h).

Surface of the filament

Sommer et al. [3] suggested that under the condition where the hot filament is coated by graphite, non-diamond is formed. To check this possibility, we analyzed the filament surface whether the filament after deposition was coated by graphite or not. When the filament was carburized under the filament temperature of 2100 °C, the filament was not coated with graphite at methane concentration of 1 % as shown in Fig. 34 (a) but it was almost fully graphite coating on the filament surface at methane concentration of 3 % as shown in Fig. 34 (b). At the filament temperature of 1900 °C, the graphite coating on the filament surface was only partially formed at methane concentration of 1 % as shown in Fig. 34 (c) but the graphite coating was fully covered on the filament surface at methane concentration 3 % as shown in Fig. 34 (d). The behaviors of graphite coating on the filament surface agree with the thermodynamic calculations by a Thermo-Calc software using a SGTE (Scientifica Group Thermodata Europe) database [56] as shown in Fig. 35. Fig. 35 shows that at 1 % CH_4 - 99 % H_2, the graphite would partially precipitate at 1900 °C. However, at 3 % CH_4 - 97 % H_2, the graphite would precipitate on the filament surface at the filament temperature of 2300 °C.

At the filament temperature of 2100 °C, the diamond particles at 1 % CH_4 – 99 % H_2 has well defined faceted surfaces, whereas the diamond particles at 3 % CH_4 – 97 % H_2 has a cauliflower shape surfaces. The crystallinity of diamond particles reflects that the diamond particles at 3 % CH_4 – 97 % H_2 contains some non–diamond phase, which was mainly consisted of sp^2–bonded carbon structure. Due to the atomic hydrogen etching, the weak stability of the graphitic carbon structure would be easily etched. However, Fig. 31 shows that the size of the cauliflower diamond is larger than that of the diamond with faceted surfaces. Fig. 31 shows that the growth rate of the diamond particles at 3 % CH_4 – 97 % H_2 is higher than that of the diamond particles at 1 % CH_4 – 99 % H_2. Even though the higher etching rate at 3 % CH_4 – 97 % H_2 than that at 1 % CH_4 – 99 % H_2, the flux of the source for diamond deposition outweighs the higher etching rate of the diamond particles at 3 % CH_4 – 97 % H_2 than that of the diamond particles at 1 % CH_4 – 99 % H_2. However, at the filament temperature of 1900 °C the diamond deposited at 1 % CH_4 – 99 % H_2 has a cauliflower shape reflecting the non–diamond phase, and the diamond deposited at 3 % CH_4 – 97 % H_2 also has a ball–like shape as shown in Fig. 32. The size of the diamond particles at 1 % CH_4 – 99 % H_2 was larger than that of the diamond particles at 3 % CH_4 – 97 % H_2. This results shows that the growth

rate of the diamond particles at 3 % CH_4 – 97 % H_2 was lower than that of the diamond particles at 1 % CH_4 – 99 % H_2. In other words, the higher etching rate would be attributed to the higher content of the non–diamond phase in the ball–like diamond deposited at 3 % CH_4 – 97 % H_2 than that deposited at 1 % CH_4 – 99 % H_2 at the filament temperature of 1900 °C. It should be noted that the amount of atomic hydrogen formed at the filament temperature of 2100 °C would be larger than that of 1900 °C, and thereby the etching rate at 2100 °C is expected to be higher than that at 1900 °C.

From the above results, we assumed that the filament temperature plays an important role in the etching rate of the diamond particles. When the filament temperature increased, the amount of atomic hydrogen increased. This means that the amount of atomic hydrogen generated at 1900 °C would be much smaller than that at 2100 °C. However, since the etching rate of the diamond particles deposited at 2100 °C is much less than that at 1900 °C, the role of the filament temperature cannot explain the reversible dependence of the diamond growth rate alone. To understand the phenomena, we tried to understand the etching of the diamond particles.

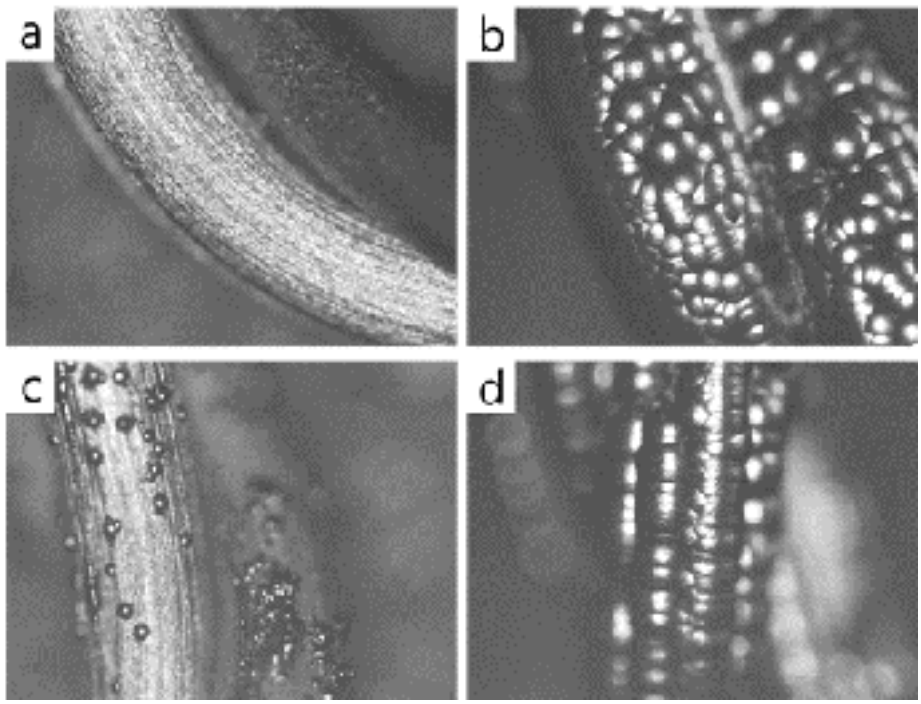

Fig. 34. Optical microscope images of the filament surface (a) at a filament temperature of 2100 °C at the gas mixture of 1 % CH_4 – 99 % H_2 and (b) at a filament temperature of 2100 °C at the gas mixture of 3 % CH_4 – 97 % H_2, (c) at a filament temperature of 1900 °C at the gas mixture of 1 % CH_4 – 99 % H_2, and (d) at a filament temperature of 1900 °C at the gas mixture of 3 % CH_4 – 97 % H_2.

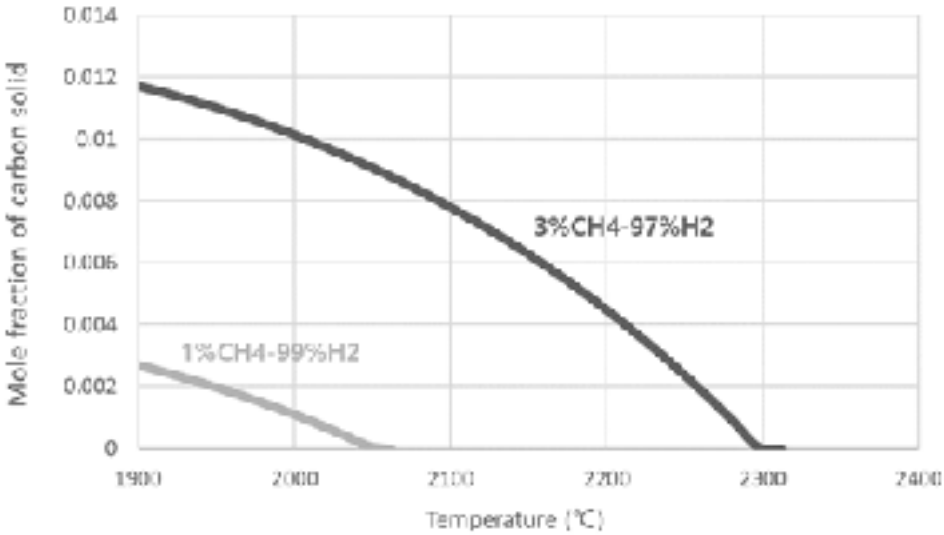

Fig. 35. Thermodynamic calculations of the equilibrium mole fraction of carbon precipitation at gas mixture of 1 % CH_4 – 99 % H_2 and 3 % CH_4 – 97 % H_2 by using a Thermo–Calc software based on a SGTE (Scientifica Group Thermodata Europe) database [56].

Electron emission from the hot-filament

The stability of the diamond particles was highly related to the amount of the electrons. We investigated the relationship between the electrons and the stability of the diamond nanoparticles at the chapter 4. We measured the electrons thermally emitted from the hot filament at each experimental condition. Fig. 36 shows the current measured at filament temperatures of 1900 °C, 2000 °C, and 2100 °C at 1 % CH_4 - 99 % H_2 and 3 % CH_4 - 97 % H_2. In Fig. 36, the amount of negative current increases with increasing filament temperature and is larger at 1 % CH_4 - 99 % H_2 than at 3 % CH_4 - 97 % H_2. At 1 % CH_4 - 99 % H_2, the amount of current increases from- 7.10 $\mu A/cm^2$ to - 17.3 $\mu A/cm^2$ when the filament temperature increases from 1900 °C to 2100 °C. At 3 % CH_4 - 97 % H_2, the amount of current increases from - 0.49 $\mu A/cm^2$ to -5.57 $\mu A/cm^2$ when the filament temperature increases from 1900 °C to 2100 °C. The tendency of the negative current with increasing filament temperature can be explained by considering the Richardson equation [97].

The measurement of current tendency -dramatically decreases when the methane concentration changes from 1 % CH_4 - 99 % H_2 to 3 % CH_4 - 97 % H_2. Those would be explained by the graphite

coating on the filament surface as shown in Fig. 34 (c-d). The work function of the surface was closely related to the electron emission described by the Richardson-Dushman equation [97-98]. When the filament surface is not coated by graphite, the components of the filament surface is tungsten carbide, which has a work function of 3.6 eV [99]. When the filament surface is coated by graphite, the components of the filament surface is graphite, which has a work function of 4.6 eV [100]. Because of the work functions, the thermionic emission from the filament could be affected by the work functions of the surface of the filament. As a result, the amount of the electrons at the gas phase at 3 % CH_4 - 97 % H_2 is smaller than that of the electrons at 1 % CH_4 - 99 % H_2.

In chapter 4, the diamond quality is related to the amount of the current. We also thought that the number of electric charges might affect the stability of diamond nanoparticles generated in the gas phase. To investigate the effect of charge on the nanoparticles at the filament temperature of 1900 ^oC and 2100 ^oC, diamond nanoparticles generated in the gas phase were captured at the filament temperature of 1900 ^oC and 2100 ^oC at the gas mixture of 3 % CH_4 - 97 % H_2.

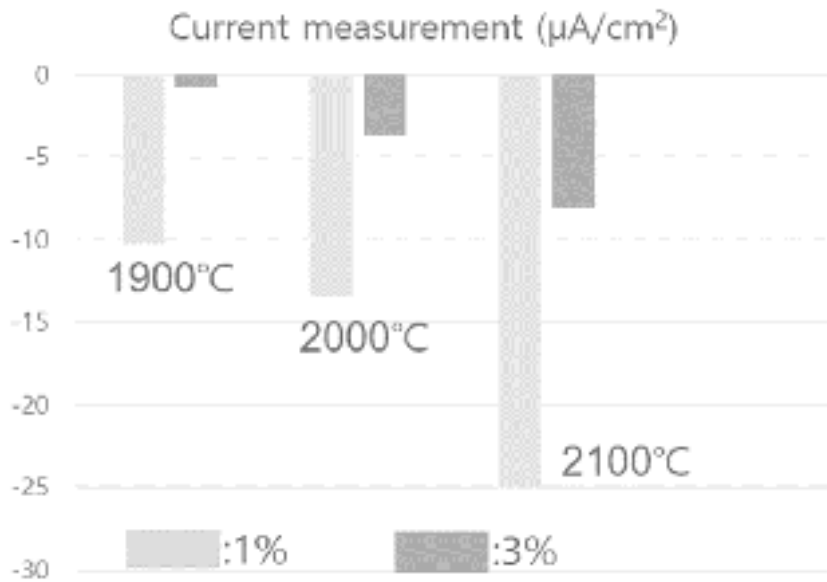

Fig. 36. Current measured at filament temperatures of 1900 °C, 2000 °C and 2100 °C. The light gray bars show the current measurement at 1 % CH_4 – 99 % H_2 and the dark gray bars show the current measurement at 3 % CH_4 – 97 % H_2.

Investigate the relationship between the captured nanoparticles and the diamond particles

Fig. 37 is TEM images of nanoparticles captured on the SiO membrane of the TEM grid for 15 s. Fig. 37 (a−b) show the scanning TEM (STEM) images of nanoparticles captured at 1900 °C and 2100 °C, respectively. When smaller nanoparticles are analyzed, the STEM mode have a much higher contrast between the membrane and the nanoparticles [101]. The crystalline nanoparticles tend to appear bright because of incoherently scattered electrons [102]. White spots in Fig. 36 (a−b) indicate the captured nanoparticles. The number of nanoparticles per μm^2, captured at the filament temperature of 1900 °C and 2100 °C, are 58 and 26, respectively. HRTEM images of nanoparticles captured at 1900 °C and 2100 °C, respectively, with the inset of FFT image are shown in Fig. 37 (c−d).

At the filament temperature 1900 °C, the crystal structure of captured nanoparticles is almost polycrystalline structure with the size of ~ 12 nm. 2.06 Å, 2.2 Å, and 2.5 Å d−spacing values were observed in the captured nanoparticles, which were measured within an error of 5 % by FFT of the HRTEM images. Four kind of carbon allotropes such as i−carbon, hexagonal diamond, n−diamond,

and cubic diamond were identified in the HFCVD diamond process [103]. D-spacing values of 2.06 Å, 2.2 Å, and 2.5 Å were related to various carbon allotropes such as a cubic diamond, n-diamond, hexagonal diamond, and i-carbon. [1, 103]. Considering the crystal structure of carbon allotropes, we confirmed that polycrystalline nanoparticles in Fig. 37 (a-c) mainly consist of i-carbon.

At the filament temperature 1900 °C, the crystal structure of captured nanoparticles is identified such as n-diamond and i-carbon with the size of ~ 5 nm. 2.06 Å, 2.2 Å, and 2.5 Å d-spacing values were observed in the captured nanoparticles. However, the frequencies of observed d-spacing values were definitely different at the filament temperature of 1900 °C and 2100 °C. As increasing the filament temperature, the frequency of 2.06 Å and 2.2 Å d-spacing values increased. However, as increasing the filament temperature, the frequency of 2.5 Å d-spacing value decrease. It means that nanoparticles captured at 2100 °C contained much less i-carbon than those captured at 1900 °C.

As a results, the deficient in excess charges would lead to the relatively lower charging state of nanoparticles generated in the gas phase. This would explain the possibility that carbon nanoparticles generated at 1900 °C at 3 % CH_4 - 97 % H_2 have a large

polycrystalline structure with i-carbon d-spacing. Such a structure would be formed by the agglomeration of nanoparticles. The diameter of nanoparticles in Fig. 37 (c) is 3 times larger than that of the nanoparticles captured at 2100 °C in Fig. 37 (d). In addition to these results, the nanoparticles with the size of ~ 5nm also were observed. In Fig. 38, the nanoparticles were captured under the same condition with the nanoparticles shown in Fig. 37. But the graphene membrane was used to capture the nanoparticles. In this condition, the nanoparticles were damaged during the TEM observation. As shown in Fig. 38 (a-c), the nanoparticles in the Fig. 38 were etched and became smaller. Fig. 38 shows that the crystal structure of captured nanoparticles has an amorphous structure, which can be easily damaged by the electron beam. Considering above results, the unusual dependence of the diamond growth rate at the filament temperature of 1900 °C would be related to the generation of amorphous carbon and i-carbon nanoparticles.

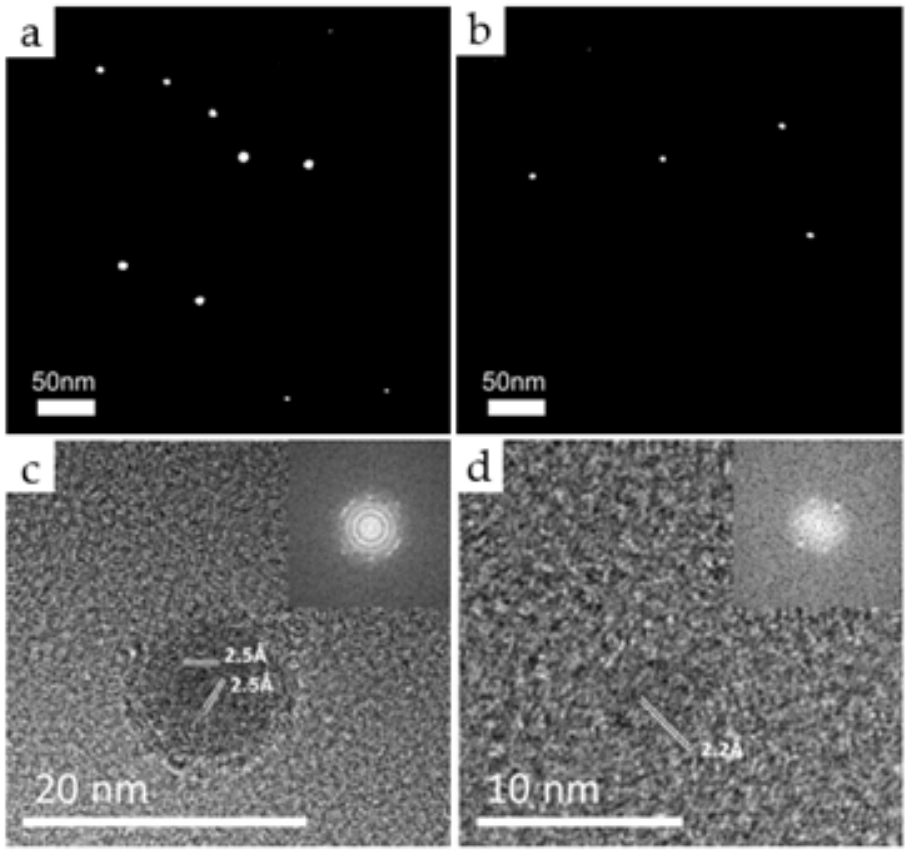

Fig. 37. TEM images of carbon nanoparticles captured at the gas mixture of 3 % CH_4 – 97 % H_2 for 15 s on the SiO membrane of the TEM grid. (a–b) are the STEM images of the nanoparticles captured at 1900 °C and 2100 °C, respectively. (c–d) are the HRTEM images of (a–b), respectively.

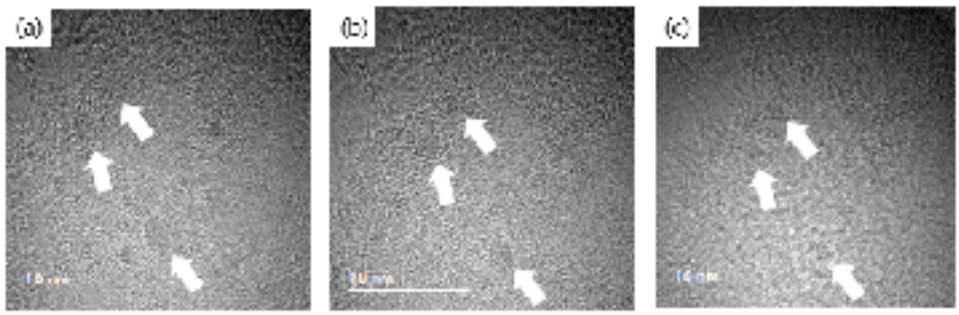

Fig. 38. HRTEM images of carbon nanoparticles for 10 s on the carbon membrane of the TEM grid. (a) shows the nanoparticles captured at 1900 °C at 3 % CH_4 – 97 % H_2 (b) after 2 s (c) 4 s.

5.4 Conclusions

At the filament temperature of 1900 °C, the deposition rate of diamond nanoparticles at 3 % CH_4 – 97 % H_2 decreases. The amount of the electrons at the gas phase is related to the filament temperature. As increasing the filament temperature, the amount of the electrons also increases. The graphite coating on the filament surface is related to the work function of the filament surface. The amount of electrons would stabilize the sp^3 bonding of captured nanoparticles. This unusual growth rate of the diamond particles is attributed to the higher content of the non-diamond phase, such as i-carbon and amorphous carbon in the cauliflower diamond structure at 3 % CH_4 – 97 % H_2. The higher content of the graphitic structure and amorphous phase appears to come from the less amount of electrons, which is again attributed to the hot filament coated by graphite at the filament temperature of 1900 °C and 3 % CH_4 – 97 % H_2.

Ch.6 summary

We have studied the various allotropes of diamond nanoparticles and their contribution to growth of diamond in the HFCVD. We found that crystal structure of the nanoparticles was related to the crystal structure of the deposited diamond, which was affected by the capture temperature, methane concentration, and electrons. Furthermore, we experimentally confirmed a charge-induced reconstruction of the carbon allotropes.

Chapter 2. About 600 nanoparticles captured in the HFCVD diamond process at various experimental conditions were analyzed by HRTEM and FFT images and identified as cubic diamond, n-diamond, hexagonal diamond and i-carbon. The cubic diamond and n-diamond become more stable as the size increases and i-carbon becomes more stable as the size decreases in the size range of 2 ~ 7 nm of nanoparticles generated in the gas phase of HFCVD. Diamond crystals deposited for 8 h under the condition of the capture temperature of 900 ^{o}C and 1 % CH_4 - 99 % H_2, where mainly cubic diamond and n-diamond nanoparticles were captured, have well-developed (100) facets whereas diamond crystals deposited for 8 h under the condition of the capture temperature of

900 ° C and 3 % CH_4 – 97 % H_2, where mainly i–carbon nanoparticles were captured, have ball–like or cauliflower structures.

Chapter 3. The number density of nanoparticles captured in the grounded condition was much larger than that in the floating condition. Nanoparticles captured in the floating condition consisted mainly of cubic diamond and n–diamond, whereas those captured in the grounded condition consisted mainly of i–carbon. Diamond particles deposited in the floating condition displayed an octahedral shape with well–developed facets, and had a high–intensity 1,332 cm^{-1} diamond Raman peak, whereas those deposited in the grounded condition showed an overall spherical shape and were partially covered with crystalline facets with a broad G–band Raman peak. These results indicate that negative charging stabilizes the diamond structure of nanoparticles, which contributes to the deposition of crystalline diamond with well–developed facets.

Chapter 4. It is shown that the size of the captured nanodiamonds was increased as increasing the filament temperature. The number of 2.06 Å d–spacing, which is related to diamond allotropes, is proportional to the current and the average size of the nanodiamonds. In addition, the additional bias ranged of – 100 V to

+ 50 V was applied to the filament. As decreasing the filament bias, the number of electrons increased. The growth rate of diamond film was related to the filament bias. The electrons stabilized the nanoparticles at the gas phase and enhanced the growth rate of the diamond film.

Chapter 5. In the diamond HFCVD process, the deposition rate is depended on the amount of precursor. However, the deposition rate at 3 % CH_4 – 97 % H_2 is drastically changed as decreasing the filament temperature from the 2100 °C to 1900 °C. This unusual growth rate of diamond particles is related to the higher content of the non-diamond phase. i-Carbon and amorphous carbon nanoparticles were mainly observed at the filament temperature of 1900 °C at the gas mixture of 3 % CH_4 – 97 % H_2. This can be explained that the stability of the nanoparticles generated at the gas phase is related to the amount of the electrons at the gas phase. By using the theory of the charged nanoparticles, the unusual phenomena in the diamond growth at 1900 °C is clearly explained.

I think that the understanding the relationship between the nanoparticles and the charge will open new science, technology and applications.

Bibliography

[1] H. Vora and T. J. Moraec, J. Appl. Phys. 52, 1981, 6151.

[2] L. Holland and S. M. Ojha, Thin Solid Films 58, 1979, 107.

[3] Y. Gogotsi, S. Wiez, D. A. Ersoy, and M. J. Mcnallan, Lett. Nat. 411,2011, 577-585.

[4] H. Hirai and K. Kondo, Science 253, 1991, 772-774.

[5] K. Yamada and A. B. Sawaoka, Carbon 32, 1994, 665-673.

[6] A. L. Vereshchagin, Combustion, Explosion and shock Waves 38, 2002, 358-359.

[7] A. S. Barnard, S. P. Russo, and I. K. Snook, Phys. Rev. B 68, 2003, 073406.

[8] J. W. Park, K. S. Kim, and N. M. Hwang, Carbon 106, 2016, 289-294.

[9] N. M. Hwang et al. Journal of Crystal Growth 162, 1996, 55-68.

[10] H.F. Calcote, Combust. Flame 42, 1981, 215.

[11] K.H. Homann, Angew. Chem. Int. Edit. 7, 1968, 414.

[12] D. G. Keil, R. J. Gill, D. B. OIson and H. F. Calcote, in: 20th Symp. Int. on Combustion (The Combustion Institute, 1984, pp. 1129.

[13] C. S. Kim, Y. B. Chung, W. K. Youn, and N. M. Hwang, Carbon 47, 2009, 2511-2518.

[14] C. S. Kim, W. K. Youn, amd N. M. Hwang, Journal of Applied Physics 108, 2010, 014313.

[15] C. S. Kim, W. K. Youn, D. K. Lee, K. S. Seol, and N. M. Hwang, Journal of Crystal Growth 311, 2009, 3938-3942.

[16] C. S. Kim, Y. B. Chung, W. K. Youn, and N. M. Hwang, Aerosol Science and Technology 43, 2009, 120-125.

[17] S. S. Lee, C. S. Kim, and N. M. Hwang, Aerosol Science and Technology 46, 2012, 1100-1108.

[18] C.T.R. Wilson, Phil. Trans. R. Soc. A 189, 1897, 265-307.

[19] C.T.R. Wilson, Phil. Trans. R. Soc. A 193, 1900, 289-308.

[20] C.T.R. Wilson, LXXV., Philos. Mag. Series 6 7, 1904, 681-690.

[21] B. V. Spitsyn, L. L. Bouilov, and B. V. Derjaguin, J. Cryst. Growth 52, 1981, 219-226.

[22] W. A. Yarbrough, J. Am. Ceram. Soc. 75, 1992, 3179-3200.

[23] N. M. Hwang, J. H. Hahn, and D. Y. Yoon, J. Cryst. Growth 160, 1996, 87-97.

[24] N. M. Hwang, D. Y. Yoon, J. Cryst. Growth 160, 1996, 98-103.

[25] I. D. Jeon, C. J. Park, D. Y. Kim, and N. M. Hwang, J. Cryst. Growth 213, 2000, 79-82.

[26] I. D. Jeon, C. J. Park, D. Y. Kim, and N. M. Hwang, J. Cryst. Growth 223, 2001, 6-14.

[27] S. Mitura, J. Cryst. Growth 80, 1987, 417-424.

[28] M. Frenkiach, R. Kematick, D. Huang, W. Howard, and K.E. Spear, J. Appl. Phys. 66, 1989, 395-399.

[29] R. Peter, Buerki, and S. Leutwyler, J. Appl. Phys. 69, 1989, 3739-3744.

[30] J. Y. Raty, G. Galli, C. Bostedt, T. W. V. Buuren, and L. J. Terminello, Phys. Rev. Lett. 90, 2003, 037401.

[31] V. L. Kuznetsov, I. L. Zilberberg, Yu. V. Butenko, and A. L. Chuvilin, J. Appl. Phys. 86, 1999, 863-870.

[32] J. C. Angus and C. C. Hayman, Science 241, 1988, 913.

[33] P. K. Bachmann, D. Leers, and H. Lydtin, Diamond Relat. Mater. 1, 1991, 1021-1034.

[34] P. Badziag, W. S. Verwoerd, W. P. Ellis, and N. R. Greiner, Nature 343, 1999, 244.

[35] D. M. Gruen, S. Liu, A. R. Krauss, J. Luo, and X. Pan, Appl. Phys.Lett. 64, 1994, 1502-1504.

[36] M. Yoshimoto, K. Yoshida, H. Maruta, Y. Hishitani, H. Koinuma, S. Nishio, M. Kakihana, and T. Tachibana, Nature 399, 1999, 340.

[37] N. J. Park, S. G. Park, N. M. Hwang, J. S. Ihm, S. Tejima, and H. Nakamura, Phys. Rev. B 69, 2004, 195411.

[38] L. Lai and A. S. Barnard, J. Mat. Chem. 22, 2012, 13141−13147.

[39] M. Y. Gamarnik, Nanostructured Mat. 7, 1996, 651−658.

[40] G. W. Yang, J. B. Wang, Q. X. Liu, J. Phys.: Condens. Matter 10, 1998, 7923−7927.

[41] T. L. Daulton, M. A. Kirk, R. S. Lewis, and L. E. Rehn, Nucl. Instr. and Meth. B 175, 2001, 12−20.

[42] V. Y. Dolmatov, Russ. Chem. Rev. 76, 2007, 339−360.

[43] S. M. Pimenov, G. A. Shafeev, A. A. Smolin, V. I. Konov, and B. K. Vodolaga, Appl. Surf. Sci. 86, 1995, 208−212.

[44] F. Banhart, and P. M. Ajayan, Nature 382, 1996, 433−435.

[45] É. M. Galimov, A. M. Kudin, V. N. Skorobogatskii, V. G. Plotnichenko, O. L. Bondarev, B. G. Zarubin, V. V. Strazdovskii, A. S. Aronin, A. V. Fisenko, I. V. Bykov, and A. Yu. Barinov, Doklady Phys.49, 2004, 150−153.

[46] J. P. Boudou, P. A. Curmi, F. Jelezko, J. Wrachtrup, P. Aubert, M. Sennour, G. Balasubramanian, R. Reuter, A. Thorel, and E. Gaffet, Nanotechnology 20, 2009, 235602.

[47] Y. R. Chang, H. Y. Lee, K. Chen, C. C. Chang, D. S. Tsai, C. C. Fu, T. S. Lim, Y. K. Tzeng, C. Y. Fang, C. C. Han, H. C. Chang, and W. Fann, Nat. Nanotechnol. 3, 2008, 284−288.

[48] A. D. Greentree, B. A. Fairchild, F. M. Hossain, and S. Prawer, Mater. Today 11, 2008, 22−31.

[49] I. I. Vlasov, A. S. Barnard, V. G. Ralchenko, O. I. Lebedev, M. V. Kanzyuba, A. V. Saveliev, V. I. Konov, and E. Goovaerts, Adv. Mater. 21, 2009, 808−812.

[50] E. Ōsawa, Diam. Relat. Mater. 16, 2007, 2018−2022.

[51] S. Turner, O. L. Lebedev, O. Shenderova, I. I. Vlasov, J. Verbeeck, and G. V. Tendeloo, Adv. Funct. Mater. 19, 2009, 2116–2124.

[52] H. Vora, T. J. Moravec, J. Appl. Phys. 52, 1981, 6151–6157.

[53] J. L. Peng, J. O. Orwa, B. Jiang, S. Prawer, L. A. Bursill, Int. J. Mod. Phys. B 15, 2001, 3107–3123.

[54] K. Yamada and A. B. Sawaoka, Carbon 32, 1994, 665–673.

[55] M. J. Bucknum, C. J. Pickard, I. Stamatin, and E. A. Castro, J. Theor. Comput. Chem. 5, 2006, 175–185.

[56] B. Sundman B. Jansson, and J. O. Andersson, Calphad, 1985, 153–190.

[57] F. Teng, J. Wang, X. An, B. Lu, Y. Su, C. Gong, P. Zhang, Z. Zhang, and E. Xie, RSC Adv. 2, 2012, 7403–7405.

[58] S. Mathur, The thermionic work function of graphite—III, Proc. Nat. Acad. Sci.19, 1952.

[59] L. Gueroudji and N.M. Hwang, Diam. Relat. Mat. 9, 2000, 205–211.

[60] M. Sommer, K. Mui, and F.W. Smith, Solid State Communications 69, 1989, 775–778.

[61] A.R. Badzian, T. Badzian, R. Roy, R. Messier, and K.E. Spear, Mat. Res. Bull. 23, 1988, 531–548.

[62] A.V. Palnichenko, A.M. Jonas, J.C. Charlier, A.S. Aronin, J.P. Issi, Nature 402, 1999, 162–165.

[63] M. Yoshimoto, K. Yoshida, H. Maruta, Y. Hishitani, H. Koinuma, S. Nishio, M. Kakihana, and T. Tachibana, Nature 399, 1999, 340–342.

[64] D.M. Gruen, S. Liu, A.R. Krauss, J. Luo, and X. Pan, Appl. Phys. Lett. 64, 1994, 1502–1504.

[65] N.M. Hwang and D.Y. Kim, J. Cryst. Growth 218, 2000, 40–44.

[66] H.M. Jang and N.M. Hwang, J. Mat. Res. 13, 1998, 3536–3549.

[67] A. Glasner and J. Kenat, J. Cryst. Growth 2, 1968, 119–127.

[68] A. Glasner and S. Skumik, Isr. J. Chem. 6, 1968, 69–72.

[69] A. Glasner and M. Tassa, Isr. J. Chem. 12, 1974, 799–816.

[70] A. Glasner and M. Tassa, Isr. J. Chem. 12, 1974, 817–826.

[71] I. Sunagawa, J. Cryst. Growth 99, 1990, 1156–1161.

[72] J. Blažek, J. Kousal, H. Biederman, O. Kylián, J. Hanuš, and D. Slavínská, J. Phys. D: Appl. Phys. 48, 2015, 415202.

[73] C.M. Donnelly, R.W. McCullough, and J. Geddes, Diam. Relat. Mat. 6, 1997, 787–790.

[74] H. Fujita, J. Electron Microscopy Tech. 3, 1986, 45–56.

[75] H. Fujita, Mat. Transactions 35, 1994, 563–575.

[76] S. Iijima and T. Ichihashi, Phys. Rev. Lett. 56, 1986, 616.

[77] H. W. Whitlock and M. W. Siefkien, J. Am. Chem. Soc. 90, 1968, 4929–4939.

[78] T. M. Grund, P. R. Schleyer, P. H. Gund and W. T. Wipke, J. Am. Chem. Soc. 97, 1975, 743–751.

[79] J. Y. Raty, G. Galli, C. Bostedt, T. W. van Buuren and L. J. Terminello, Phys. Rev. Lett. 90, 2003, 037401.

[80] A. S. Barnard and M. Sternberg, J. Mater. Chem. 2007, 17, 4811–4819.

[81] B. Palosz, C. Pantea, E. Grzanka, S. Stelmakh, et al., Diamond Relat. Mater. 15, 2006, 1813–1817.

[82] L. Lai and A. S. Barnard, J. Mater. Chem. 22, 2012, 13141.

[83] V. V. Roddatis, V. L. Kuznetsov, Y. V. Butenko, D. S. Su and R. Schlogl, Phys. Chem. Chem. Phys., 4, 2002, 1964–1967.

[84] J. Hiraki, H. Mori, E. Taguchi, H. Yasuda, et al., Appl. Phys. Lett., 86, 2005, 223101.

[85] N. M. Hwang, Non-Classical Crystallization of Thin Films and Nanostructures in CVD and PVD Processes, Springer, Dordrecht, 1st edn, 2016, ch. 5–6, pp. 101–158.

[86] J. D. Watts and R. J. Bartle2tt, J. Chem. Phys. 96, 1992, 6073–6084

[87] A. S. Barnard, S. P. Russo and I. K. Snook, Diam. Relat. Mater. 12, 2003,1867–1872.

[88] A. S. Barnard, S. P. Russo and I. K. Snook, Philos. Mag. Lett. 83, 2003, 39–45.

[89] N. W. Winter and F. H. Ree, J. Comput. Aided Mater. Des. 5, 1998, 279–294.

[90] P. K. Chu and L. Li, Mater. Chem. Phys. 96, 2006, 253–277.

[91] S. Prawer and R. J. Nemanich, Phil. Trans. R. Soc. 362, 2004, 2537–2565.

[92] L. Abello, G. Lucazeau, B. Andre and T. Priem, Diam. Relat. Mater. 1, 1992, 512–518.

[93] A. C. Ferrari and J. Robertson, Phys. Rev. B, 61, 2000, 14095.

[94] C. M. Donnelly, R. W. McCullough and J. Geddes, Diam. Relat. Mat., 6, 1997, 787–790.

[95] C. Kanai, K. Watanabe and Y. Takakuwa, Phys. Rev. B, 63, 2001, 235311.

[96] L. Lai and A.S. Barnard, Nanoscale 4, 2012, 1130-1137.

[97] O.W. Richardson, Phys. Rev. 23, 1924, 153–155.

[98] S. Dushman, Rev. Modern Phys. 2, 1930, 381–476.

[99] S. Jianping, S. Field emission from tungsten carbide on W tips, ICAIT'08: Proceedings of the 2008 International Conference on Advanced Infocomm Technology 2008, pp. 1–4.

[100] K. S. Krishnan, S. C. Jain, Nature 169, 1952, 702–703.

[101] B. S. Zhang, W. Zhang, D. S. Su, Microsc. Anal. 26, 2012, 15–21.

[102] Krumeick, F. Properties of Electrons, their Interactions with matter and applications in electron microscopy, Laboratory of Inorganic Chemistry dispon□el em, http://www.microscopy.ethz.ch/downloads/Interactions.pdf. consultado em 2011; pp. 3–8.

[103] H. Y. Kim, Nanomaterials 10, 2020, 2504.

요약 (국문 초록)

Hot-filament 화학 기상 증착에서의 다이아몬드 나노입자의 다양한 동소체와 다이아몬드의 성장 거동

다이아몬드를 합성하는 방법에는 다양한 방법이 있다. 최근에는 나노다이아몬드를 합성하는 방법에 대한 연구도 활발하게 이루어지고 있다. 그 중에서도 폭발법을 이용하여 나노다이아몬드를 합성하는 방법에 대한 연구가 가장 활발하게 이루어져왔다. 최근에는 Hot-filament 화학 기상 증착 과정동안 나노입자가 기상에서 생성되는 것을 활용하여 기상에 존재하는 나노다이아몬드를 직접 포집하는 방법에 대해서도 연구가 진행되었다. 하지만 Hot-filament 화학 기상 증착에서의 나노다이아몬드와 공정 변수간 관계에 대해 연구가 부족한 상황이며, 이러한 기상에서 형성된 나노다이아몬드 입자들이 다이아몬드 입자로 성장하게 되었을 때 미치는 관계에 대해서는 연구가 부족한 상황이다.

본 연구에서는 포집 온도, membrane의 전기적 특성, 필라멘트의 온도, 필라멘트 bias, 그리고 기상에 존재하는 전자가 나노다이아몬드에 미치는 영향과 이 때 나노다이아몬드의 특성이 다이아몬드의 입자 성장 및 박막 성장에 미치는 영향을 확인하였다. 우선 나노다이아몬드의 결정 구조를 확인하는 과정에서 나노다이아몬드는 네 가지 동소체의 형태로 존재하는 것을 확인 할 수 있었다. 기상에서 형성되는 나노다이아몬드 입자는 음의 하전을 띄는 특성을 가지는 특성을 활용하여 나노다이아몬드가 합성되는 외부 환경이 변화하게 되었을 때 포집된 나노입자들을 분석해 보았을 때, 나노다이아몬드의 동소체의 분율이 변화하는 것을 확인할 수 있었으며 이는 나노다이아몬드가 여러가지 변수로 인하여 기상에서 혹은 포집이 되는 membrane에서 결정성이 변화하는 것을 알 수 있

었다.

기상에서 형성되는 나노입자의 특성의 연구가 중요한 이유는 고전적인 박막 및 입자 성장 관점에서 설명하지 못하는 문제를 해결하는 새로운 관점을 제시하는 데에 있다. 가령 예를 들어서 화학 증착 방법을 이용하게 되었을 때에, 일반적으로는 시스템에 투입되는 precursor의 양이 증가하게 되었을 때 박막 혹은 입자의 성장이 증가한다는 지극히 당연하고 간단한 현상이, hot-filament 화학 증착 방법을 사용하는 경우에는 필라멘트의 온도가 2000도 아래로 가게 되면 이러한 당연한 현상이 반대로 관찰이 되기도 한다. 또한 기존의 다이아몬드 박막 증착에서 증착 속도에 가장 중요한 변수로 atomic hydrogen에 의한 etching이 중요한 이유로 다루어 졌는데, 하전된 나노입자 이론을 활용하여 기상에 존재하는 나노입자의 phase stability를 변화시킬 수 있었고, atomic hydrogen에 의한 etching을 억제하는 것을 확인하였다. 이처럼 하전된 나노입자 이론을 활용하여 지금까지 다이아몬드의 입자와 박막 성장에서 이해가 되지 않는 여러 현상을 설명하는 새로운 관점을 제시 하였다.

주요어 : Hot-filament CVD; 하전된 나노입자; 나노다이아몬드 동소체; 하전 유도 재결정화; TEM;

학번: 2015-22743